PNNL-16652

Pacific Northwest
National Laboratory
Operated by Battelle for the
U.S. Department of Energy

Site-Specific Velocity and Density Model for the Waste Treatment Plant, Hanford, Washington

A. C. Rohay
T. M. Brouns

June 2007

Prepared for the U.S. Department of Energy
Office of River Protection
under Contract DE-AC05-76RL01830

DISCLAIMER

PACIFIC NORTHWEST NATIONAL LABORATORY
operated by
BATTELLE
for the
UNITED STATES DEPARTMENT OF ENERGY
under Contract DE-AC05-76RL01830

Printed in the United States of America

Available to DOE and DOE contractors from the
Office of Scientific and Technical Information,
P.O. Box 62, Oak Ridge, TN 37831-0062;
ph: (865) 576-8401
fax: (865) 576-5728
email: reports@adonis.osti.gov

Available to the public from the National Technical Information Service,
U.S. Department of Commerce, 5285 Port Royal Rd., Springfield, VA 22161
ph: (800) 553-6847
fax: (703) 605-6900
email: orders@ntis.fedworld.gov
online ordering: http://www.ntis.gov/ordering.htm


This document was printed on recycled paper.
(8/00)

PNNL-16652

Site-Specific Velocity and Density Model for the Waste Treatment Plant, Hanford, Washington

A. C. Rohay
T. M. Brouns

June 2007

Prepared for
the U.S. Department of Energy
Office of River Protection
under Contract DE-AC05-76RL01830

Pacific Northwest National Laboratory
Richland, Washington 99352

Summary

The U.S. Department of Energy (DOE) is constructing a Waste Treatment and Immobilization Plant (WTP) to treat and vitrify underground tank waste stored on the Hanford Site in southeastern Washington State. The seismic design basis for the WTP was re-evaluated in 2005, resulting in an increase by up to 40% in the seismic design basis. The original seismic design basis for the WTP was established in 1999 based on a probabilistic seismic hazard analysis completed in 1996. The 2005 analysis was performed by Pacific Northwest National Laboratory (PNNL) to address questions raised by the Defense Nuclear Facilities Safety Board about the assumptions used in developing the original seismic criteria and adequacy of the site geotechnical surveys. The updated seismic response analysis used existing and newly acquired seismic velocity data, statistical analysis, expert elicitation, and ground motion simulation to develop interim design ground motion response spectra that enveloped the remaining uncertainties. The uncertainties in these response spectra were enveloped at approximately the 84th percentile to produce conservative design spectra, which contributed significantly to the increase in the seismic design basis.

A key uncertainty identified in the 2005 analysis was the contrasts in velocity between the basalt flows and sedimentary interbeds below the WTP. The velocity structure of the upper four basalt flows (Saddle Mountains Basalt) and the interlayered sedimentary interbeds (Ellensburg Formation) produces strong reductions in modeled earthquake ground motions propagating through them. Uncertainty in the magnitude of velocity contrasts between these basalts and interbeds resulted primarily from an absence of measured shear wave velocities (Vs) in the interbeds. For the 2005 study, Vs in the interbeds was estimated from older, limited compression wave (Vp) data using estimated ranges for the ratio of the two velocities (Vp/Vs) based on analogues in similar materials. A range of possible Vs for the interbeds and basalts was used and produced additional uncertainty in the resulting response spectra.

Because of the sensitivity of the calculated response spectra to the velocity contrasts between the basalts and interbedded sediments, DOE initiated the seismic boreholes project (SBP) to emplace additional boreholes at the WTP site and obtain direct Vs measurements and other physical property measurements in these layers. The approach to the SBP involved four main elements: 1) planning and site preparation, 2) new borehole installation, 3) geological and geophysical data collection and analysis, and 4) site seismic response analysis.

The three boreholes are within 500 feet of and surrounding the high-level waste vitrification and pretreatment facilities of the WTP, which were the structures affected by the interim design spectra. The core hole is co-located with the borehole closest to those two structures.

This report documents the geophysical data collection and analysis element managed and conducted by PNNL. Previously published reports document the planning and installation of three boreholes and single core hole in which the geophysical measurements were made, as well as the geological data collection and analysis from the drilling. The seismic response analysis was performed and documented separately by Geomatrix Consultants, Inc., in parallel with this PNNL study.

Geophysical data were collected in 2006–2007 in the three boreholes and one core hole to a maximum depth of nearly 1,500 feet below ground surface. Multiple geophysical methods were used to measure the shear and compression wave velocities of the sediments above the basalts and in the basalts

and interbeds that were penetrated by all four borings. In addition, density measurements were made that aided the interpretation of the geology in the boreholes and were used as input to the seismic response modeling.

Shear and compression wave velocity measurements were made using two basic techniques, suspension and downhole logging. Suspension logging measures the velocities near the borehole wall using high-frequency signals produced and recorded on a string of instruments suspended in the boreholes. Downhole logging measures velocities over a larger area surrounding the borehole by using a lower-frequency surface energy source with a geophone clamped at depth. Two different types of energy sources were used at the surface for the downhole measurements—an impulsive source that produces a single, unambiguous signal, and a vibratory source, which is more difficult to interpret but has the greater energy required to reach the depths of these boreholes. The first source was either a sledgehammer or small mechanical device. The second source was a large truck-mounted electro-hydraulic vibrator.

Systematic differences were found between the suspension and downhole logging measurements. Suspension logging gives a very high-resolution measurement, but the signal frequencies of the downhole method are similar to those of earthquakes important in ground-motion response modeling. The suspension logging measurements gave velocities significantly higher than the downhole measurements in the basalts for both shear and compression. Suspension logging results were used to shape the downhole velocity profiles to address details of velocity reductions in the basalt flow tops that were not modeled previously.

Density measurements were made also using two different methods. A standard geophysical logging method measured density at the borehole wall. A second method using a borehole gravity meter measured density far from the borehole wall. The second method is not affected by drill fluid invasion, cement, or metal casing in the borehole. Comparison of the two density measurements gave good agreement except where borehole irregularities or steel casing were present.

The shear wave velocity and density data from the three boreholes and the core hole were combined statistically to produce an average velocity and density model of the WTP site. The final set of profiles integrated data from the new boreholes and previous studies and provided a set of updated input parameters for subsequent use in evaluating the seismic site response of the WTP site. The statistical analysis also provided bounds on the variability and uncertainty of the profiles. The final velocity and density profiles are represented by a set of input parameters required for seismic site response analyses that include densities of all stratigraphic units, stratigraphic unit thicknesses, basalt flow top thicknesses, Vs of all stratigraphic units, and basalt flow top velocity gradients.

The basalt Vs values in the new model are comparable to the upper limit of the 2005 analyses, and the interbed Vs values are significantly lower than the upper limit of the 2005 analyses. The reductions in velocity through the basalt flow tops are higher than in 2005 and also are different for each basalt layer. Uncertainties in both the shear wave velocity and density models were reduced significantly relative to the model constructed in 2005. These updated models are based on measured properties from directly below the pretreatment and high-level waste vitrification facilities of the WTP and provide the necessary technical foundation for updating the seismic site response analysis and site-specific ground motion design spectra for the WTP site.

Abbreviations

bgs	below ground surface
BHGM	borehole gravity meter
CCU	Cold Creek unit
CRBG	Columbia River Basalt Group
DNFSB	Defense Nuclear Facilities Safety Board
DOE	U.S. Department of Energy
DOE-ORP	DOE Office of River Protection
fps	feet per second
ft	foot, feet
GPS	Global Positioning System
H2 unit	Hanford formation sands
H3 unit	Hanford formation gravels
HLW	high-level waste
in.	inch, inches
LAW	low-activity waste
m	meter, meters
MGL	Micro-g Lacoste, Inc.
MSL	mean sea level
NGS	National Geodetic Survey
OD	outside diameter
ORP	Office of River Protection
PC-3	Performance Category 3
PNNL	Pacific Northwest National Laboratory
PVC	polyvinyl chloride

PT	Pretreatment Facility
Redpath	Redpath Geophysics
SASW	spectral analysis of shear wave
SBP	Seismic Boreholes Project
SCPT	seismic cone penetrometer test
Shannon & Wilson	Shannon & Wilson, Inc., Geotechnical and Environmental Consultants
Texas	University of Texas at Austin
USACE	U.S. Army Corps of Engineers
Vp	compression wave velocity
Vs	shear wave velocity
WTP	Waste Treatment and Immobilization Plant

Contents

Figures

Tables

1.0 Introduction

The U.S. Department of Energy (DOE) is constructing a Waste Treatment and Immobilization Plant (WTP) to treat and vitrify legacy nuclear wastes stored in underground tanks at the Hanford Site in southeastern Washington State. The geology underlying both the Hanford Site and the WTP is a sequence of sedimentary units overlying a series of flood basalt flows. The original seismic design basis for the WTP was established in 1999 based on a probabilistic seismic hazard analysis completed in 1996 (Geomatrix Consultants 1996).

The Defense Nuclear Facilities Safety Board (DNFSB) subsequently initiated a review of the seismic design basis of the WTP. In March 2002, DNFSB staff questioned the assumptions used in developing the seismic design basis, particularly the adequacy of the site geotechnical surveys, and subsequently raised additional questions about the probability of earthquakes, adequacy of the "attenuation relationships" that describe how ground motion changes as it moves from its source in the earth to the site, and the large uncertainty in the extrapolation of California attenuation models to the Hanford Site.

Between 2002 and 2004, the DOE Office of River Protection (ORP) responded, resolving many of the questions raised, and developed a plan to acquire additional site data and analysis to address remaining questions. The key features of this plan were 1) acquiring new soil data down to about 500 ft, 2) reanalyzing the effects of deeper layers of sediments interbedded with basalt down to about 2,000 ft that may affect the attenuation of earthquake ground motions more than previously understood, and 3) applying new models for ground motions as a function of magnitude and distance at the Hanford Site.

In 2004 and 2005, the Pacific Northwest National Laboratory (PNNL) led efforts for DOE-ORP to address features 1 and 2 of the plan by collecting site-specific geologic and geophysical data at the WTP site and conducting modeling of the WTP site-specific ground motion response. New geophysical data were acquired, analyzed, and interpreted with respect to existing geologic information gathered from other Hanford-related projects in the WTP area. Information from deep boreholes was collected and interpreted to produce a realistic model of the deeper rock layers consisting of the interlayered basalts and sedimentary interbeds. The earthquake ground motion response was modeled, and a series of sensitivity studies was conducted to address areas in which the geologic and geophysical information has significant remaining uncertainties. This effort culminated in 2005 with issuance of an updated seismic response analysis for the WTP site (Rohay and Reidel 2005).

The updated seismic response analysis used existing and newly acquired seismic velocity data, statistical analysis, expert elicitation, and ground motion simulation to develop interim design ground motion response spectra that enveloped the remaining uncertainties. The uncertainties in these response spectra were enveloped at approximately the 84th percentile to produce conservative design spectra, which contributed significantly to the increase in the seismic design basis (Figure 1.1).

A key uncertainty identified in the 2005 analysis was the velocity contrasts between the basalt flows and sedimentary interbeds beneath the WTP. The velocity structure of the upper four basalt flows and the interlayered sedimentary interbeds produces strong reductions in modeled earthquake ground motions propagating through them. Uncertainty in the strength of velocity contrasts between these basalts and interbeds resulted primarily from an absence of measured shear wave velocities (Vs) in the interbeds. For

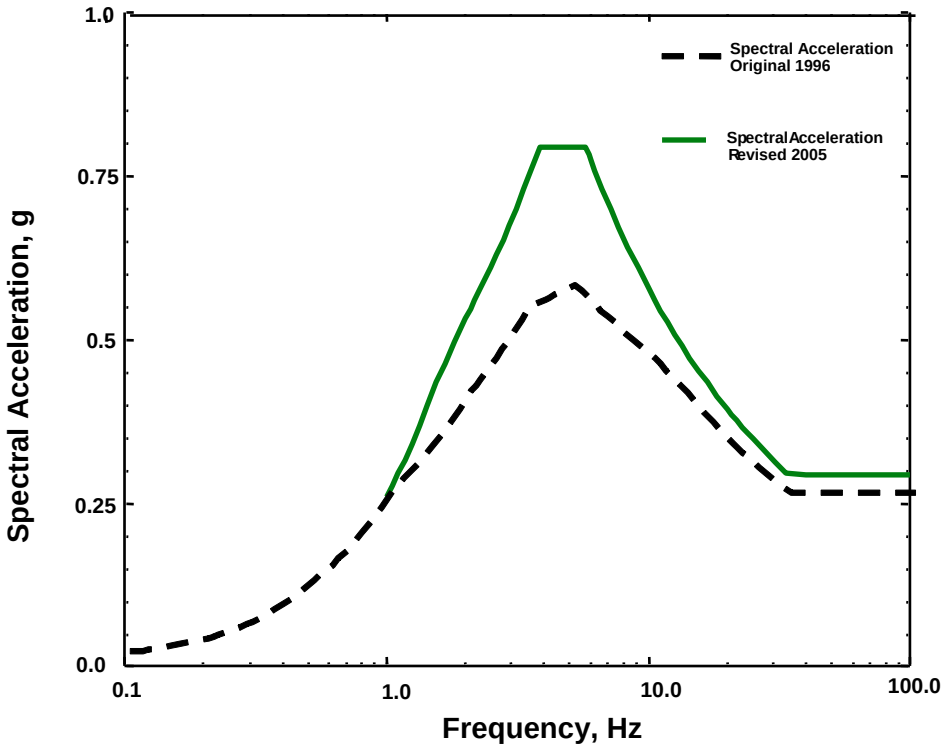

Figure 1.1. Original 1996 and Revised 2005 Horizontal Design Spectra at 5% Damping (Rohay and Reidel 2005)

the 2005 study, Vs in the interbeds was estimated from older, limited compression wave (Vp) data using estimated ranges for the ratio of the two velocities (Vp/Vs) based on analogues in similar materials. The range of possible Vs used for the interbeds produced additional uncertainty in the resulting response spectra.

In late 2005, DOE-ORP initiated planning for the Seismic Boreholes Project (SBP) to emplace additional boreholes at the WTP site and obtain direct measurements of Vs and other physical properties in these layers. The goal was to reduce the uncertainty in the response spectra and seismic design basis and potentially recover design margin for the WTP. PNNL was selected to manage the SBP, with oversight from DOE-ORP and the U.S. Army Corps of Engineers (USACE).

This report documents the work conducted under the SBP to develop a shear wave and compression wave velocity and density model specific to the WTP site. Section 2 provides detailed background information on the WTP site and its underlying geology. Seismic Boreholes Project activities leading up to the measurements of Vs and Vp also are documented in Section 2. In Section 3, methods employed and results obtained are documented for measurements of Vs and Vp velocities in basalts and interbeds. Section 4 provides details on velocity measurements in the sediments underlying the WTP. Borehole gravity measurements of density of the subsurface basalt and sediments are described in Section 5. Section 6 describes the analysis of data presented in Sections 3 through 5 and presents the overall velocity and density model for the WTP site. References cited are listed in Section 7.

2.0 Background

This section provides detailed background information on the WTP site and an overview of the work conducted under the SBP to prepare for obtaining the measurements of velocity and density needed to construct the statistical model.

2.1 Waste Treatment Plant Location and Underlying Geology

The WTP, under construction on the Hanford Site in southeastern Washington State (Figure 2.1), will treat and vitrify underground tank waste stored at the Site. The WTP comprises four major facilities: a

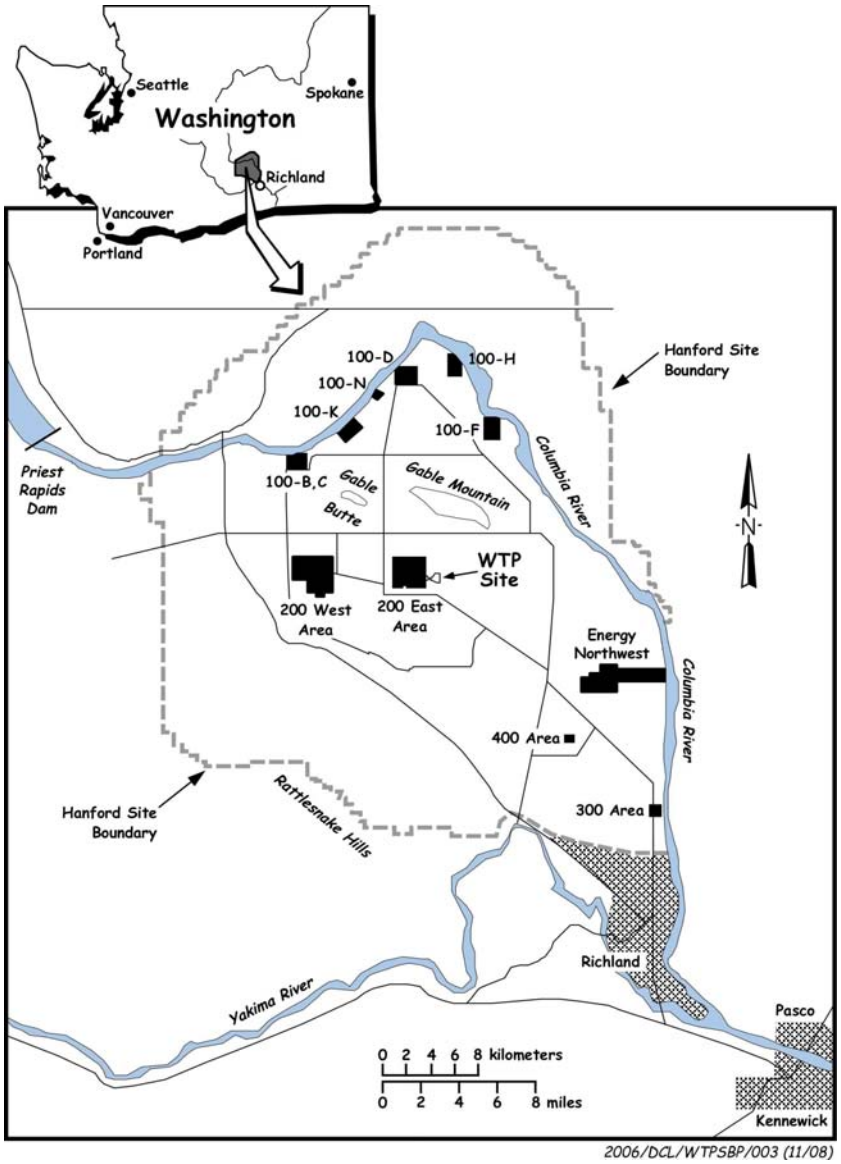

Figure 2.1. Location of the Waste Treatment and Immobilization Plant Site

pretreatment facility to separate the tank waste into high-level waste (HLW) and low-activity waste (LAW) fractions; an HLW vitrification facility to immobilize the HLW fraction in borosilicate glass; an LAW vitrification facility to immobilize the LAW fraction in borosilicate glass; and an analytical laboratory to support operations of the three treatment facilities.

The Hanford Site and the WTP are situated on a sequence of sedimentary units (Hanford and Ringold formations) that overlie the Columbia River Basalt Group (CRBG). The CRBG is a sequence of flood basalt flows that erupted between 17 and 6 million years ago from fissures or vent systems in Oregon, Washington, and Idaho, and forms the main bedrock of the WTP. The upper four basalt flows (Saddle Mountains Basalt) were laid down over a period of time that allowed sediments of the Ellensburg Formation to accumulate between basalt layers. The general stratigraphy of geologic units of interest beneath the WTP is shown in Figure 2.2.

2.2 Seismic Boreholes Project

In late 2005, DOE-ORP initiated planning for the Seismic Boreholes Project (SBP) to emplace additional boreholes at the WTP site and obtain direct Vs measurements and other physical property measurements in these layers. The goal was to reduce the uncertainty in the response spectra and seismic design basis, and potentially recover design margin for the WTP. PNNL was selected to manage the SBP, with oversight from DOE-ORP and the U.S. Army Corps of Engineers (USACE). The priority of the SBP activities was elevated in 2006 as a result of fiscal year 2007 congressional authorization that limited fiscal year 2007 expenditures for the WTP until "…the date on which the Secretary of Energy certifies to the congressional defense committees that the final seismic and ground motion criteria have been approved by the Secretary …."[(a)]

The approach to the SBP involved four main elements:

1. planning and site preparation
2. new borehole installation
3. data collection
4. site seismic response analysis.

2.2.1 Implementation

To plan and implement the SBP, a project team was established to effectively control all elements of the project. The overall project structure involved a multi-contractor onsite project team that provided technical, project, and field operations direction and oversight. PNNL provided overall management and technical leadership for the project. EnergySolutions provided field oversight for all site operations, including technical direction for drilling activities. Fluor Hanford, Inc., provided well-site geology, radiological controls, and waste management support. Bechtel National, Inc., provided access to and supporting facilities on the WTP site. Interfaces between project team members were controlled via contractual relationships between PNNL, EnergySolutions, and Fluor Hanford, and via a Memorandum of Understanding between PNNL and Bechtel National.

(a) John Warner National Defense Authorization Act for Fiscal Year 2007. Public Law 109-364 (H.R.5122 ENR), Sec. 3120, Limitations on Availability of Funds for Waste Treatment and Immobilization Plant.

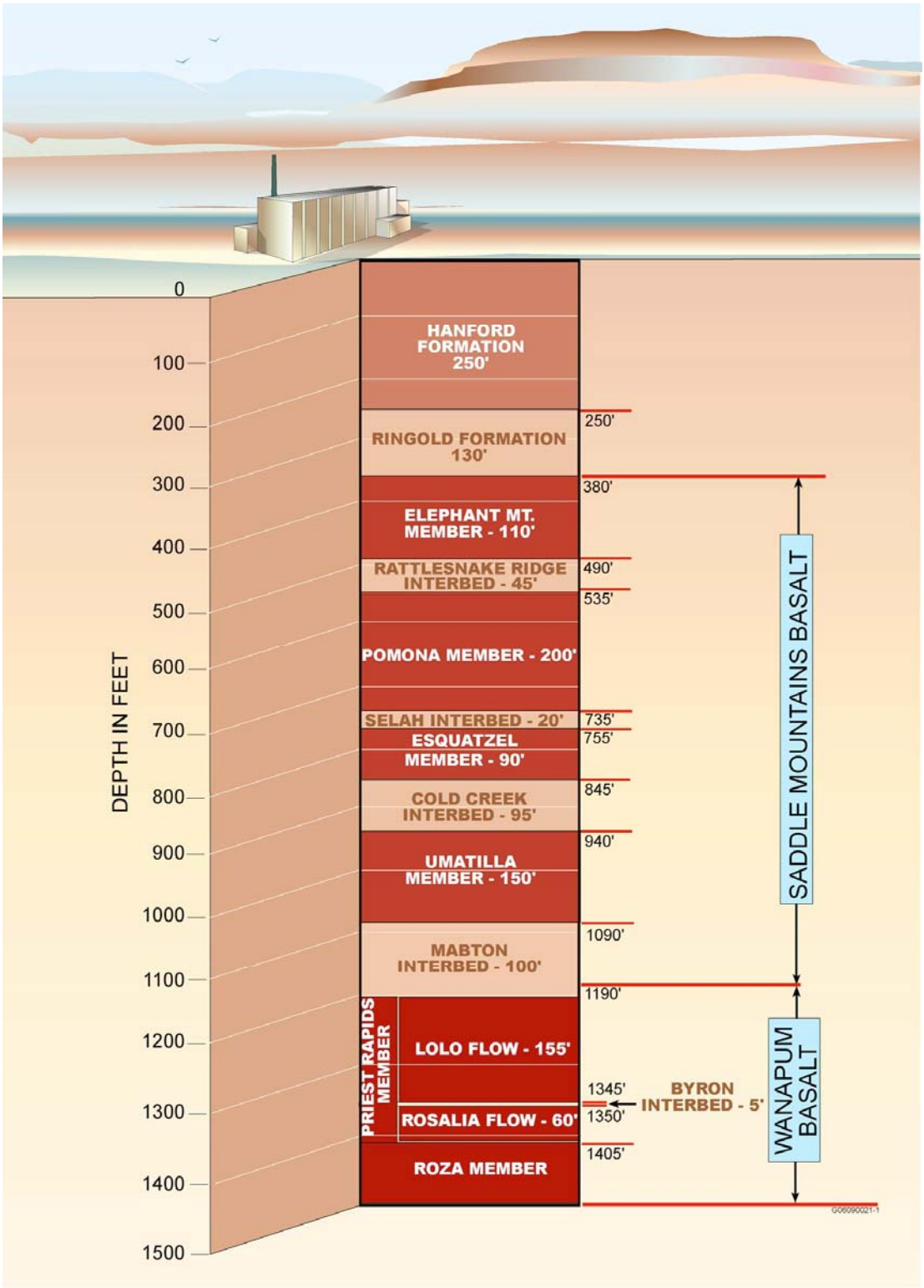

Figure 2.2. General Stratigraphy and Approximate Depths Below Ground Surface of Geologic Units of Interest Beneath the Waste Treatment Plant Site

2.2.2 New Borehole Installation

A drilling plan (Gardner et al. 2005) was developed to guide the installation of the four boreholes. The locations of the boreholes on the WTP site and their designations (C4993, C4996, C4997, and C4998) are shown in Figure 2.3. The drilling plan provided a technical basis for subsequent drilling contracts as well as environmental, health, and safety planning activities. A separate sampling and analysis plan (PNNL 2006) specified the physical characterization, geophysical logging, in situ seismic velocity and density measurements to be collected, and physical testing of core samples to be performed.

Installation of the four planned boreholes required several different drilling techniques to address Hanford site-specific geologic conditions and to ensure collection of the required subsurface information. Detailed summaries of the drilling program for each borehole are provided in Adams et al. (2007), Barnett and Garcia (2006), DiFebbo (2007), Horner (2007), and Rust et al. (2007).

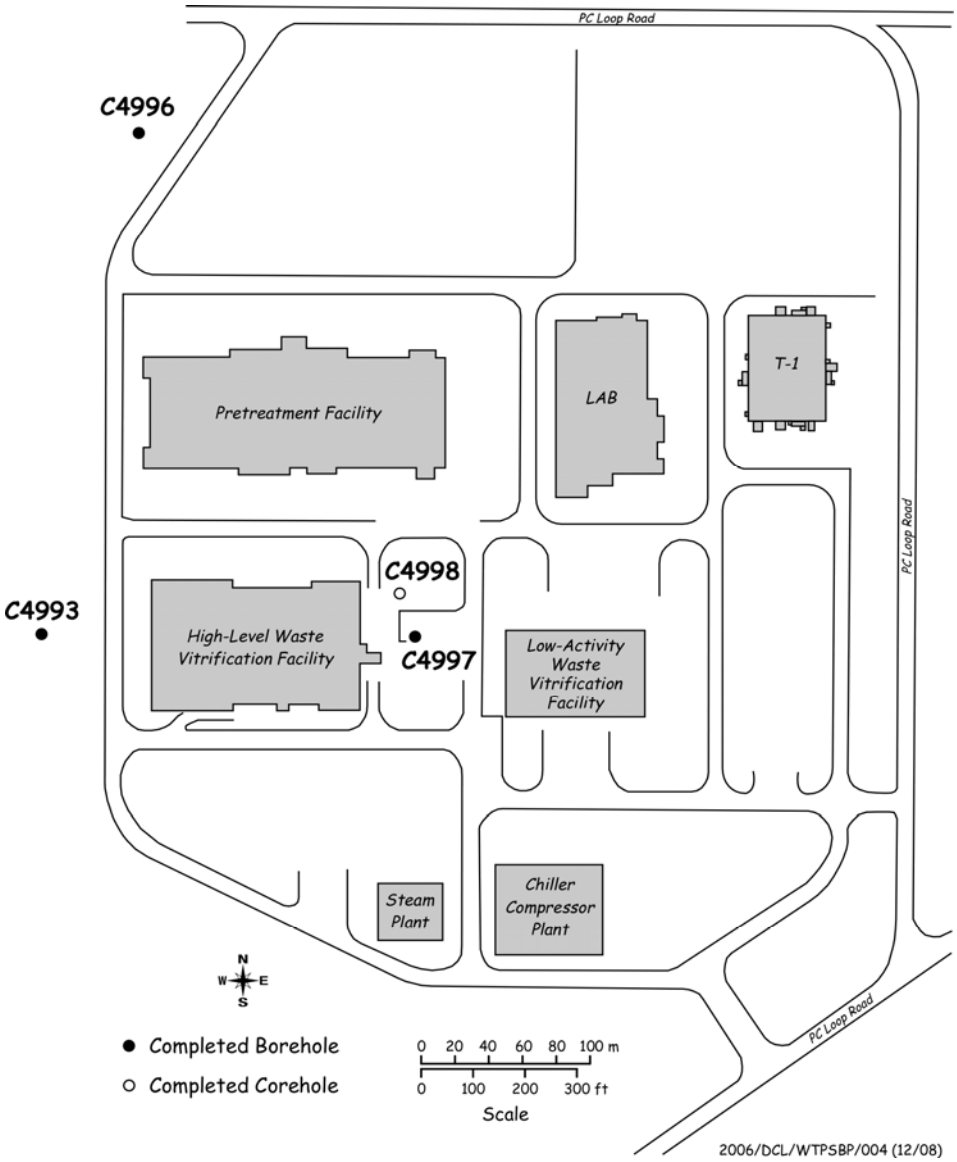

Figure 2.3. Seismic Boreholes Drilled in 2006 at the Waste Treatment Plant

2.2.3 Data Collection

The characterization effort within the deep boreholes included

- downhole measurements of the velocity properties (including uncertainties) of the suprabasalt sediments (Hanford formation sands and gravels, Cold Creek unit, and Ringold Formation Unit A), basalt, and sedimentary interbed sequences
- downhole measurements of the density of these layers
- confirmation of the geometry of the contact between the various basalt and interbedded sediments through examination of retrieved core from the corehole and data collected through geophysical logging of each borehole.

Additional laboratory dynamic testing of the suprabasalt sediments, basalts, and sedimentary interbeds was performed to evaluate nonlinear response to strong earthquake ground motion. The characterization effort was guided by the sampling and analysis plan and referenced standards and procedures.

A suite of geophysical logs also was performed to support confirmation of the contact between basalt and interbed sediments, evaluate straightness and the condition of the borehole wall, and evaluate the magnetic deviation as a function of depth (Gardner and Price 2007).

Physical samples of suprabasalt sediments, basalts, and sedimentary interbeds were collected and subjected to one or more physical testing methods at the direction of the USACE. Selected samples were transferred to the University of Texas at Austin for resonant column/torsional shear, large-diameter resonant column, or free-free resonant column tests. Additional sediment samples from the Hanford and Ringold formations underwent particle size gradation testing at a USACE-selected testing laboratory.

2.2.4 Site Response Analysis

The project culminated with new site response modeling and analysis to process the new borehole data and determine the overall impact of reduced uncertainty on the response spectra for the WTP site. Geomatrix Consultants, Oakland, California, was selected to update the WTP site seismic response calculations completed in 2005 by incorporating the new geology and geophysical data collected from the WTP site boreholes. In addition, the site response analysis evaluates soil-site earthquake ground motion models that have been developed and published subsequent to the previous studies (Geomatrix Consultants 1996; Rohay and Reidel 2005). The site response analysis is documented in Youngs (2007).

3.0 Velocity Measurements in Basalts and Interbeds

The characterization effort within the deep boreholes included downhole measurements of the velocity properties of the basalt and sedimentary interbed sequences. Measurements of Vs and Vp were obtained using two techniques—suspension logging and downhole logging.

3.1 Suspension Logging Measurements

Suspension logging, or P-S logging, uses a downhole shear wave and compression wave source joined to two triaxial receivers (i.e., geophones). The suspension logging system, manufactured by OYO Corporation, is suspended in the borehole by a cable. The source motion creates a high-frequency (1,000-Hz) impulsive seismic wave that propagates through the borehole fluid and surrounding soil and rock, and is detected by the two receivers on the opposite end of the downhole system assembly. A concept illustration of the P-S logging system is shown in Figure 3.1.

Measurements were taken every 1.6 to 3.3 ft (0.5 to 1.0 m) from the top of basalt to the bottom of the borehole. Geovision Geophysical Services, Inc., Corona, California, performed and documented the suspension logging. Data were acquired from both interval logs (1.6 ft [0.5 m] intervals) and an overall log (3.3 ft [1.0 m] intervals). The interval logs were performed in freshly drilled segments. Drilling of each borehole progressed in segments, advancing through an overlying basalt member and sedimentary interbed before stopping after penetrating the underlying basalt member. Suspension logging was then performed through this interval or segment of freshly drilled borehole (Diehl and Steller 2007a). After logging, the borehole was cemented to stabilize the borehole wall, and drilled out and advanced through the next deeper basalt and sedimentary interbed. An overall log was performed after the borehole was drilled to total depth, and after each segment had been cemented to improve borehole stability (Diehl and Steller 2007b). A description of the drilling and cementing operations can be found in Gardner and Price (2007).

Suspension logging results for the overall logs of each borehole are presented in Figures 3.2, 3.3, and 3.4 for boreholes C4993, C4996, and C4997, respectively. Both Vs and Vp measurements are presented. Delineation of the basalt and sedimentary interbed sequences is evident in each borehole. The basalt flows are indicated by data points with higher Vs values in the range of 8,000 to 12,000 ft/sec, whereas the sedimentary interbeds are noted by lower Vs values of 2,000 to 4,000 ft/sec. The Vp data are indicated by significantly higher values, but follow the same overall trend as the Vs data with regard to lower values in the interbeds and higher values in the basalt flows.

Results from interval and overall logs showed good agreement with each other, indicating that the cementing of the borehole had little impact on the results. A comparison of data from interval and overall logs of one segment of borehole C4993 is shown in Figure 3.5. While there are some differences in results, the overall shape and magnitude of the measured velocities are consistent between logs. In this specific case, differences between logs are most notable within the upper portion of the Esquatzel Member (from 760 to 780 ft bgs), at the top of the Cold Creek interbed (from 830 to 850 ft bgs), and again at the top of the Umatilla Member (950 ft bgs). Differences in measured Vs are generally less than 10% between the two logs except for small regions noted above.

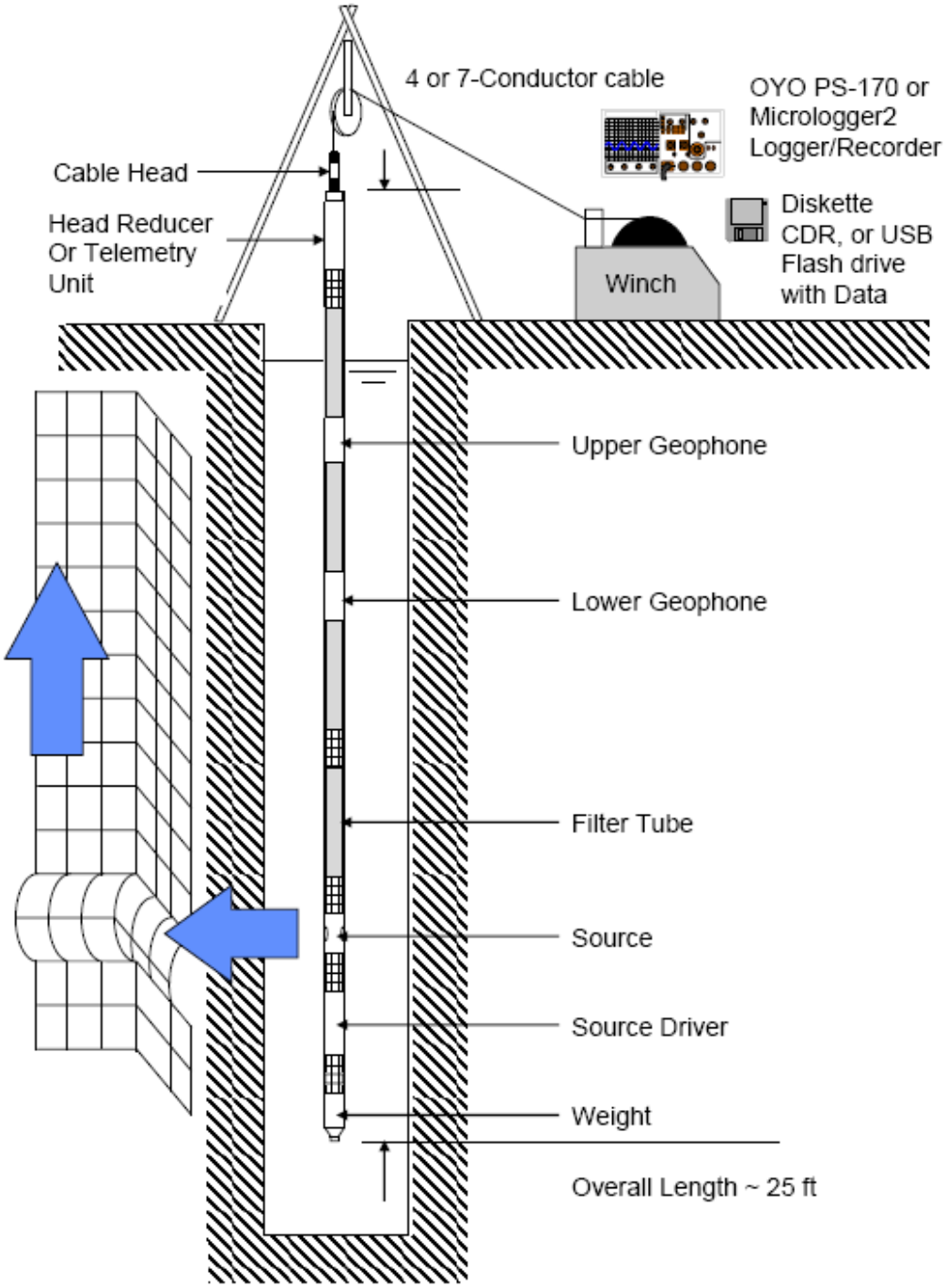

Figure 3.1. Concept Illustration of Suspension Logging System (Diehl and Steller 2007a)

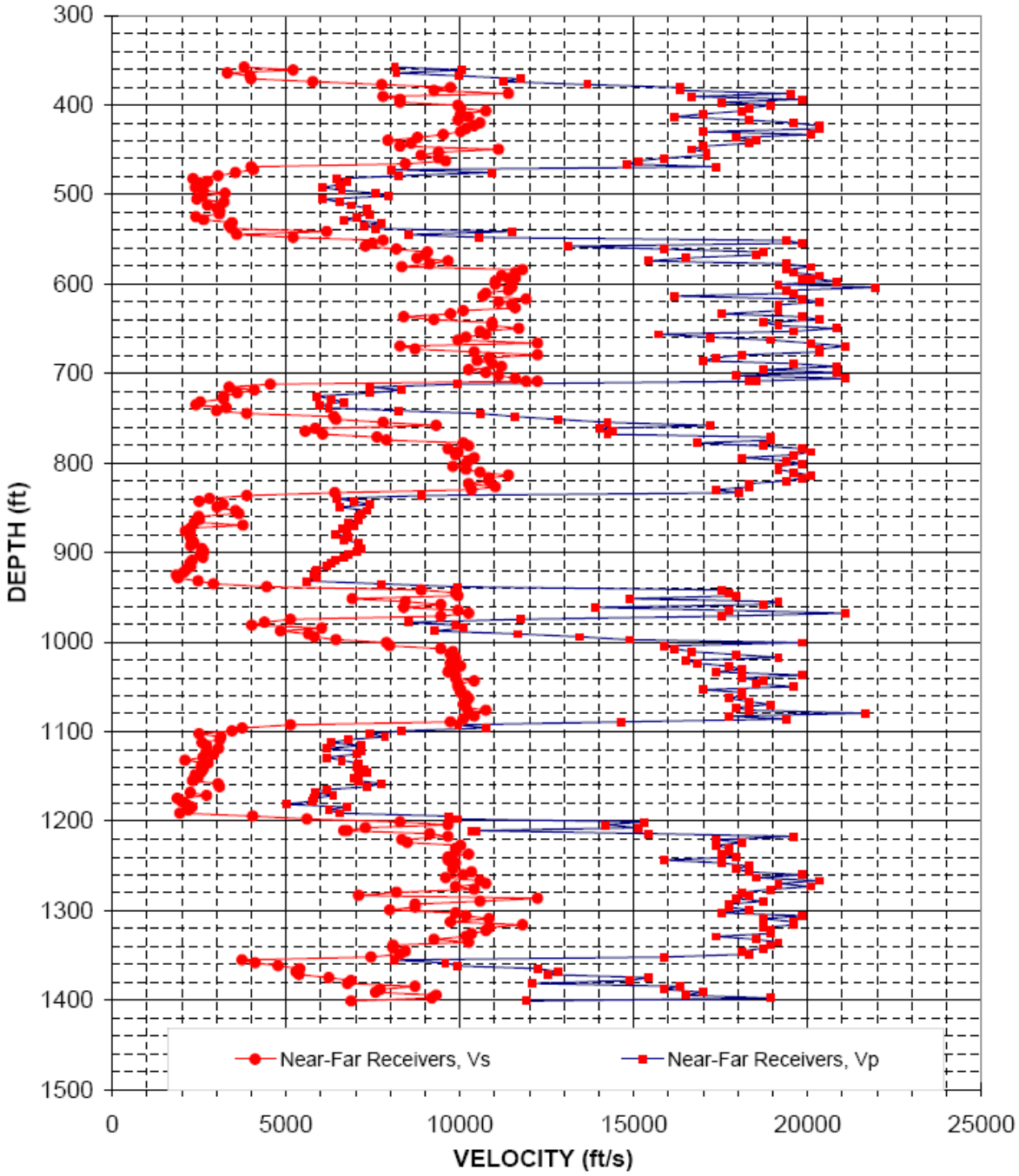

Figure 3.2. Borehole C4993 Suspension Shear Wave and Compression Wave Velocity Data (Diehl and Steller 2007b)

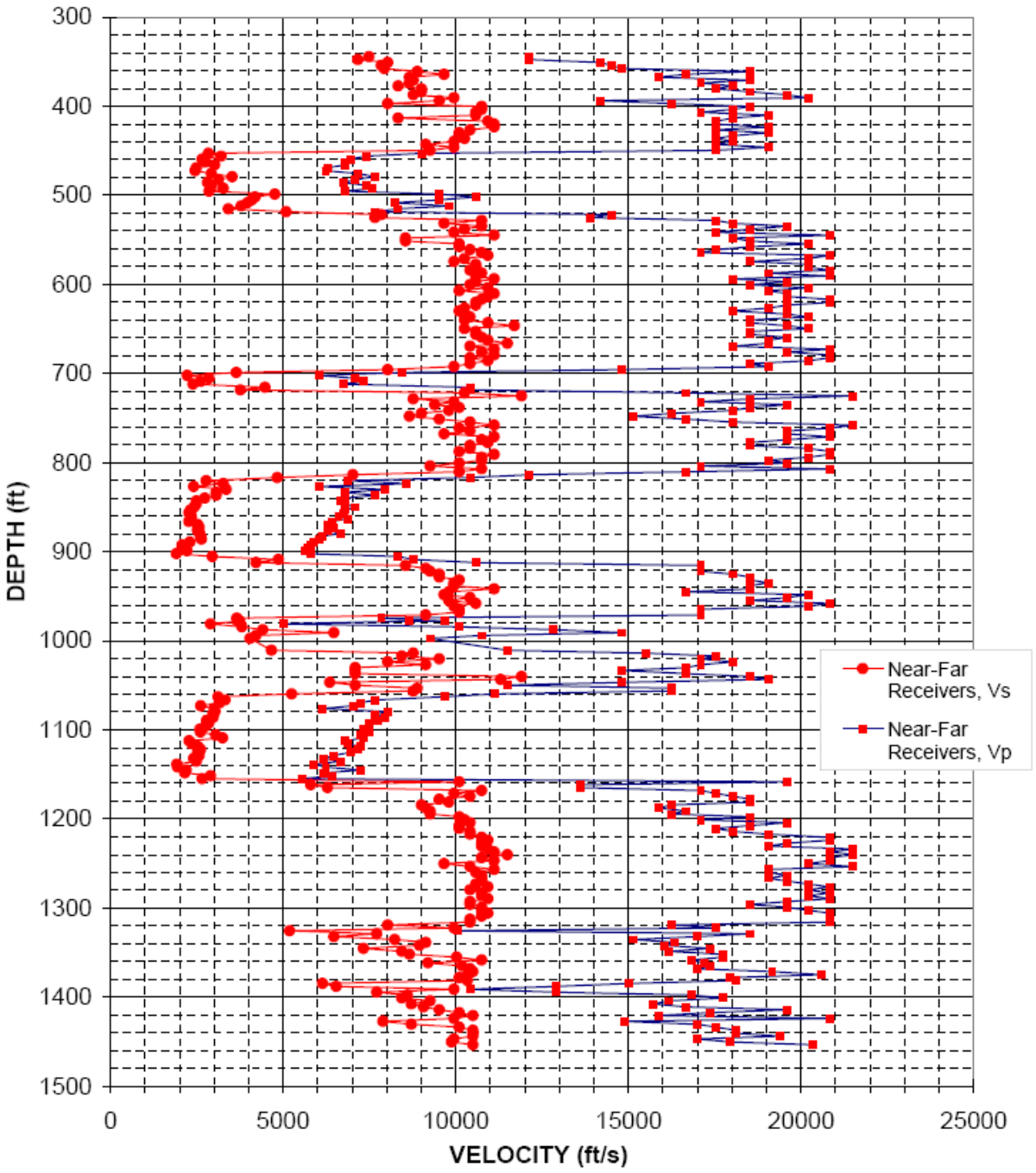

Figure 3.3. Borehole C4996 Suspension Shear Wave and Compression Wave Velocity Data (Diehl and Steller 2007b)

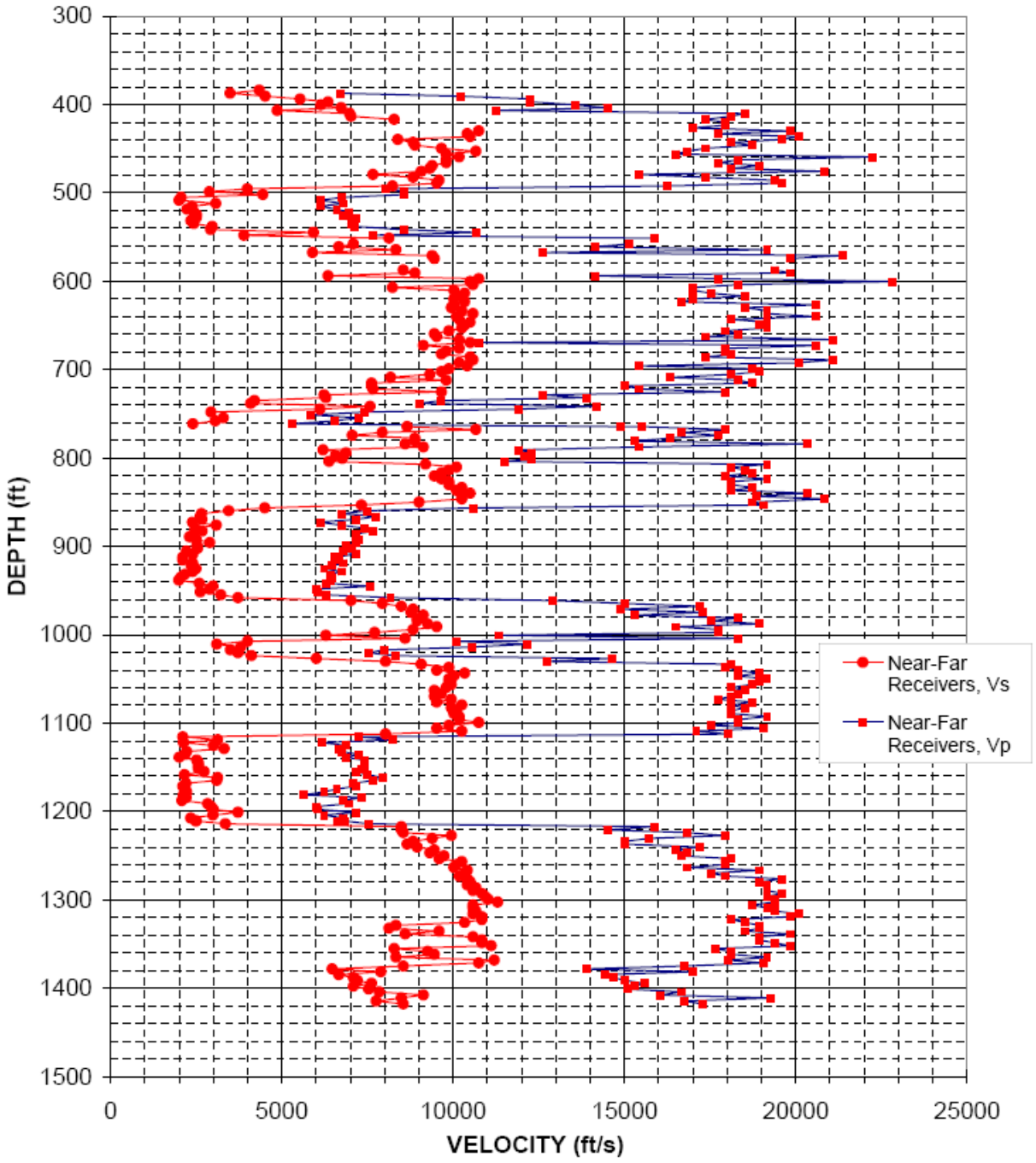

Figure 3.4. Borehole C4997 Suspension Shear Wave and Compression Wave Velocity Data (Diehl and Steller 2007b)

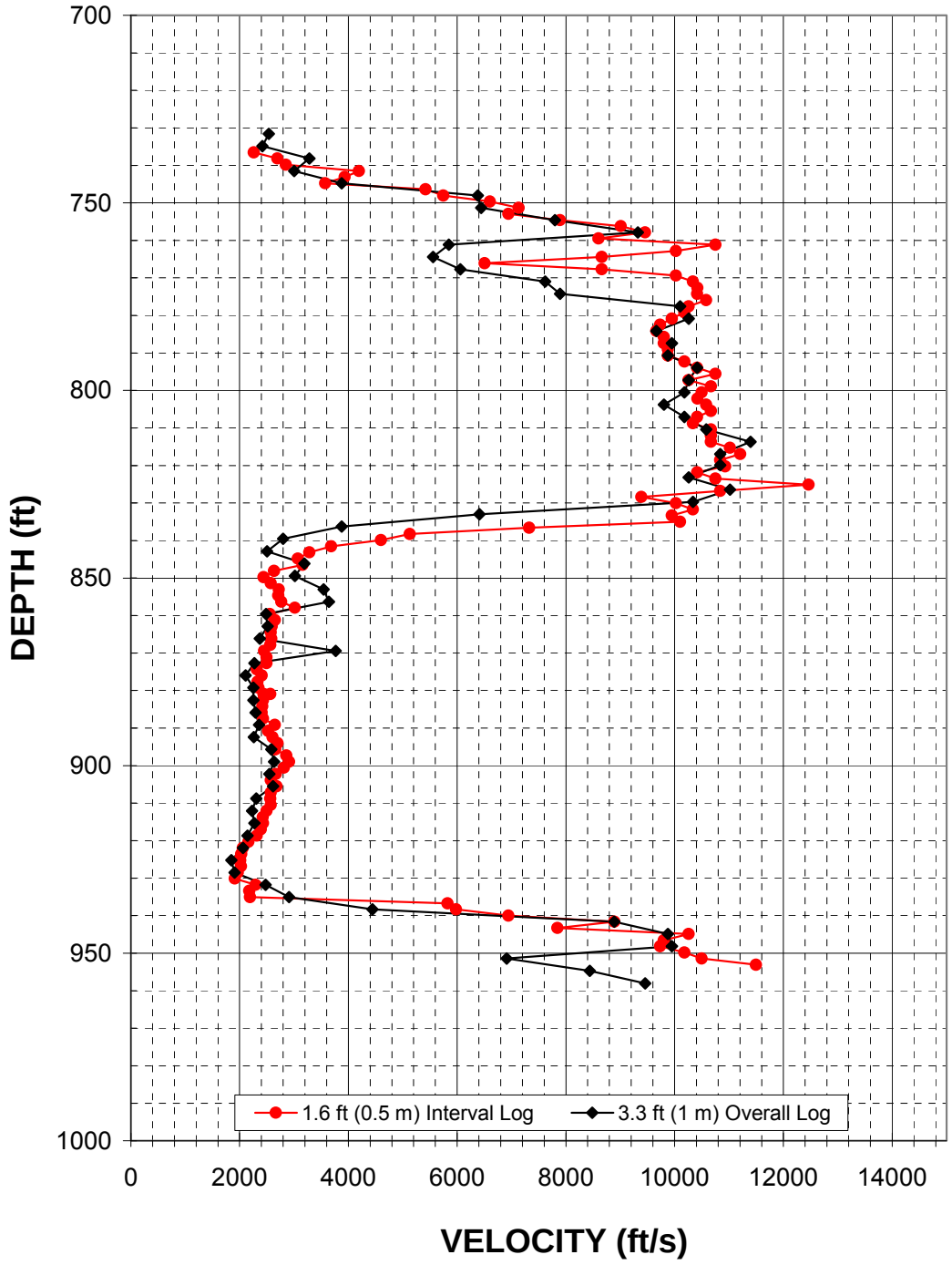

Figure 3.5. Comparison of Near-Far Receivers, Shear Wave Velocity Results from Interval, and Overall Logs for Segment of Borehole C4993 (adapted from Diehl and Steller 2007a and 2007b)

3.2 Downhole Measurements

Downhole seismic logging uses shear and compression wave sources at the ground surface and one or more receivers downhole to detect the seismic waves at depth. The receivers are deployed down the borehole by cable and clamped against the borehole wall to assure measurement of seismic wave propagation through the subsurface formation rather than the borehole fluid.

Two types of sources were used—impulsive and vibratory. Lightweight downhole geophone systems (Figure 3.6) using impulsive seismic sources were effective in both cased and uncased boreholes to depths of 750 ft or less. However, the strength of the impulsive signal was inadequate to reach deeper depths within the formation below the WTP. In addition, the lightweight geophone had difficulty consistently deploying to depths below 1,000 ft in the uncased borehole. The geophone system hung up along the irregular surface of the borehole wall. A heavyweight geophone system (Figure 3.6) with accompanying wireline truck and vibratory seismic source was required to consistently reach the deeper depths of each of the three deep boreholes and obtain acceptable Vs data. Redpath Geophysics of Murphys, California, and researchers from the University of Texas at Austin (Texas) performed the downhole logging (Redpath 2007; Stokoe et al. 2007).

Figure 3.6. Geophone Systems Used for Downhole Seismic Logging

3.2.1 Impulsive Source Measurements

Shear and compression wave velocity measurements using a sledgehammer or an accelerated-weight impact "slingshot" source were effectively collected by Redpath Geophysics in both cased and uncased boreholes to depths of 750 ft or less. For the basalts and interbeds, the lightweight geophone system and

slingshot impulsive source (Figure 3.7) was deployed in boreholes C4993, C4996, and C4997 between October 2006 and February 2007. A more detailed description of the methods and procedure is presented in Redpath (2007).

Figure 3.8 presents results of shear or compression wave travel-time measurements and interpreted Vs or Vp results using the impulsive sources in boreholes C4993, C4996, and C4997. Figure 3.8a presents Vs results and data collected in the two uppermost basalt units (Elephant Mountain and Pomona) and sedimentary interbeds (Rattlesnake Ridge and Selah) in borehole C4993 before and after installation of stainless steel casing. Results indicate good agreement between data from before and after casing of the borehole. For completeness, Vs results and data from the suprabasalt sediments also are shown. See Section 4 for more discussion on sediment velocity measurements.

Figure 3.8b contains Vs and Vp results and travel-time data collected in the Elephant Mountain and Pomona members and Rattlesnake Ridge interbed in borehole C4996. Shear wave data before and after installation of polyvinyl chloride (PVC) casing show good agreement. Compression wave data from the PVC-cased borehole also are shown, along with sediment Vs and Vp results for completeness.

Figure 3.8c presents the limited Vs results and travel-time data collected in the Elephant Mountain and Pomona members and Rattlesnake Ridge interbed in borehole C4997. For comparison and completeness, the sediment Vs results from the adjacent borehole C4998 also are shown.

Figure 3.7. Accelerated-Weight Impact Shear Wave "Slingshot" Source Used for Shear Wave Velocity Measurements in the Shallow Basalts and Interbeds

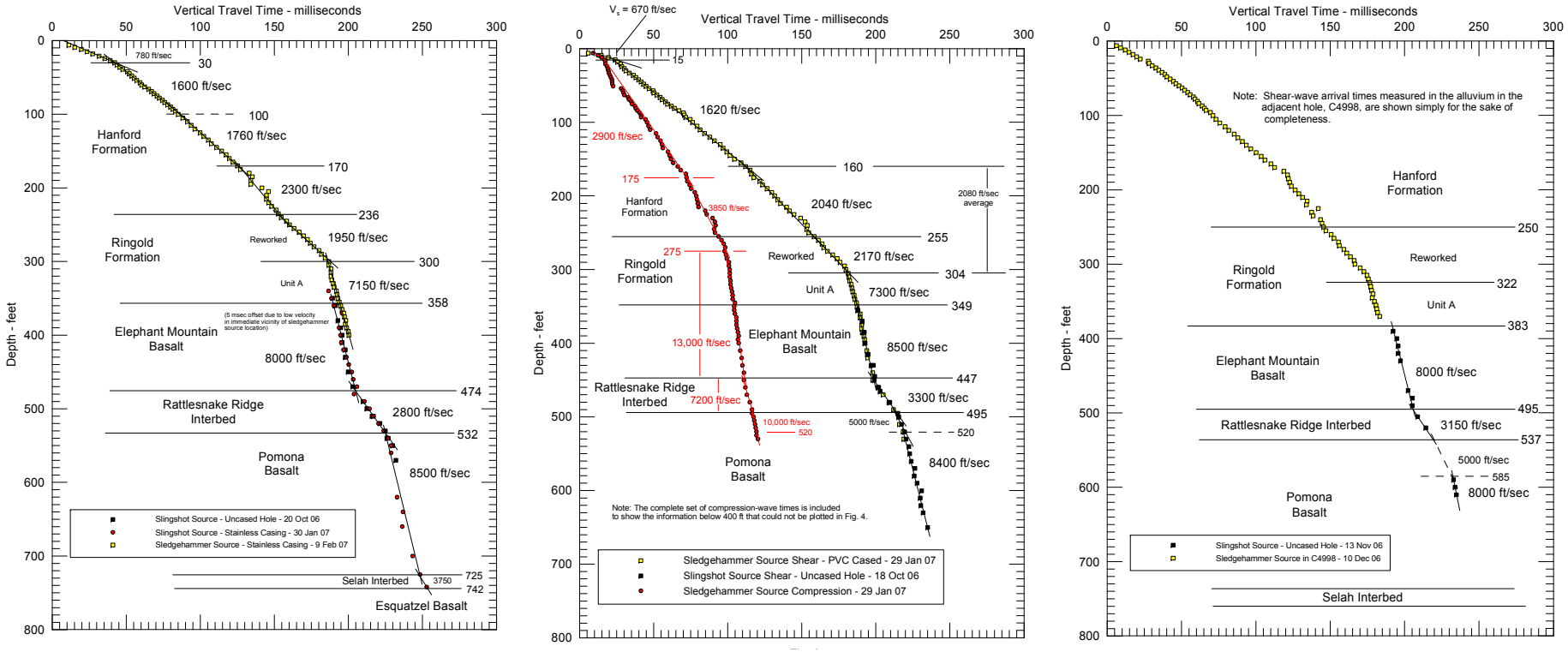

a) Borehole C4993 shear

b) Borehole C4996 shear and compression

c) Borehole C4997 shear

Figure 3.8. Shear Wave and Compression Wave Velocity Measurements Using an Impulsive Seismic Source in Boreholes a) C4993, b) C4996, and c) C4997 (from Redpath 2007)

3.2.2 Vibratory Source Measurements

A large 60,000-lb triaxial vibratory source (aka T-Rex; Figure 3.9; Industrial Vehicles International, Inc., Tulsa, Oklahoma) operating at 20 to 50 Hz was required to effectively measure Vs and Vp below 750 ft. Measurements were taken using the heavyweight geophone system deployed by a wireline logging truck at intervals in the borehole of approximately 5 to 20 ft. In addition to the downhole geophone system, both surface and near-surface geophones were deployed to provide reference times for the source input. Even with the T-Rex source at full signal strength, only compression wave signals were measurable at the deepest depths (e.g., 1,400 ft) by reducing the 50-Hz frequency to 20 or 30 Hz. Shear wave signals were attenuated significantly below the Cold Creek interbed (approximately 950 ft), and lower-frequency input signals (20 or 30 Hz versus 50 Hz) also were required. Equipment operations and data collection and processing were performed by staff from the University of Texas at Austin, with data collection support from Redpath Geophysics, PNNL, and EnergySolutions personnel. The equipment was deployed and the principal measurements taken in boreholes C4993, C4996, and C4997 in December 2006.

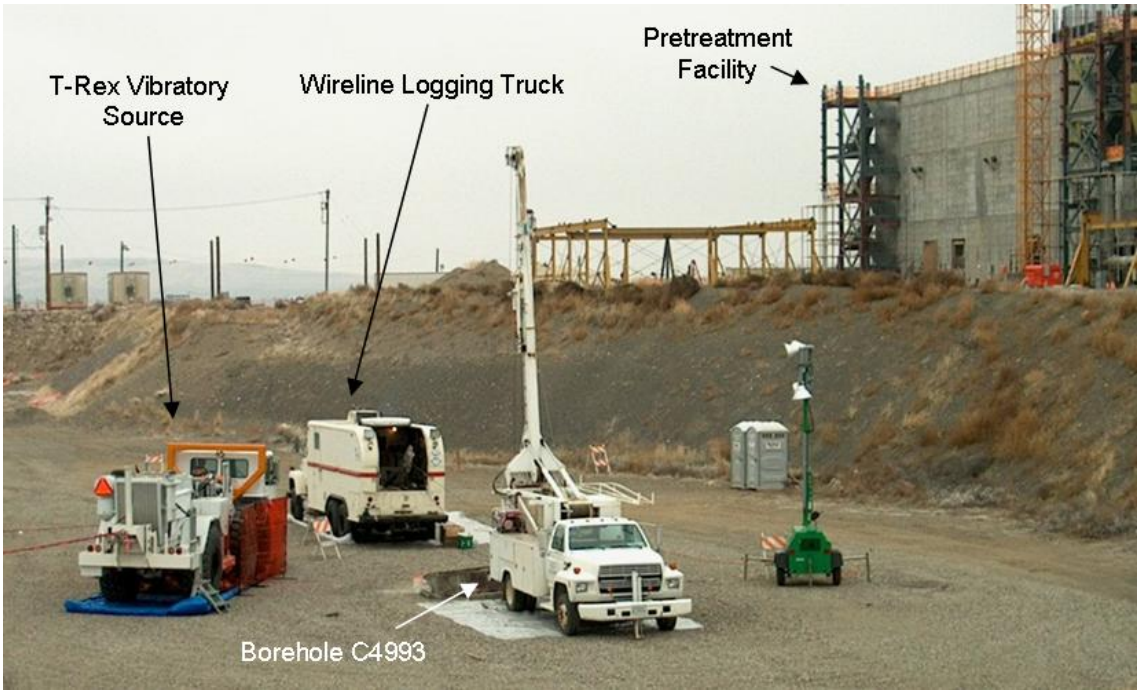

Figure 3.9. Downhole Seismic Logging of Borehole C4993 with Vibratory Source

Figure 3.10 presents results of shear wave travel-time measurements and interpreted Vs results using the vibratory source in boreholes C4993, C4996, and C4997. Relative travel times from the surface reference geophone to the downhole geophone are plotted against depth, and Vs values are interpreted from the slope of a line fit to the data. In all three boreholes, a frequency change of the input signal was required to achieve measurements within and below the Umatilla Member. These frequency changes are noted on Figure 3.10 and are evident from the shift of fitted lines to greater travel times. As noted previously, lower frequency was required to obtain adequate signal strength. Increased scatter in the travel-time data is seen also at the lower frequency within and below the Umatilla Member.

a)

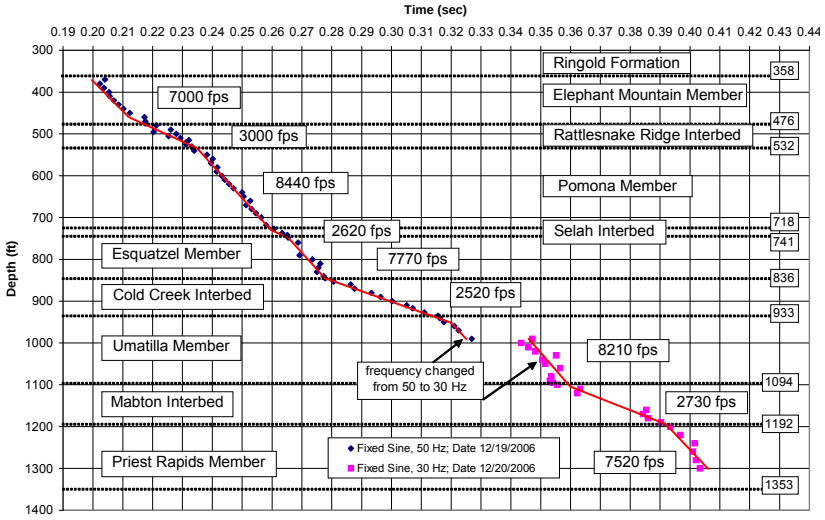

b)

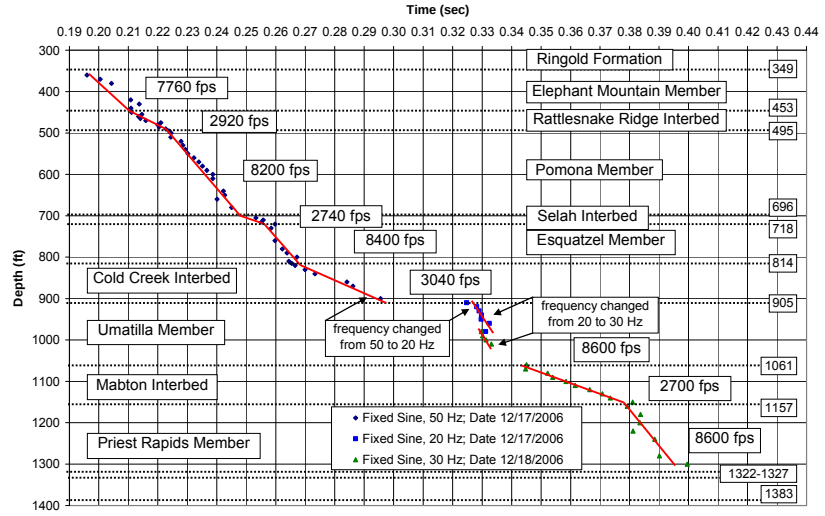

c)

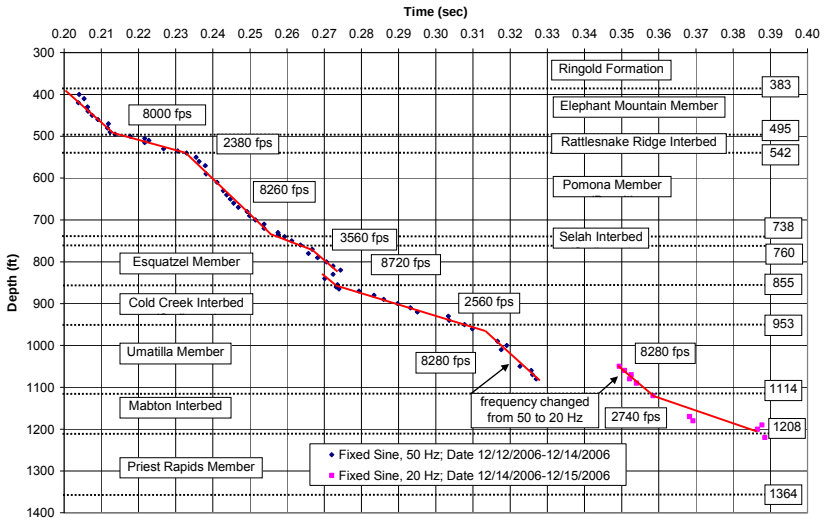

Figure 3.10. Relative Shear Wave Travel Times and Interpreted Shear Wave Velocity Profile for Boreholes a) C4993, b) C4996, and c) C4997

Measurements were made to a maximum depth of approximately 1,300 ft bgs in boreholes C4993 and C4996 before signal strength was inadequate. Measurements were adequate to only approximately 1,200 ft bgs in borehole C4997.

Figure 3.11 presents results of compression wave travel-time measurements and interpreted Vp results using the vibratory source in boreholes C4993, C4996, and C4997. As with the Vs measurements, relative travel times from the surface reference geophone to the downhole geophone are plotted against depth. Values for Vp are interpreted from the slope of a line fit to the data. The compression wave travel-time data are significantly less scattered than those from the shear wave measurements. Measurements were made to a maximum depth of approximately 1,400 ft bgs in boreholes C4993 and C4996, and to approximately 1,200 ft bgs in borehole C4997.

3.3 Comparison of Suspension and Downhole Measurements

Comparing overall results of Vs and Vp measurements from suspension logging (Figures 3.2 through 3.4) and downhole logging (Figures 3.8, 3.10, and 3.11) within the basalts and interbeds, several significant differences are evident. The magnitude of measured velocities and the level of detail that can be obtained are noticeably different between the two methods.

For the basalt flows, interpreted Vs and Vp values from suspension logging are significantly higher than results from downhole logging. For example, Vs values from suspension logging are centered around 10,000 ft/sec, compared to values from downhole logging around 8,000 ft/sec. For the interbeds, the results from the two measurement methods appear to be comparable. The technical reason for observed differences in the denser and higher velocity basalts is not known. It has been hypothesized that differences may be related to the volume and nature of the materials in and around the borehole that are being interrogated by the two different methods. For example, suspension logging, with its higher-frequency source and tool dimension, is interrogating materials very close to the borehole wall. The properties of these materials may have been affected by the drilling operation. In contrast, downhole logging is interrogating a larger volume of subsurface material, including formation that has not been directly affected by the drilling. Researching the technical reason for observed differences was outside the scope of the SBP. However, seismologists and geotechnical engineers consulted to evaluate the data concurred that the downhole logging data provided results more relevant to the seismic analysis for which the data were needed. Downhole logging used source input frequencies in a range much closer to frequencies of concern for earthquake-based ground motions than did suspension logging input frequencies.

Suspension logging does provide higher-resolution data that allow for identification of changes in Vs and Vp at a finer scale. For example, changes in velocity through the basalt flow top and flow bottom transition zones are observed in both the interval and overall suspension logs. Therefore, the suspension logging results are used in interpreting the geology at a finer scale than is possible with downhole logging.

3.4 Comparison of Velocities Measured in Three Boreholes

Comparison of shear and compression wave velocities from the same stratigraphic units across the three boreholes indicates generally consistent values. Downhole logging Vs results from Figures 3.8, 3.10, and 3.11 are combined and tabulated in Table 3.1. Variability across boreholes is generally less

a)

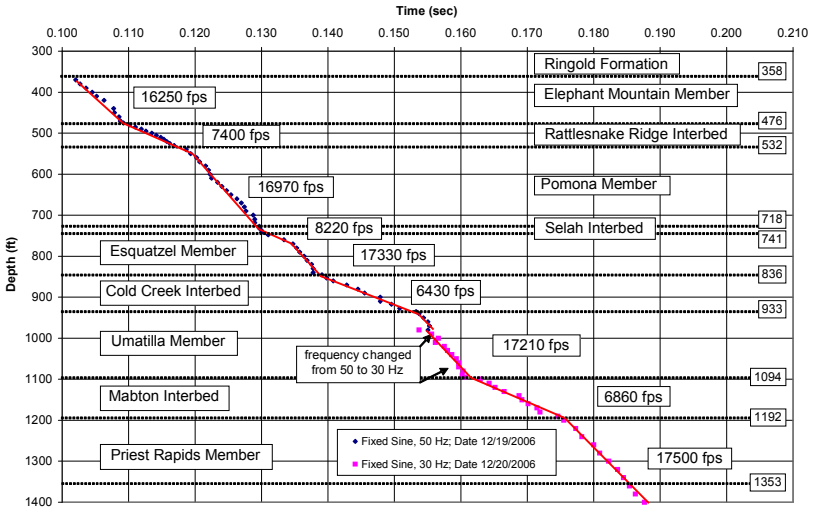

b)

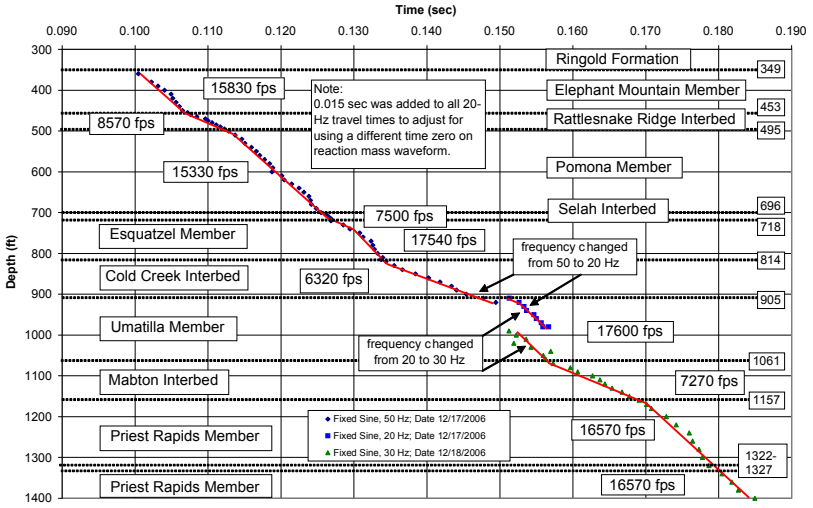

c)

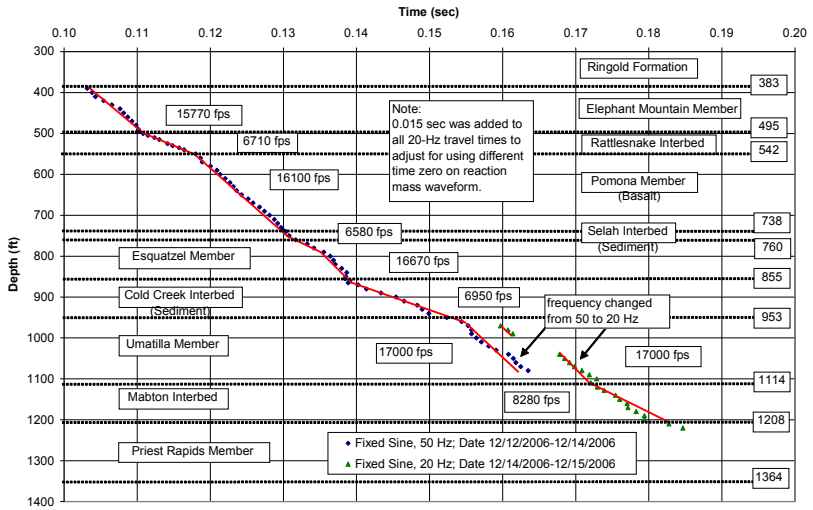

Figure 3.11. Relative Compression Wave Travel Times and Interpreted Vp Profile for Boreholes a) C4993, b) C4996, and c) C4997

than 20%, with the exception of the shallowest three interbeds, where variability across boreholes and seismic source methods is higher. The Vs for all basalt flows in all boreholes ranges from 7,000 to 8,720 ft/sec. The Vs for all interbeds ranges from 2,380 to 3,560 ft/sec.

Table 3.1. Summary of Interpreted Shear Wave Velocity Results from Downhole Seismic Logging

Stratigraphic Unit, Flow	Borehole C4993 Vs (ft/sec)		Borehole C4996 Vs (ft/sec)		Borehole C4997 Vs (ft/sec)	
	Vibratory Source	Impulsive Source	Vibratory Source	Impulsive Source	Vibratory Source	Impulsive Source
Elephant Mountain Member	7,000	8,000	7,760	8,500	8,000	8,000
Rattlesnake Ridge Interbed	3,000	2,800	2,920	3,300	2,380	3,150
Pomona Member	8,440	8,500	8,200	8,400	8,260	8,000
Selah Interbed	2,620	--	2,740	--	3,560	--
Esquatzel Member	7,770	--	8,400	--	8,720	--
Cold Creek Interbed	2,520	--	3,040	--	2,560	--
Umatilla Member	8,210	--	8,600	--	8,280	--
Mabton Interbed	2,730	--	2,700	--	2,740	--
Priest Rapids Member	7,520	--	8,600	--	--	--

Downhole logging Vp results are combined and tabulated in Table 3.2. The few Vp measurements in basalts from the impulsive source were noticeably lower than results using the vibratory source. For all other downhole logging Vp results, variability across boreholes was similar to that observed with the Vs results. For vibratory source measurements only, the Vp ranged from 15,330 to 17,600 ft/sec across all basalt flows and all boreholes. The Vp for all interbeds ranged from 6,320 to 8,570 ft/sec.

Table 3.2. Summary of Interpreted Compression Wave Velocity Results from Downhole Seismic Logging

Stratigraphic Unit, Flow	Borehole C4993 Vp (ft/sec)		Borehole C4996 Vp (ft/sec)		Borehole C4997 Vp (ft/sec)	
	Vibratory Source	Impulsive Source	Vibratory Source	Impulsive Source	Vibratory Source	Impulsive Source[(b)]
Elephant Mountain Member	16,250	11,000[(a)]	15,830	13,000	15,770	--
Rattlesnake Ridge Interbed	7,400	--	8,570	7,200	6,710	--
Pomona Member	16,970	--	15,330	10,000	16,100	--
Selah Interbed	8,220	--	7,500	--	6,580	--
Esquatzel Member	17,330	--	17,540	--	16,670	--
Cold Creek Interbed	6,430	--	6,320	--	6,950	--
Umatilla Member	17,210	--	17,600	--	17,000	--
Mabton Interbed	6,860	--	7,270	--	8,280	--
Priest Rapids Member	17,500	--	16,570	--	--	--

(a) See Figure 4.3a.
(b) Impulsive source data not taken in basalts and interbeds.

4.0 Velocity Measurements in Sediments

Shear wave and compression wave velocity measurements in the suprabasalt sediments were collected using the impulsive source methods described previously in Section 3.1.1. Although the deeper basalt and interbed Vs and Vp measurements were collected in both uncased (i.e., open) and cased boreholes, sediment measurements could be made only in cased boreholes. The unconsolidated nature of the sands and gravels that make up most of the Hanford and Ringold formations precludes open borehole access and measurements. The general lithology of the suprabasalt sediments is shown in Figure 4.1 (Barnett et al. 2007).

4.1 Downhole Measurements Using Impulsive Source

To enable velocity measurements in the sediments, three of the four boreholes were cased following completion of deeper open-borehole geophysical and/or seismic logging. Borehole C4998 was lined with 4.5-in.-outside diameter schedule 80 PVC casing from ground surface to a depth of 378 ft bgs. Borehole C4996 was lined with the same-size PVC casing from ground surface to a depth of approximately 547 ft bgs. Borehole C4993 was lined with 4.5-in.-outside diameter schedule 80 stainless steel casing from ground surface to total borehole depth of 1,411 ft bgs.

For the sediments, a sledgehammer impulsive source was deployed with the lightweight geophone system by Redpath Geophysics to collect Vs and Vp data from cased boreholes C4993, C4996, and C4998 between December 2006 and February 2007. The lightweight geophone system shown with a rigid clamping arm in Figure 3.6 was used with a bow-spring clamping mechanism for the cased boreholes. The typical procedure in the shallow cased holes was to lower the geophone to depth and extend the bow spring. The geophone could then be dragged upward to the desired measurement point without the bow-spring clamp being released. Measurements were made at 5-ft intervals below 100 ft bgs and 3-ft intervals above 100 ft bgs. A more detailed description of the methods and procedure is presented in Redpath (2007).

Figure 4.2 presents results of shear wave travel-time measurements and interpreted Vs results using the sledgehammer impulsive source in boreholes C4993, C4996, and C4998. Figure 4.2a presents Vs results and data collected to a depth of 400 ft bgs in borehole C4993, through the Hanford and Ringold formations and into the top of the Elephant Mountain Member. Horizontal lines denote transition depths where a change in Vs has been interpreted. The depth of the transition is also shown. The label *Reworked* refers to the Cold Creek unit, which is known also as the Reworked Ringold.

Figure 4.2b presents Vs results and travel-time data collected to a depth of 400 ft bgs in borehole C4996. Figure 4.2c presents similar results and data collected to a depth of 370 ft bgs in borehole C4998. Compression wave travel-time measurements and interpreted Vp results using the sledgehammer impulsive source in the same three boreholes are shown in Figure 4.3. Figures 4.3a, b, and c present Vp results and data collected to the same depths in boreholes C4993, C4996, and C4998 as reported for Vs results, respectively.

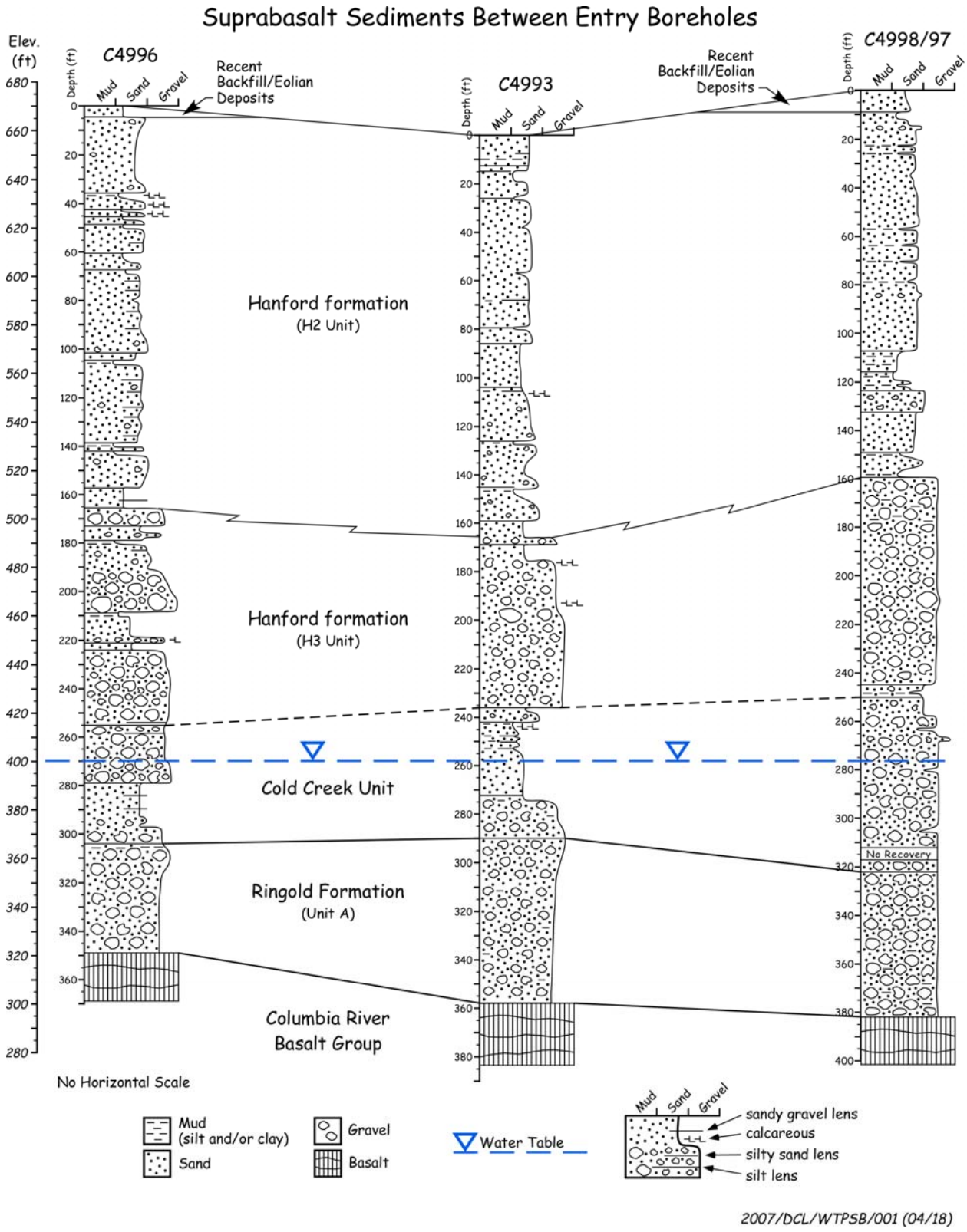

Figure 4.1. Suprabasalt Sediments Between Entry Boreholes (Barnett et al. 2007)

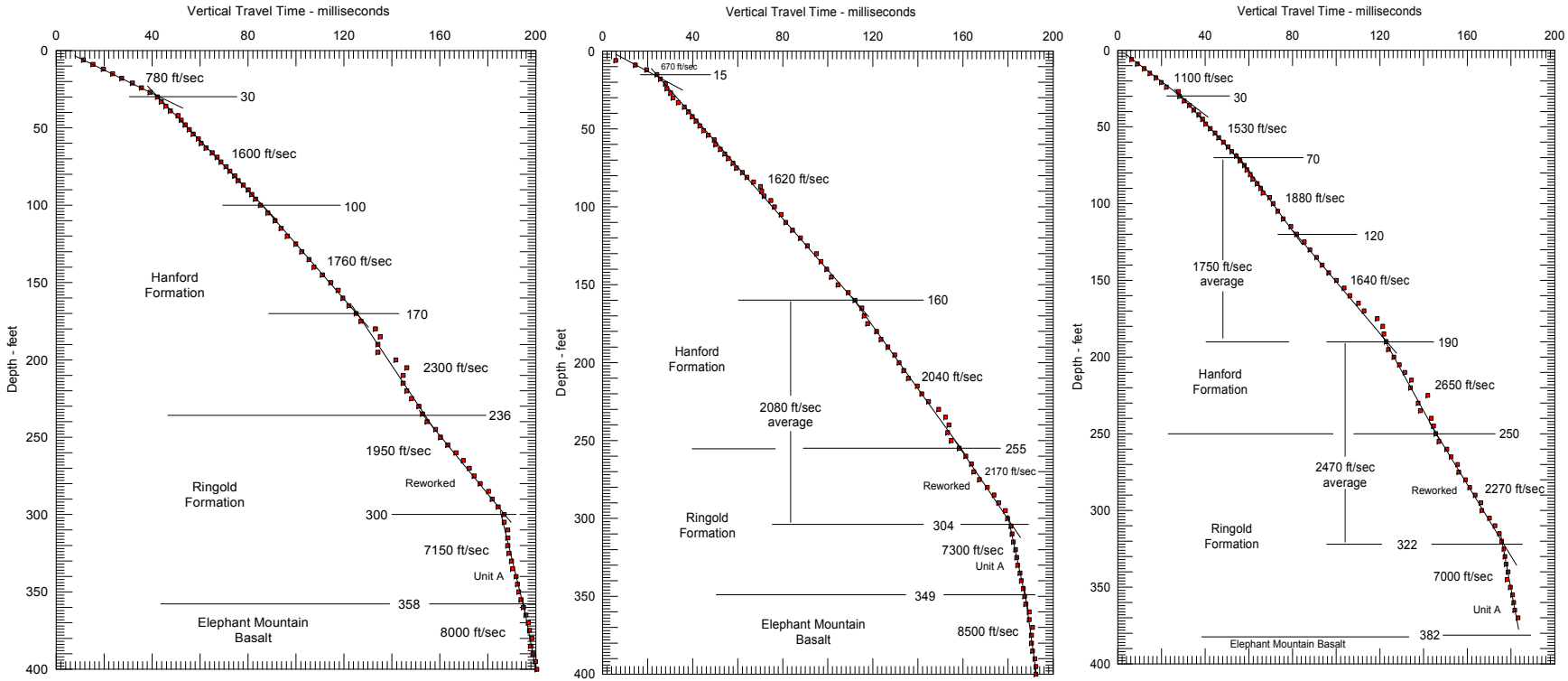

a) Borehole C4993 shear b) Borehole C4996 shear c) Borehole C4998 shear

Figure 4.2. Shear Wave Travel Times and Velocities for Sediments in Boreholes C4993, C4996, and C4998. Figures adapted from Redpath (2007).

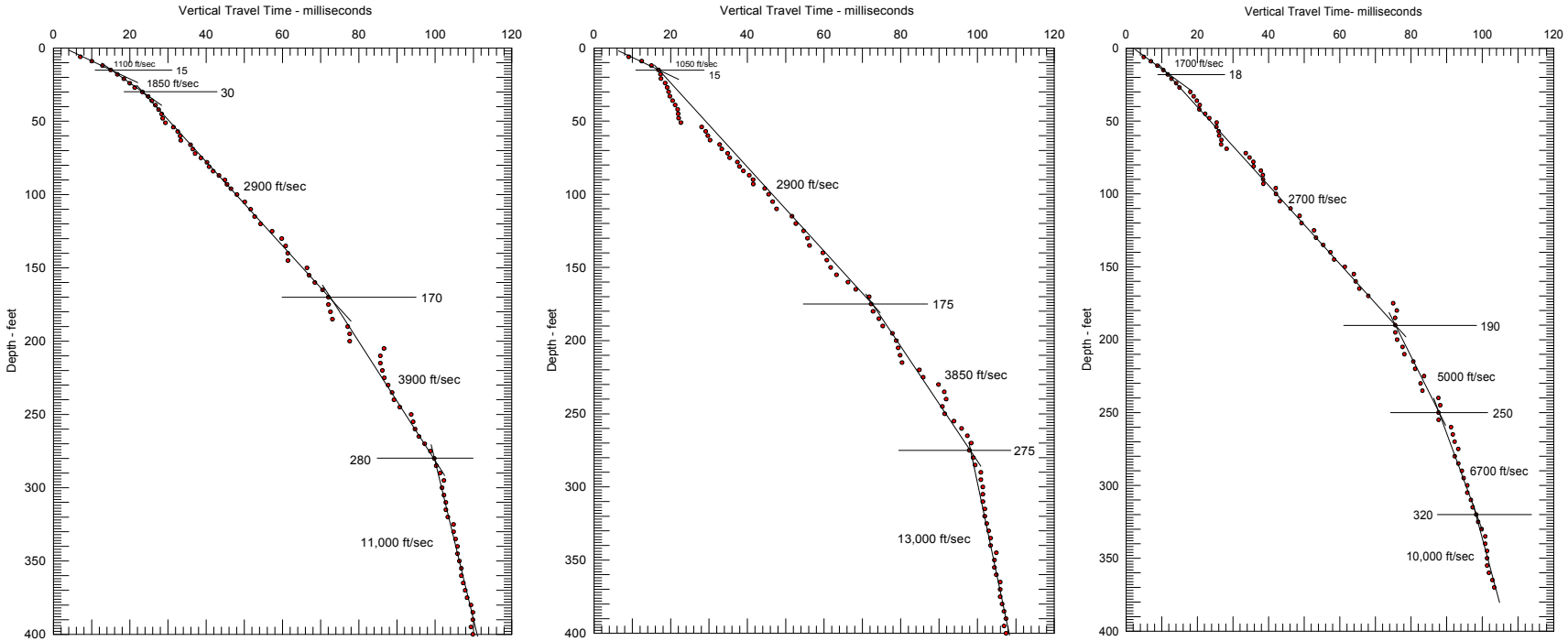

a) Borehole C4993 compression b) Borehole C4996 compression c) Borehole C4998 compression

Figure 4.3. Compression Wave Travel Times and Velocities for Sediments in Boreholes C4993, C4996, and C4998. Figures adapted from Redpath (2007).

4.2 Comparison of Velocities Measured in Three Boreholes

Comparison of shear and compression wave velocities from the same stratigraphic units across the three boreholes indicates generally consistent values. Downhole sediment logging Vs and Vp results from Figures 4.2 and 4.3 are combined and tabulated in Table 4.1. Excluding the near surface (<30 ft bgs) sediment measurements representing mixtures of backfill, eolian deposits, and H2 Unit sand, variability in Vs across the three boreholes is generally less than 30%. Variability in Vp results also is generally 30% or less when the near-surface sediments are excluded.

Table 4.1. Summary of Velocities of Suprabasalt Sediments Measured in Downhole Surveys at the WTP Site (Adapted from Redpath 2007)

Borehole Number	Stratigraphic Unit[(a)] (from Figure 4.1)	Depth Below Ground Surface (ft bgs)	Shear Wave Velocity (ft/sec)	Compression Wave Velocity (ft/sec)
C4993	Backfill & H2 unit	0–15	780	1,100
	H2 unit	15–30	780	1,850
		30–100	1,600	2,900
		100–170	1,760	2,900
	H3 unit	170–236	2,300	3,900
	CCU	236–280	1,950	3,900
	CCU & Ringold A	280–300	1,950	11,000
	Ringold A	300–358	7,150	11,000
C4996	Backfill & H2 unit	0–15	670	1,050
	H2 unit	15–160	1,620	2,900
	H2 & H3 units	160–175	2,040	2,900
	H3 unit	175–255	2,040	3,850
	CCU	255–275	2,170	3,850
	CCU	275–304	2,170	13,000
	Ringold A	304–349	7,300	13,000
C4998	Backfill & H2 unit	0–18	1,100	1,700
	H2 unit	18–30	1,100	2,700
	H2 unit	30–70	1,530	2,700
	H2 unit	70–120	1,880	2,700
	H2 & H3 units	120–190	1,640	2,700
	H3 unit	190–250	2,650	5,000
	CCU	250–322	2,270	6,700
	Ringold A	322–360	7,000	10,000

(a) Backfill = Recent backfill/eolian deposits; H2 unit = Hanford formation, H2 unit; H3 unit = Hanford formation, H3 unit; CCU = Cold Creek unit (aka Reworked Ringold); Ringold A = Ringold Formation Unit A.

5.0 Borehole Gravity Meter Measurements of Density

The characterization effort within the deep boreholes also included downhole measurements of the density of the subsurface basalt and sediments.

A borehole gravity meter (BHGM) was used to obtain accurate in situ density measurements with resolution of the depth variation of the density within the suprabasalt sediments, basalts, and sedimentary interbeds. Micro-g LaCoste (MGL) of Layfayette, Colorado, collected the BHGM density data (MacQueen and Mann 2007). In addition to the BHGM density measurements, a compensated density log was run using a gamma-gamma density logging tool (Gardner and Price 2007).

5.1 Method Description

Borehole gravimetry measures gravity as a function of depth with a downhole BHGM. The change in gravity over intervals of depth is a function of the density of the formation; therefore, density of the formation surrounding the borehole can be estimated from differences in the gravity measurements. Borehole gravimetry surveys a much larger volume of the formation surrounding the borehole than do other downhole density measurement techniques. The gravimetry surveys allow density measurements to be made through multiple casing strings, cement-filled washouts, and areas of drill fluid invasion. The BHGM is capable of providing density measurements with an estimated error of less than ± 0.05 g/cm^3 and was selected to make density measurements within boreholes C4993, C4996, and C4997 at the WTP site. The survey was designed to provide highly accurate density information from ground surface to the bottom of each borehole, in the suprabasalt sediments, basalt flows, and sedimentary interbeds. Because BHGM methods are effective in both cased and uncased boreholes, it is the only downhole method that was able to measure densities within the steel-cased suprabasalt region (i.e., upper 349 to 383 ft below ground surface) of each borehole. Measurements were made using 10-ft intervals. An introduction to borehole gravimetry can be found elsewhere (Beyer 1983), and additional details on the methods used for WTP site measurements can be found in MacQueen and Mann (2007).

Gamma-gamma density logging was also performed in each of the three WTP boreholes C4993, C4996, and C4997. The density logging tool contained a radioactive source (cesium-137) and two gamma detectors to measure long-spaced, short-spaced, and compensated densities as a function of depth. Measurements were made by COLOG of Denver, Colorado, and were recorded on 0.1-ft intervals. The compensated density measurements require contact of the logging tool with the formation wall, and results are affected by the presence of the temporary steel casing in the upper suprabasalt region. Therefore, compensated density measurements are affected by washout zones within the interbed and are not considered accurate within the Hanford and Ringold formations because of the steel casing. Additional details on the gamma-gamma density logging methods used for the WTP site measurements can be found in Gardner and Price (2007).

5.2 Borehole Gravity Meter Topographic Corrections

An underlying assumption in the process of calculating formation density from the BHGM gravity measurements is that the surrounding earth is composed of homogeneous flat layers. The most significant departure from this assumption occurs at the earth-air interface, where the land surface may vary significantly from a level plane near the top of each borehole. Micro-g LaCoste implemented terrain

corrections for each of the three BHGM borehole surveys to account for significant variations in the ground surface. To accomplish these terrain corrections, MGL used a current topographic map of the near zone of the WTP provided by PNNL, and far zone terrain data from the U.S. Geological Survey (USGS).

PNNL received a digital topographic map of the WTP site from Bechtel National, Inc. along with construction drawings of the basemats for the HLW Vitrification (HLW) and Pretreatment (PT) facilities. Construction drawings of the grout vault facility west of borehole C4993 were obtained from the DOE Records Management Information System. Because the site topography had changed due to construction activities since the development of the Bechtel National topographic map, PNNL conducted confirmatory surveys around the HLW and PT facilities and the four new boreholes to generate a topographic map representative of the conditions at the time of the BHGM surveys. PNNL provided MGL a near-zone current ground elevations map based on the real-time kinematic Global Positioning System (GPS) surveys and facility construction drawings.

The topographic survey conducted at the WTP was based upon a first-order National Geodetic Survey (NGS) benchmark atop Gable Mountain. The GPS base station setup on the Gable benchmark was verified using first-order NGS benchmark PID SA0780 (Hanford) and Hanford Well ID W-699-50-59. Both validations revealed a relative accuracy of 2 cm in the horizontal and vertical axes. To have local control of the GPS base station, a benchmark location was established upon an existing WTP benchmark, SL-2 and SL-3 on the upper western edge of the grout vault pit. Once the new GPS base station was established at SL-2, the benchmark was validated against the Gable and Hanford NGS benchmarks and revealed accuracy consistent with the original survey setup. Benchmark SL-3 was used as a local verification for daily base station setup.

A total of 4,234 three-dimensional topographic data points were collected to supplement existing WTP survey points, with the ultimate goal of developing a detailed and continuous topographic data set. WTP survey data were collected originally in a local WTP datum, officially referred to as Project Coordinate System (PCS). These data underwent a simple coordinate transformation process.[(a)] A total of 2,103 WTP survey points were transformed and incorporated into the topographic surface generation process, along with the additional 4,234 discussed earlier.

The topographic survey data were collected on a highly-irregular grid with the intent to capture the topographic details of the WTP site rather than maintaining a consistent spatial resolution. This approach provides a clear benefit for the development of an accurate topographic surface where fine detail is required, so long as an appropriate terrain processing method is used. The base topographic surface derived from the survey point data was processed into a continuous 0.6-m resolution raster-based data set utilizing a finite difference and inverse distance weighting (IDW) method (Hutchinson 1989, 1996). For areas exhibiting complex terrain features, this method is computationally expensive, but is well-suited for preserving and accurately representing topography. Once ground based topographic features were established, CAD drawings of the grout vaults and PT and HLW facilities were referenced and developed into three-dimensional surfaces. These “empty-space” surfaces were joined with the original topographic surface. Figure 5.1 displays the final results of the processing, which PNNL provided to MGL for use

(a) The coordinate transformation process was developed by Thomas G. Arneson, lead area surveyor, Bechtel National, Inc.

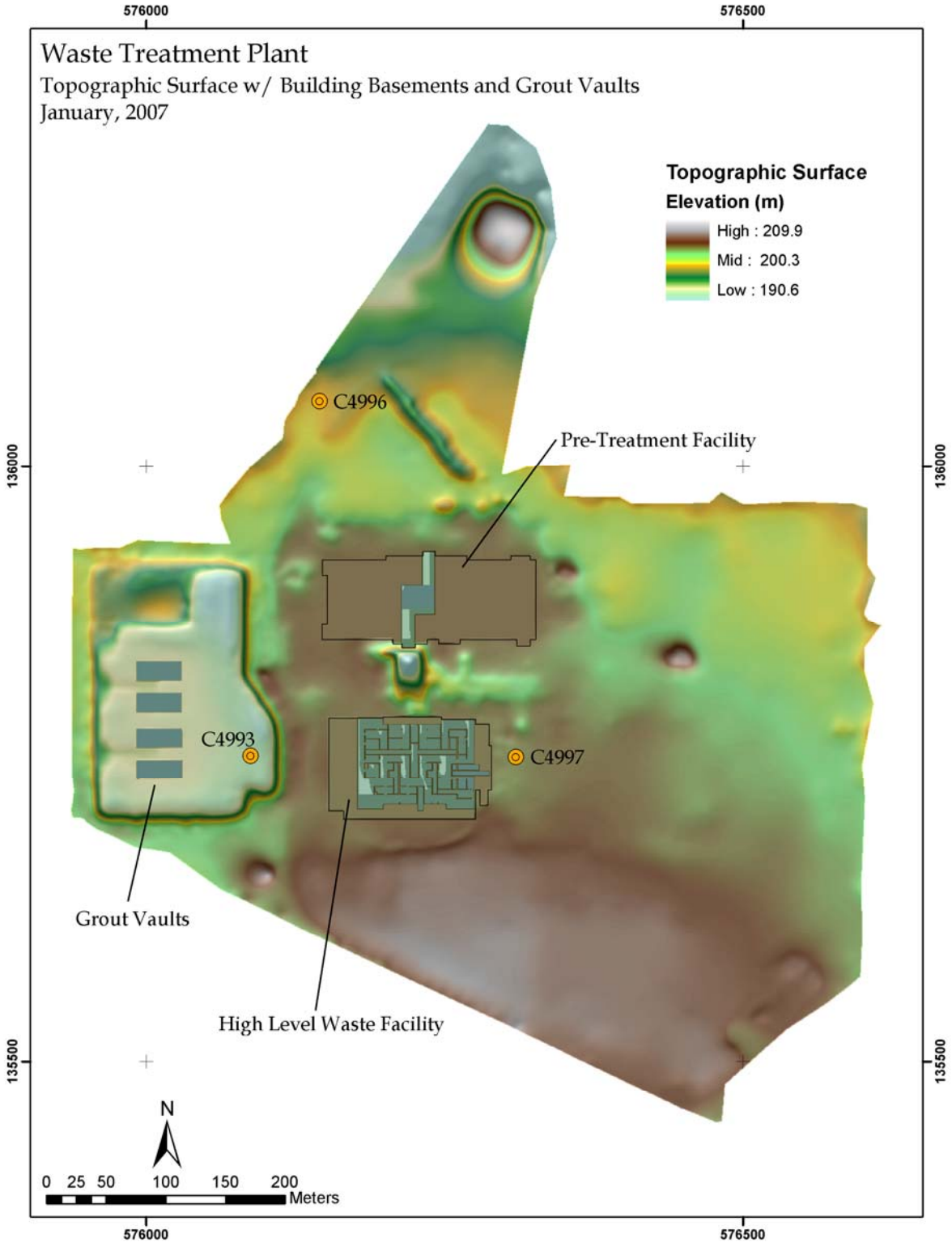

Figure 5.1. Near-Zone Terrain of the WTP Site from Global Positioning System Surveys and Facility Schematics

with the BHGM. The BHGM terrain correction methodology and results employed by MGL are described in detail in MacQueen and Mann 2007. Results were converted into density corrections, and are less than the required accuracy of ±0.05 g/cm^3 for all depths greater than 100 ft bgs. The largest correction was approximately −0.14 g/cm^3 at ground surface for borehole C4993 (see Figure 5.2).

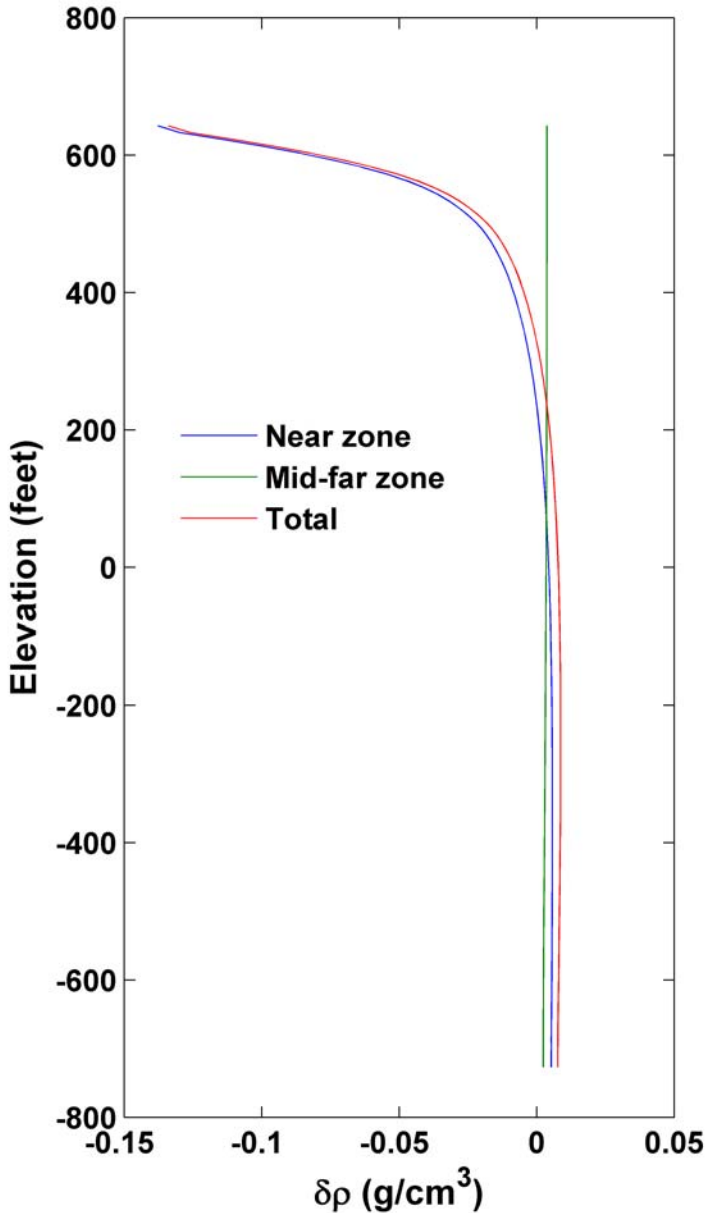

Figure 5.2. Well C4993 Terrain Corrections for Density as a Function of Depth (MacQueen and Mann 2007)

5.3 Density Profiles

The measured BHGM densities as a function of depth for each of the three boreholes are shown in Figure 5.3 along with compensated density measurements. Steel casing was present in each of boreholes C4993, C4996, and C4997 from just above ground surface to approximately 364, 351, and 383 ft bgs, respectively. Therefore, compensated density measurements above these depths are not shown in Figure 5.3. Comparison of BHGM and compensated density measurements indicates excellent agreement. Figure 5.4 shows the BHGM and compensated density log comparison for borehole C4993, with additional notation added to indicate the top of each basalt member or flow and sedimentary interbed. The compensated density measurements reflect greater scatter than BHGM measurements, including some suspect values that are observed more frequently within the sedimentary interbeds. Specifically, several regions are observed in the Selah, Cold Creek, and Mabton interbeds with significantly lower density values from the compensated gamma-gamma log compared to the BHGM log. Washouts in these interbeds were noted in the caliper logs from these zones (Gardner and Price 2007). The compensated density logging tool would have difficulty achieving close contact with the borehole wall in washout regions, and subsequently result in inaccurate measurement values.

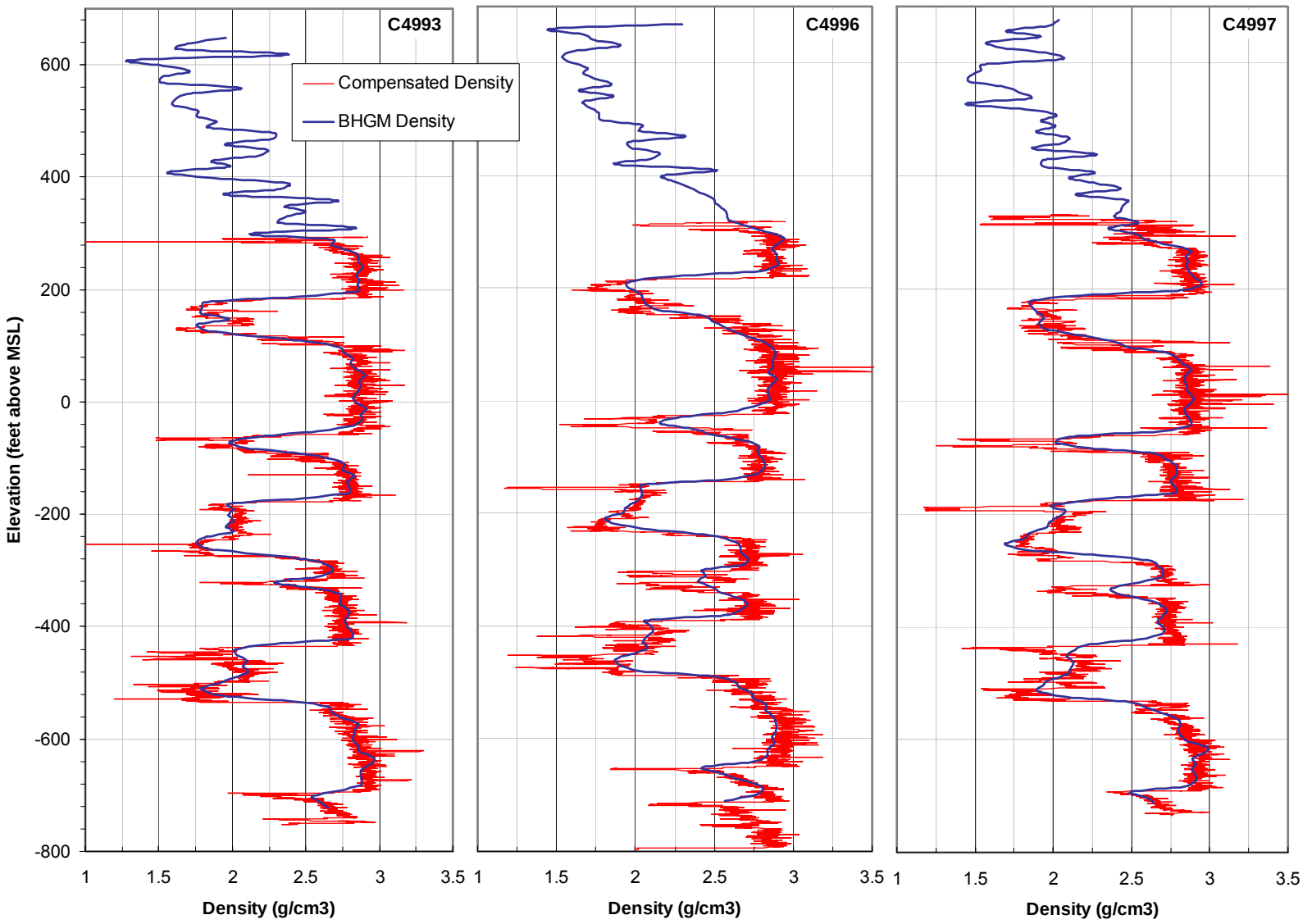

Figure 5.3. Borehole-to-Borehole Correlation of Density from Borehole Gravity Meter and Compensated Density Logs

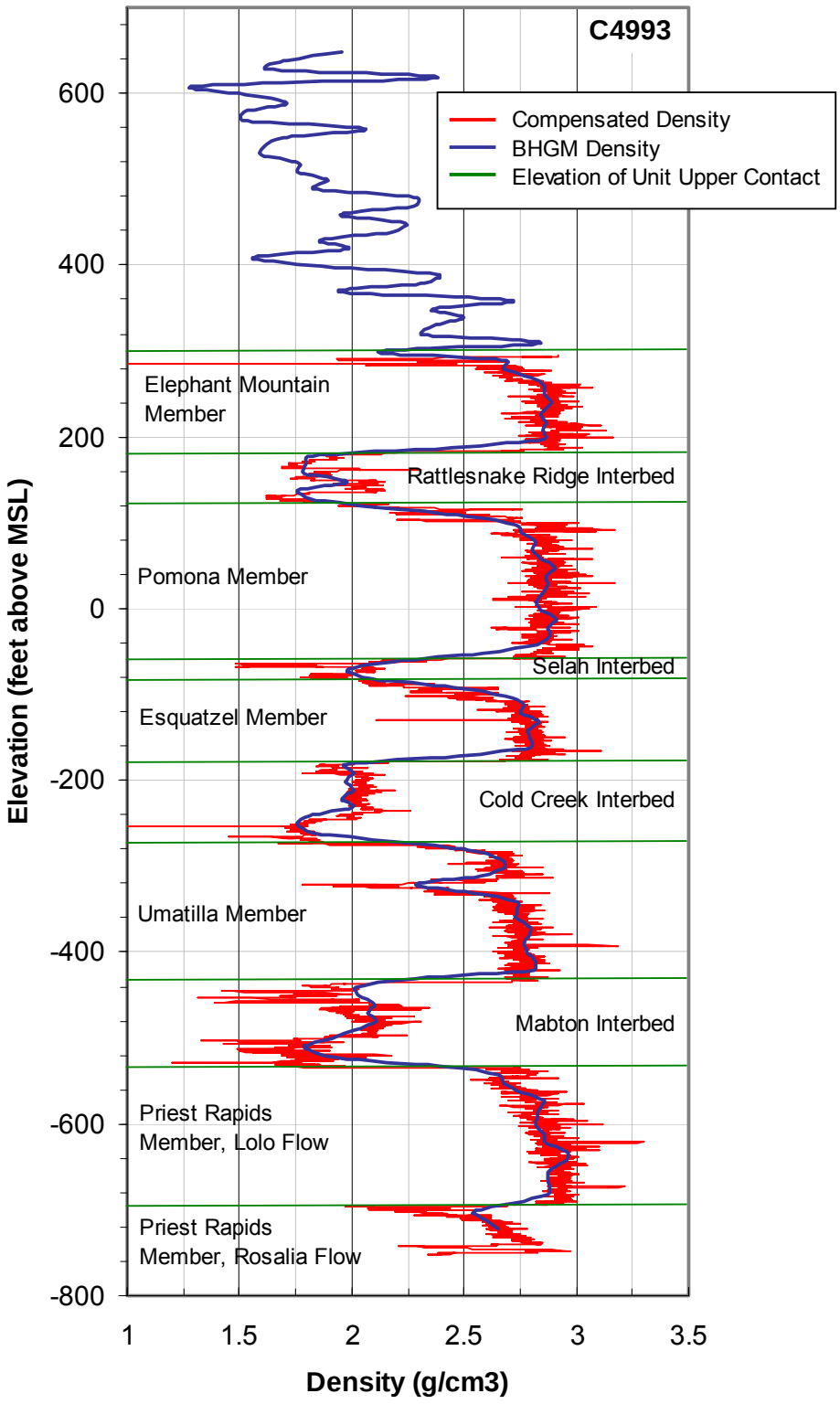

Figure 5.4. Borehole Gravity Meter and Compensated Density Logs of Borehole C4993

6.0 Generation of the Final Site-Specific Models

Data and interpreted results of in situ velocity and density measurements described in Sections 3 through 5 were evaluated and analyzed to produce a set of final site-specific velocity and density models representing the WTP site. The objective was to integrate data from the new boreholes and previous site-specific studies into a set of models for use in evaluating the seismic response of the WTP site.

6.1 Statistical Approaches to Combining Velocity-Density Profiles

Three methods of forming statistical averages of velocity and density are used. They include 1) the *arithmetic mean* (*A*), which is the straightforward average of velocities (or densities); 2) the *geometric mean* (*G*), the log of which is the average of the logarithms of the velocities; and 3) the *harmonic mean* (*H*), the reciprocal of which is the average of the inverses of the velocities (1/V) (Abramowitz and Stegun 1972). Equations used for calculating these means and their standard deviations (SD) are as follows:

$$A = \frac{1}{N}\sum_{i=1}^{N} V_i \qquad SD_A = \sqrt{\frac{1}{N-1}\sum_{i=1}^{N}\left(V_i - A\right)^2}$$

$$\log_e G = \frac{1}{N}\sum_{i=1}^{N} \log_e V_i \qquad \log_e SD_G = \sqrt{\frac{1}{N-1}\sum_{i=1}^{N}\left(\log_e V_i - \log_e G\right)^2}$$

$$1/H = \frac{1}{N}\sum_{i=1}^{N} 1/V \qquad 1/SD_H = \sqrt{\frac{1}{N-1}\sum_{i=1}^{N}\left(1/V_i - 1/H\right)^2}$$

The arithmetic mean is always the largest estimate of the averages, and the harmonic mean is always the smallest. The geometric mean also can be expressed as the *nth* root of the product of the *n* velocities.

The standard deviation is used to generate estimated 16th and 84th fractiles of the velocity distribution; this range should include 67% of the velocity values.

$$A_{16} = A - SD_A \qquad A_{84} = A + SD_A$$

$$\log_e G_{16} = \log_e G - \log_e SD_G \qquad \log_e G_{84} = \log_e G + \log_e SD_G$$

$$1/V_{16} = 1/H + 1/SD_H \qquad 1/V_{84} = 1/H - 1/SD_H$$

For the arithmetic mean, the 16th and 84th fractiles are symmetric about the mean. For the geometric mean, these fractiles are a symmetric multiplicative factor applied to the mean. For the harmonic mean, the inverses of the two fractiles are symmetric about the inverse mean. The 16th and 84th fractiles can be approximately compared in units of velocity through the derivative of the change in logarithm or the inverse velocity units,

$$\frac{dV}{dx} = V \times \frac{d\left(\log_e V\right)}{dx} \qquad \frac{dV}{dx} = -V^2 \times \frac{d\left(1/V\right)}{dx}$$

relating a small change in ($\log_e V$) or ($1/V$) , $d(\log_e V)$ and $d(1/V)$, respectively representing the standard deviations, to the corresponding change in V (Selby 1972, Derivatives 10 and 19). This is a good approximation to one-half the range between the 16th and 84th fractiles. The means, fractiles, multiplicative factors, and approximate standard deviations are tabulated in Section 6.2.

The reason for using one of these three averaging methods is that there are different interpretations regarding the underlying distribution of values being averaged. In the case of the geometric mean, it assumes that the distribution of velocity values is log-normally distributed and that errors or variability in the values tend to be multiplicative. In the case of the harmonic mean, because velocity is measured by making travel-time measurements, normally distributed errors in the travel-time measurements are introduced into the denominator of the ratio distance/travel time, implying that 1/V is normally distributed. In addition, when averaging velocities over multiple adjacent distance intervals, this average preserves the total travel time accumulated from all of the intervals.

All three types of mean are used to estimate average velocities and uncertainties in the basalts and interbeds in Section 6.2 and in the sediments in Section 6.3. The seismic response modeling requires the use of the geometric mean, even though the harmonic mean may be the most appropriate.

Arithmetic means are used for density data in Section 6.4. Laboratory measurements of basalt density (Carmichael 1989) suggest that they have a normal distribution, so the arithmetic mean is appropriate. Outliers show only lower densities from the main peak in the laboratory data, similar to the borehole measurements made at the WTP site. This is not typical of a log-normal distribution. Section 6.5 uses arithmetic means to develop average densities and density shape factors and uses harmonic means to develop average shape factors for velocity.

Weighted means could be used when there are standard error estimates for each of the measurements. This would allow for the better-determined values being given more weight. Weighted means can be used regardless of whether the arithmetic, geometric, or harmonic means are considered. In the case of the velocity data (Redpath 2007; Stokoe et al. 2007), no error estimates are given. Layer thicknesses over which velocities are calculated are not highly variable (velocity measured over a longer distance would be more accurate), and data were taken at the same depth spacing so that the number of data points also does not vary. Error estimates for density (MacQueen and Mann 2007) were calculated, but they did not vary significantly. Weighted means have not been used in this analysis.

6.2 Basalt and Interbed Model

The data from the downhole Vs measurements reported in Section 3 are examined and summarized in this section. The travel-time data plots were examined to form velocity profiles to compare the different measurements and the different boreholes. Figure 6.1 shows the Vs profiles at the three new boreholes recorded by Texas. The depth intervals conform to the geophysically picked interfaces between the basalts and interbeds. The data are shown relative to the elevation of the Priest Rapids Member flow top rather than absolute elevation, to isolate thickness variations in the layers of interest.

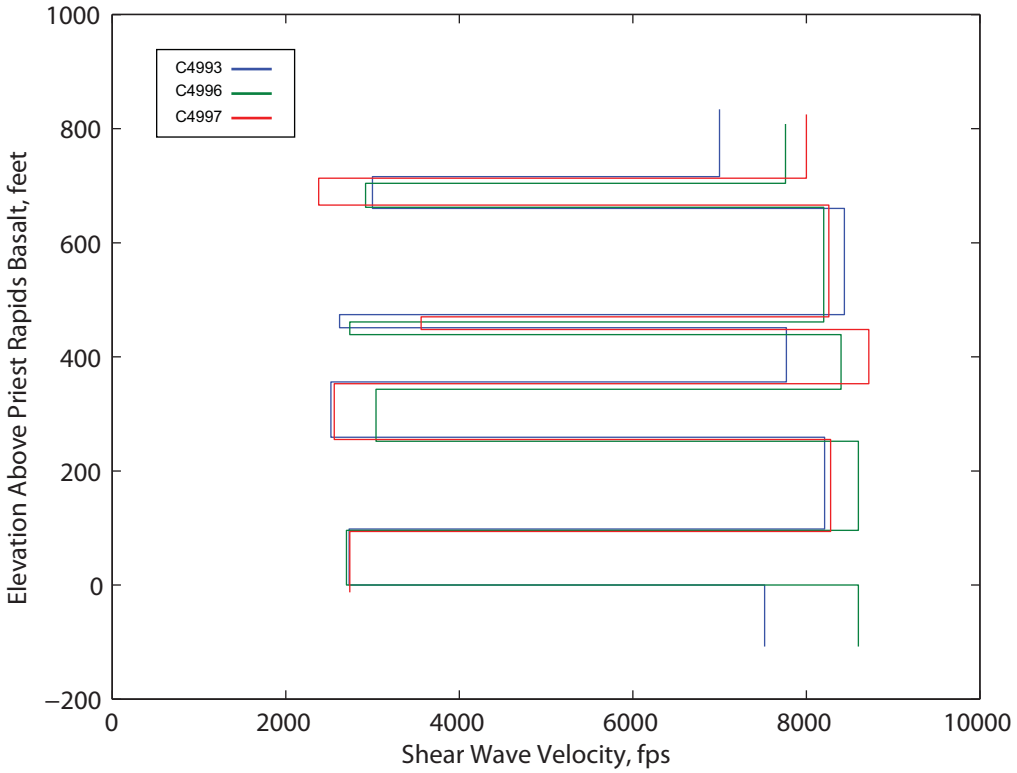

Figure 6.1. Texas Downhole Shear Wave Velocity Profiles

Figure 6.2 shows the data collected by Redpath Geophysics. The impulsive source used here had sufficient power to observe downhole signals to depths of up to 750 ft. In the data, there is evidence for a lower velocity flow top in the Pomona Member for two of the boreholes. This has been difficult to detect with downhole data because of the depth sampling of 5 to 10 ft. This was not well determined, but careful examination of the data by Redpath Geophysics suggests this.

Figure 6.3 compares the Texas and Redpath Geophysics Vs profiles. The Redpath Geophysics Vs in the Elephant Mountain Member (uppermost basalt) are, on average, slightly higher than those measured by Texas, but Vs for the second basalt (Pomona Member) are consistent. The presence of an extensive lower-velocity flow top in the Pomona Member is reflected in Vs values of 5,000 fps in two of the three boreholes.

Figures 6.4 and 6.5 display the basalt and interbed velocities in histogram form for the Texas and Redpath Geophysics data sets, respectively. These form the basis from which to generate average models under various alternative assumptions.

The thicknesses of each basalt and interbed unit from each of the four new boreholes are summarized in Table 6.1. Data presented here are from Barnett et al. (2007), with the exception of the C4996 thicknesses of the Cold Creek interbed, Umatilla Member, Mabton interbed, and Priest Rapids Member, Lolo flow. Additional suspension logging data (Diehl and Steller 2007a, 2007b) were compared with geophysical logs used by Barnett et al., and revised upper depths of contact for the Umatilla and Priest Rapids Member, Lolo flow basalts were made. These revised picks based on additional data changed the reported thicknesses of the four units.

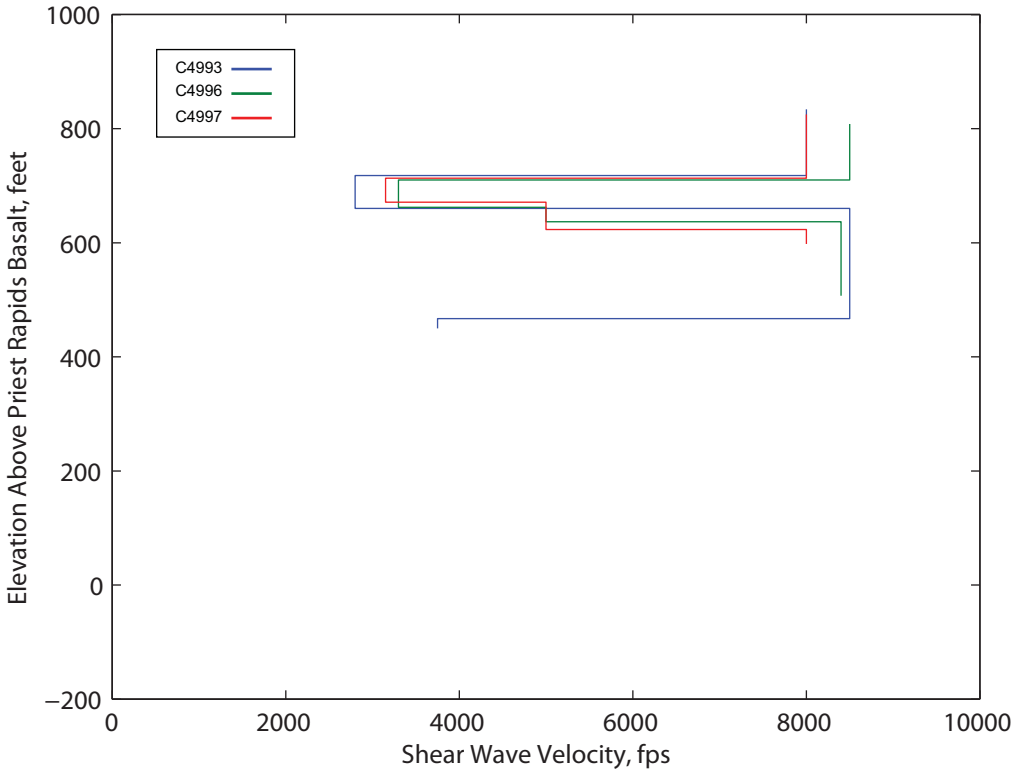

Figure 6.2. Redpath Downhole Shear Wave Velocity Profiles

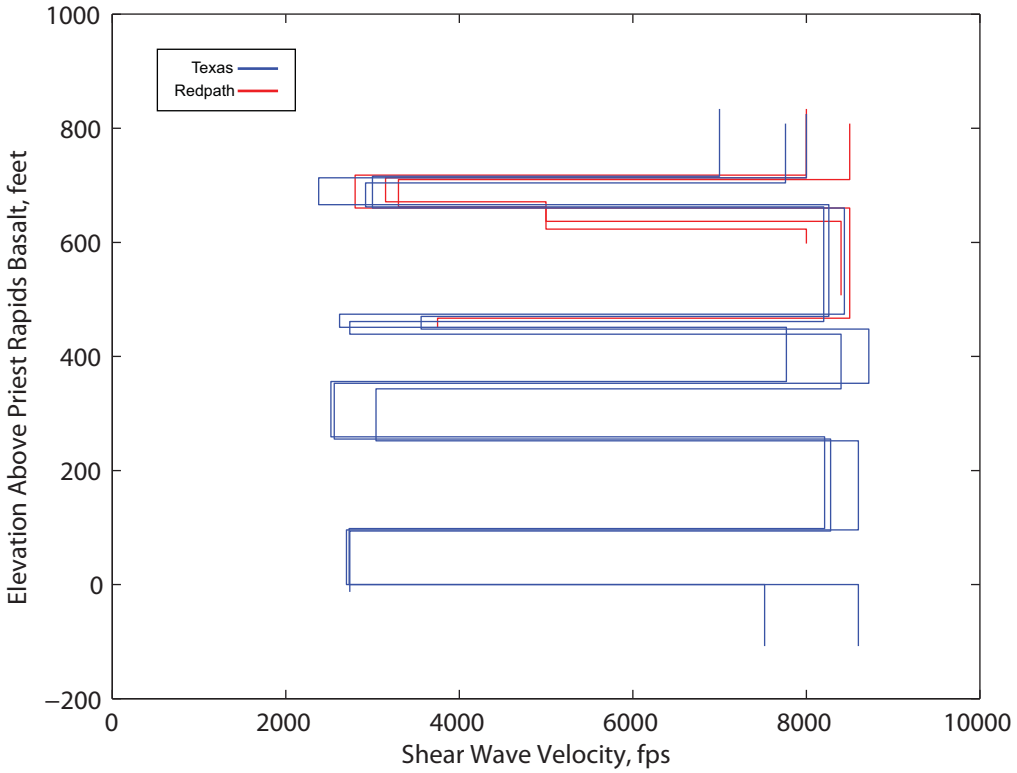

Figure 6.3. Comparison of the Texas and Redpath Downhole Shear Wave Velocity Measurements

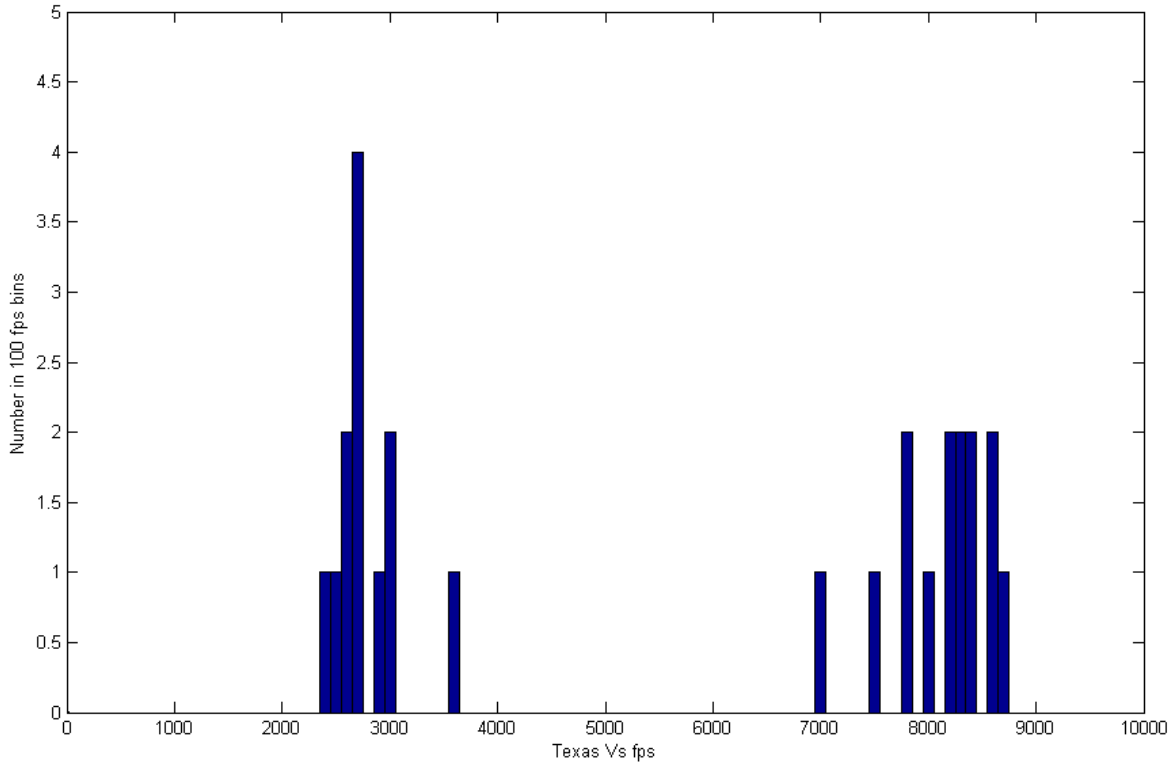

Figure 6.4. Texas Downhole Shear Wave Velocity Measurements

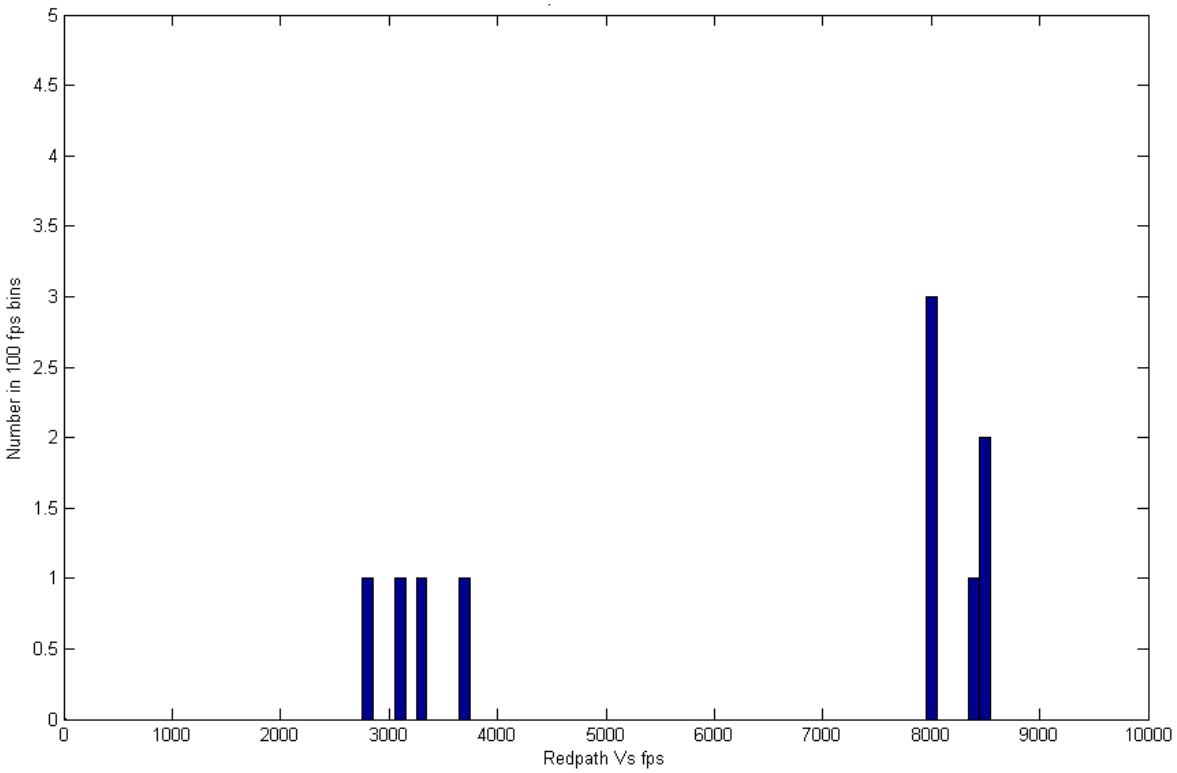

Figure 6.5. Redpath Downhole Shear Wave Velocity Measurements

Table 6.1. Thickness Variation in Basalt and Interbed Layers

Basalt and Interbed Unit Thicknesses in Feet				
	C4993	C4996	C4997	C4998
Elephant Mountain Member	118	104	112	110
Rattlesnake Ridge Interbed	56	42	47	34
Pomona Member	186	201	196	209
Selah Interbed	23	22	22	22
Esquatzel Member	95	96	95	94
Cold Creek Interbed	97	91	98	98
Umatilla Member	161	156	161	157
Mabton Interbed	98	96	94	98
Priest Rapids Member, Lolo flow	161	165	156	161

There is very little thickness variation in the lower basalt and interbed layers. The combined thickness of the Rattlesnake Ridge interbed and Pomona Member also is nearly constant, indicating that there is more topography on the interface between them than on the top or bottom of the combined basalt-interbed combination. This can be seen in Figure 6.1, where the interface between the top basalt and the underlying interbed is more variable than the bottom of the interbed.

The range of layer thicknesses in Table 6.1 is used in the seismic response modeling by Youngs (2007). In the modeling, each layer thickness is randomized from a uniform distribution between the maximum and minimum thickness for that layer. In the case of the Rattlesnake Ridge interbed and the Pomona Member, a correlation is introduced into the randomization to keep the combined thickness constant, effectively randomizing only the interface between them.

A number of alternatives to forming average Vs profiles have been suggested. These averaging alternatives are examined in Tables 6.2 through 6.4. The results are dominated by the Texas data due to its extended depth range, but the only evidence for flow tops from downhole measurements comes from the Redpath Geophysics data. Density (Section 5) and suspension logging (Section 3.2) provide strong evidence for reduced velocity in the basalt flow tops. The effect of the flow tops is to smooth out the impedance contrast between the tops of basalt and the overlying interbed. Examination of the geophysical data for similar features in the flow bottoms indicated that these are minor (on the order of 1 ft in thickness) or entirely absent, as discussed further in Section 6.4.

Three different averaging methods were used to examine and tabulate the Vs data; the geometric, arithmetic, and harmonic means were introduced in Section 6.1.

Table 6.3 shows the average Vs from Redpath (2007). These data cover only the Elephant Mountain and Pomona members' flow interiors and the Rattlesnake Ridge interbed between them. In addition, Table 6.3 shows the result of averaging the six Redpath and Texas velocities for these three layers.

Table 6.2. Average Shear Wave Velocities from All Texas Measurements

	Stratigraphic Unit								
	EMM	RRI	PM	SI	EM	CCI	UM	MI	PRM
Geometric mean (ft/sec)	7574	2752	8299	2946	8287	2697	8362	2723	8042
84th percentile (ft/sec)	8124	3124	8425	3476	8790	2993	8571	2744	8842
16th percentile (ft/sec)	7063	2425	8176	2496	7814	2430	8158	2703	7314
Approx. Vel. Std. Dev. (ft/sec)	530	348	125	488	488	281	207	21	763
Sigma	0.070	0.127	0.015	0.166	0.059	0.104	0.025	0.008	0.095
Mult. Factor	1.072	1.135	1.015	1.180	1.061	1.110	1.025	1.008	1.100
Arithmetic mean (ft/sec)	7587	2767	8300	2973	8297	2707	8363	2723	8060
84th percentile (ft/sec)	8109	3104	8425	3485	8780	2996	8571	2744	8824
16th percentile (ft/sec)	7065	2429	8175	2462	7813	2417	8155	2703	7296
Std. Dev. (ft/sec)	522	337	125	512	483	289	208	21	764
Harmonic mean (ft/sec)	7562	2737	8299	2920	8278	2687	8360	2723	8024
84th percentile (ft/sec)	8140	3149	8425	3466	8800	2989	8570	2744	8864
16th percentile (ft/sec)	7060	2421	8177	2522	7814	2441	8160	2703	7329
Approx. Vel. Std. Dev. (ft/sec)	537	358	124	460	492	271	205	21	760
Mult. Fac. High	1.076	1.150	1.015	1.187	1.063	1.112	1.025	1.008	1.105
Mult. Fac. Low	0.934	0.884	0.985	0.864	0.944	0.908	0.976	0.992	0.913
EMM = Elephant Mountain Member; RRI = Rattlesnake Ridge interbed; PM = Pomona Member; SI = Selah interbed; EM = Esquatzel Member; CCI = Cold Creek interbed; UM = Umatilla Member; MI = Mabton interbed; PRM = Priest Rapids Member.									

Comparison of the velocities in Table 6.4 should be made to the individual basalt velocity averages in Table 6.2, in particular the Elephant Mountain Member that was excluded in this average. The Elephant Mountain Member appears to have a consistently lower velocity than the deeper basalt layers in the data from Texas. In addition, Table 6.4 shows the effect of averaging all of the basalt velocities as a single velocity and all of the interbeds as a single velocity.

The standard errors or ranges from the different averaging methods generally are comparable and do not indicate that any one of them is significantly different when the variability in velocities is low. The basalt velocities have 16th and 84th percentile points that are smaller and larger than their mean values by 2% to 10%. The interbed velocities have corresponding relative errors ranging from approximately 10% to 20%, excepting the deepest Mabton interbed for which the relative error is only 1%. Given the scatter of the travel-time data within this interbed, especially in boreholes C4993 and C4997 (see Figure 3.10), and significantly wider range of interpreted Vp, the relative error in Vs for the Mabton interbed is likely underrepresented.

Table 6.3. Comparison of Average Vs from Redpath and Redpath and Texas Combined

Stratigraphic Unit			
	EMM	RRI	PM
Redpath Shear Wave Velocities in Elephant Mountain Member, Rattlesnake Ridge Interbed, and Pomona Member			
Geometric mean (ft/sec)	8163	3076	8297
84th percentile (ft/sec)	8454	3348	8568
16th percentile (ft/sec)	7883	2826	8035
Approx. Vel. Std. Dev. (ft/sec)	286	261	267
Sigma	0.035	0.085	0.032
Mult. Factor	1.036	1.088	1.033
Algebraic mean (ft/sec)	8167	3083	8300
84th percentile (ft/sec)	8455	3340	8565
16th percentile (ft/sec)	7878	2827	8035
Std. Dev. (ft/sec)	289	257	265
Harmonic mean (ft/sec)	8160	3069	8294
84th percentile (ft/sec)	8453	3357	8572
16th percentile (ft/sec)	7887	2826	8034
Approx. Vel. Std. Dev. (ft/sec)	283	264	269
Mult. Fac. High	1.036	1.094	1.033
Mult. Fac. Low	0.967	0.921	0.969
Redpath and Texas Shear Wave Velocities in Elephant Mountain Member, Rattlesnake Ridge Interbed, and Pomona Member			
Geometric mean (ft/sec)	7863	2910	8298
84th percentile (ft/sec)	8385	3261	8487
16th percentile (ft/sec)	7374	2597	8114
Approx. Vel. Std. Dev. (ft/sec)	505	332	186
Sigma	0.064	0.114	0.022
Mult. Factor	1.066	1.121	1.023
Algebraic mean (ft/sec)	7877	2925	8300
84th percentile (ft/sec)	8370	3244	8485
16th percentile (ft/sec)	7383	2606	8115
Std. Dev. (ft/sec)	493	319	185
Harmonic mean (ft/sec)	7850	2894	8297
84th percentile (ft/sec)	8404	3284	8488
16th percentile (ft/sec)	7364	2586	8113
Approx. Vel. Std. Dev. (ft/sec)	518	344	187
Mult. Fac. High	1.071	1.135	1.023
Mult. Fac. Low	0.938	0.894	0.978
EMM = Elephant Mountain Member; RRI = Rattlesnake Ridge interbed; PM = Pomona Member.			

Table 6.4. Comparison of Average Shear Wave Velocities for All Texas-Measured Basalt Velocities to Average Without Elephant Mountain Member, and Average for All Texas-Measured Interbed Velocities

	All Basalt Velocities Except Elephant Mountain Member	All Basalt Velocities	All Interbed Velocities
Geometric mean (ft/sec)	8266	8112	2778
84th percentile (ft/sec)	8640	8617	3088
16th percentile (ft/sec)	7908	7637	2499
Approx. Vel. Std. Dev. (ft/sec)	366	490	294
Sigma	0.044	0.060	0.106
Mult. Factor	1.045	1.062	1.112
Algebraic mean (ft/sec)	8273	8126	2793
84th percentile (ft/sec)	8632	8601	3102
16th percentile (ft/sec)	7914	7650	2483
St. Dev. (ft/sec)	359	476	310
Harmonic mean (ft/sec)	8258	8098	2764
84th percentile (ft/sec)	8649	8636	3076
16th percentile (ft/sec)	7901	7624	2510
Approx. Vel. Std. Dev. (ft/sec)	373	504	280
Mult. Fac. High	1.047	1.066	1.113
Multi. Fac. Low	0.957	0.941	0.908

6.3 Sediment Shear Wave Velocity Model

This section describes the data analyses used to construct a model for the shear wave velocity structure of the sedimentary Hanford and Ringold layers beneath the WTP PT and HLW buildings. The downhole Vs data collected in 2006−2007 from the three new boreholes, described in Section 4, is reviewed and then combined with similar data from earlier downhole data (to depths of 260–270 ft) collected in 1999 as part of the WTP geotechnical site investigations (Shannon & Wilson 2000). The shallow soils also were characterized by a large number (26) of shallow downhole measurements (60 to 90 ft) using a seismic cone penetrometer test (SCPT). The earlier data are particularly important because they were taken prior to excavation of foundations for the WTP buildings, which results in the uppermost portions of three of the four boreholes measuring the backfill properties instead of native soils.

The downhole Vs data collected in 2004 and used in Rohay and Reidel (2005) were limited by the selection of available boreholes surrounding the WTP site at distances up to 1 mi, and measurements were made to depths of only 250 ft. Data from a borehole drilled 1.5 mi from the WTP for that study, which did go to a depth of more than 500 ft (the basalt is deeper to the southwest) sampled the deeper gravels, but they appear to be unrepresentative of those encountered in the 2006 borings on the WTP site. Other Vs profiles were taken in 2004 using a method termed spectral analysis of shear waves (SASW) and also used in Rohay and Reidel (2005), at similar distances from the WTP, generally near the locations of the existing boreholes for which downhole measurements were made. These measurements also proved to be different from the new borehole data. The data from the downhole and SASW measurements taken in

2004 are considered to be either unrepresentative or of such weaker resolution and applicability that they are not included in the final Vs model developed here. However, the final model from Rohay and Reidel (2005) is compared to the new result after its development has been described.

6.3.1 Sediment Downhole Shear Wave Velocity Measurements in New Boreholes

Shear wave velocity data collected in the new boreholes (Redpath 2007), described in detail in Section 4, are shown plotted versus elevation in Figure 6.6. These data have been truncated near the surface to remove the depth range where the boreholes were penetrating backfill instead of native material.[(a)] These data are averaged with other data to determine an average velocity profile and "sigma," the logarithmic standard error, for use in the ground motion response modeling.

The data show Vs is just below 2,000 fps in the upper 180 ft that corresponds to the Hanford formation sands or H2 unit. In the Hanford formation gravels or H3 unit, Vs is higher—2,000–2,700 fps. A lower velocity was recorded in the underlying Cold Creek unit of the Ringold Formation (aka reworked Ringold), and a very high velocity of 7,000–8,000 fps in the lower Ringold, Unit A.

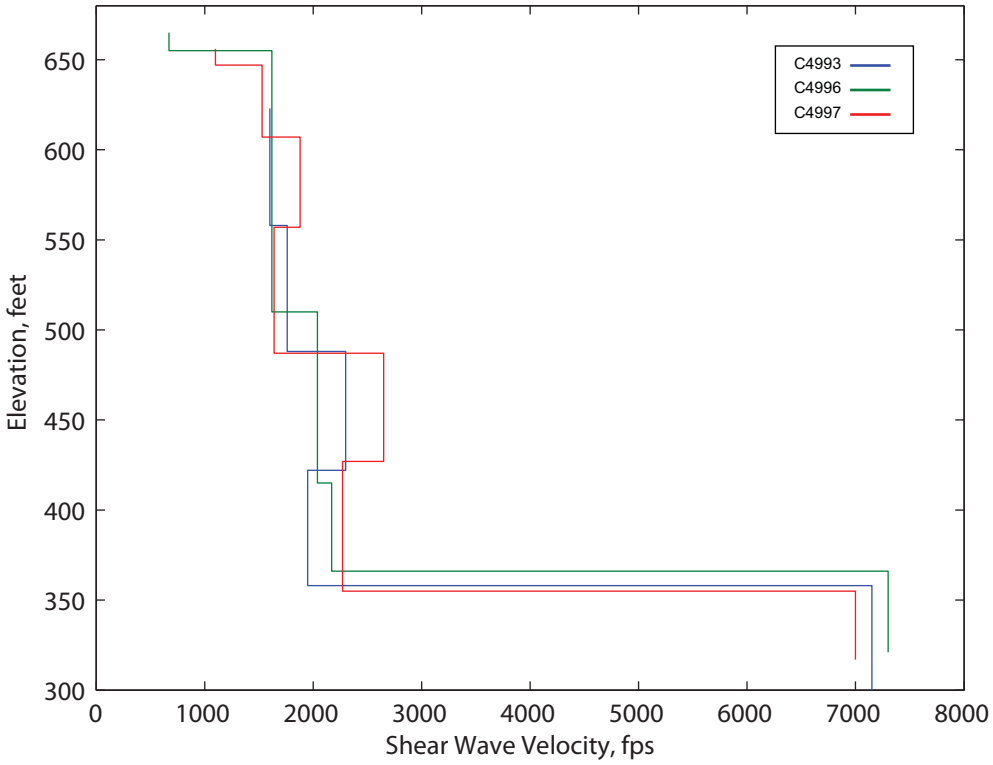

Figure 6.6. Shear Wave Velocity Versus Elevation in Sediment Section from New Deep Boreholes

(a) Borehole C4993 was located near the grout vaults, and construction drawings and elevations on maps indicated that at least 35 ft of material had been backfilled. Both C4997 and C4998 were located near the excavation of the WTP building. Construction of the excavation and the location of the boreholes suggest a backfill thickness of 21 ft, but aerial photography from that period indicates that a roadway entrance to the excavation went between the two borehole locations. A maximum excavation depth of 27 feet is possible. These estimates are different than those reported in Barnett et al. (2007) and are documented in email dated April 19, 2007, from Alan Rohay, PNNL, to Tom Brouns, PNNL, and maintained in project files.

6.3.2 Preconstruction Shear Wave Velocity Measurements

Preconstruction geophysical and geotechnical measurements were conducted by Shannon & Wilson and its subcontractors in 1999 and were reported in Shannon & Wilson (2000). At the time of these measurements, no excavations for the WTP buildings had begun, although excavation of the grout vault facilities to the west had left a 25-ft-high sand pile near the center of the WTP construction site, which was avoided. Included in these investigations were downhole shear wave measurements and SCPTs. These were re-examined in 2004 with additional geophysical data (Rohay and Reidel 2005) and are being used again to augment the data collected from the new deep boreholes. The area where borehole C4993 was drilled had been excavated previously during construction of the grout vaults. Backfilling after construction left an estimated 35 ft of backfill below the current surface elevation at C4993. The area where boreholes C4997 and C4998 were drilled was excavated to an estimated depth of 21 ft to emplace the foundation of the HLW building, and the uppermost 21 ft of these boreholes is also in non-native material (backfill). Characterization of the physical properties of native material beneath the foundations of the PT and HLW buildings therefore requires the use of these earlier data. Only the shear wave measurements are used for the site response modeling.

Blackhawk Geophysics conducted four downhole velocity tests at the WTP site in August 1999. The source of energy for these tests was a Minivib (Industrial Vehicles International, Inc., Tulsa, Oklahoma) positioned approximately 20 ft from the boreholes, and BHG-2 14-Hz downhole geophones were used to record the energy. The vibrator produced a frequency sweep from 20 to 120 Hz. The horizontal geophones were un-oriented but were rotated mathematically in post-processing and sweep cross-correlation. Additional details of the downhole data are in Appendix B of Shannon & Wilson (2000). One downhole test was made beneath each of the four major structures of the WTP in boreholes designated BD-8A, BD-23, BD-35, and BD-43. The measurements were made at 5-ft increments to 50 ft depth and 10-foot increments from 50 ft to depths of 260 or 270 ft. The locations of the downhole and later SCPT measurements are shown in Figure 6.7. Figure 6.8 shows the preconstruction Vs profiles.

Applied Research Associates, Inc. conducted 26 SCPTs in October 1999. The SCPT used a GS-14-L9 28-Hz geophone fitted into a standard cone penetrometer and impulsive compression and shear wave sources positioned 6 ft and 3 ft, respectively, from the boring. Additional details regarding the SCPTs data are in Appendix C of Shannon & Wilson (2000). The SCPTs were located beneath the planned footprints of the four major buildings of the WTP; seven SCPTs were completed beneath the planned footprints of both the PT and HLW buildings, and six were completed beneath the footprints of the analytical laboratory (LAB) and the low-activity waste (LAW) building. The measurements were made at 3-ft increments and generally extended to depths of approximately 60 or 75 ft, although five of the seven measurements beneath the PT extended to depths of approximately 90 or 100 ft.

The SCPT data were carefully checked, including borehole locations and elevations. Of a total of 146 velocity blocks from the 26 tests, three suspected outliers were censored (anomalously high velocity at shallow depth). In another two cases, pairs of adjacent blocks were averaged because these outliers had a high/low offset (indicating an underlying travel-time error at the middle point).

The SCPT velocity-elevation profiles are shown geographically grouped in Figure 6.9 and are averaged in Figure 6.10. Some relatively high velocity blocks remain, are evident in some of the profiles, and also can be seen in the average profiles.

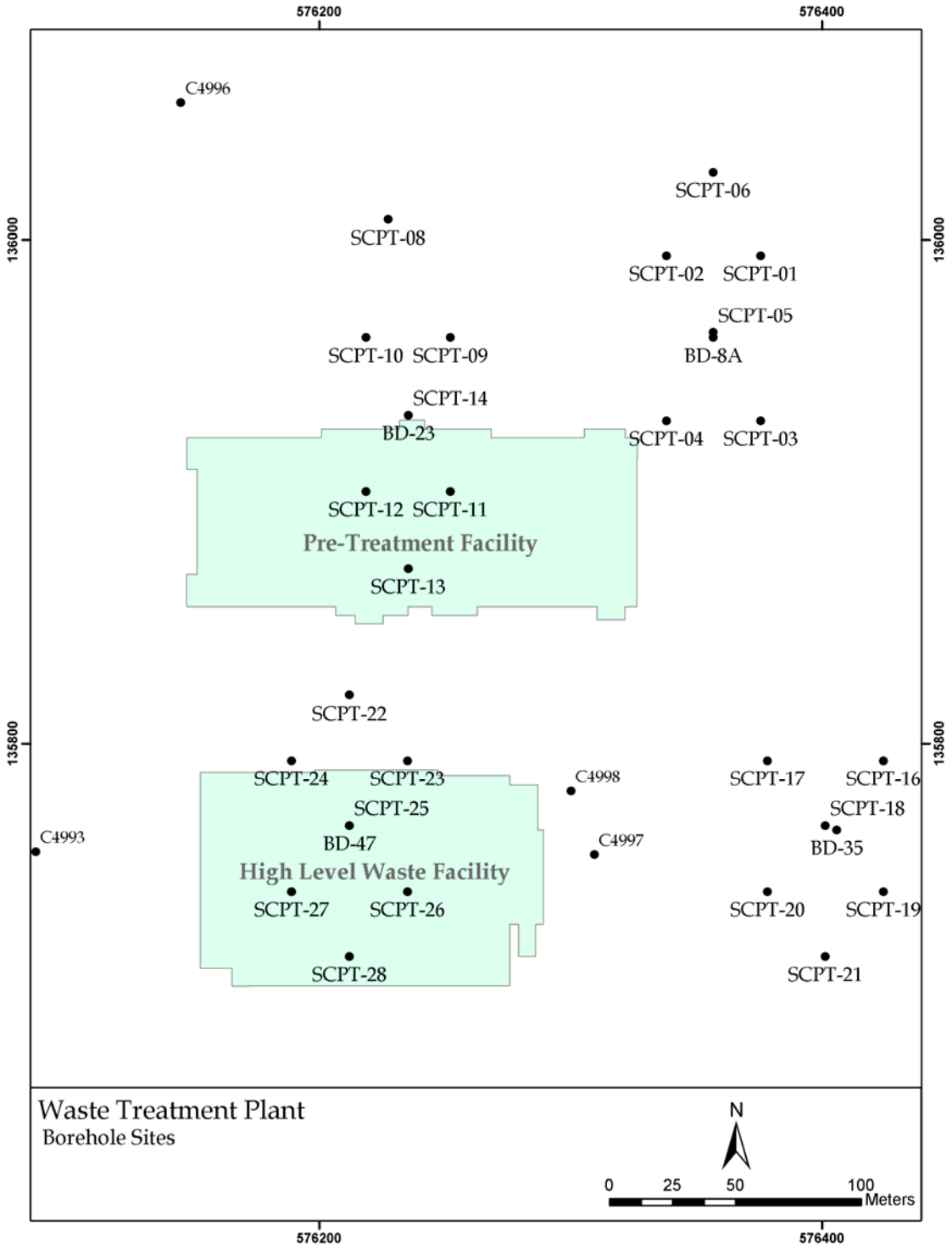

Figure 6.7. Location Map of Borings from Shannon & Wilson (2000)

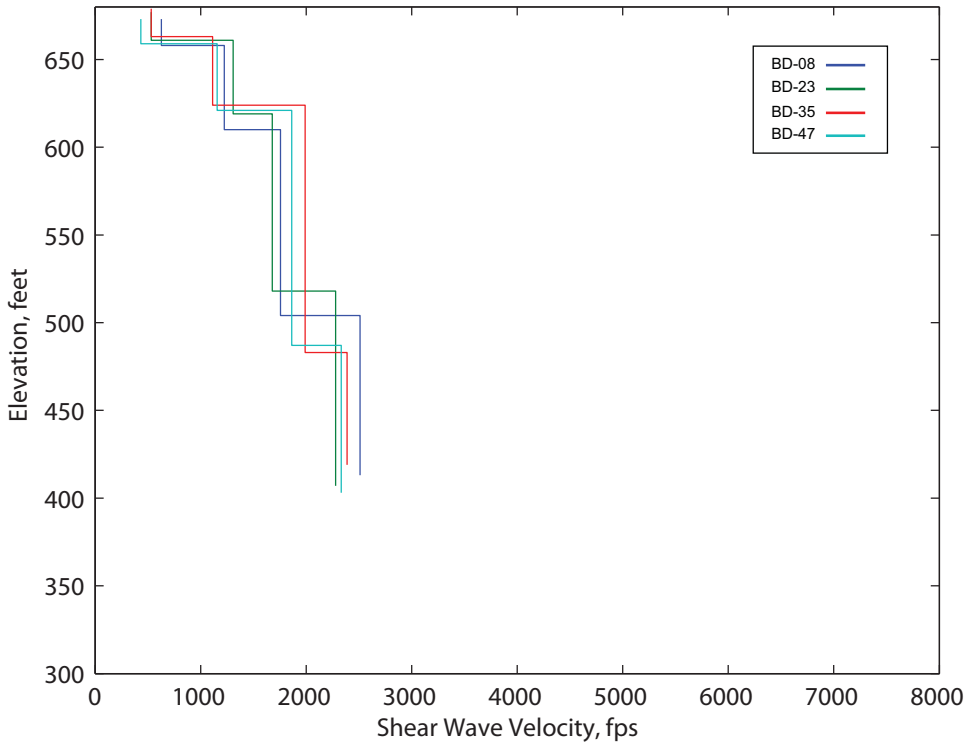

Figure 6.8. Preconstruction Downhole Shear Wave Velocity Profiles

There appears to be a tendency for the two eastern groups shown in Figure 6.9 to have some high velocity values near the surface, that are not seen at the two western groups (beneath the HLW and PT buildings). Figures 6.11 and 6.12 show the result of averaging all of the SCPT data from all four groups, and from just beneath the two buildings of interest. The analysis concludes that only the two western groups will be averaged and used in the Vs profile for modeling of ground motion.

6.3.3 Averaged Downhole and Seismic Cone Penetrometer Test Shear Wave Velocity Profiles

Figures 6.13 and 6.14 show the superposition of the Vs profiles from the new boreholes and the preconstruction boreholes, and the resulting average profile and standard deviation. Both data sets appear to be in good agreement in the upper 260- to 270-ft depth range. When these data are averaged, the disappearance of the preconstruction data at varying depth produces a gradient transition from the high Vs H3 gravel into the lower Vs Cold Creek unit. The preconstruction Vs data are dominated by the data from within the H3 layer, so this gradient is not really measured. For the new data (Redpath 2007), Vs was fit to data subsets from within the geologically determined depth range, and abrupt changes were measured. The data from the preconstruction were then truncated so as not to affect this transition and averaged again, as shown in Figure 6.15. This reduces the transition depth range substantially, to the elevation differences between the contacts in the three different boreholes.

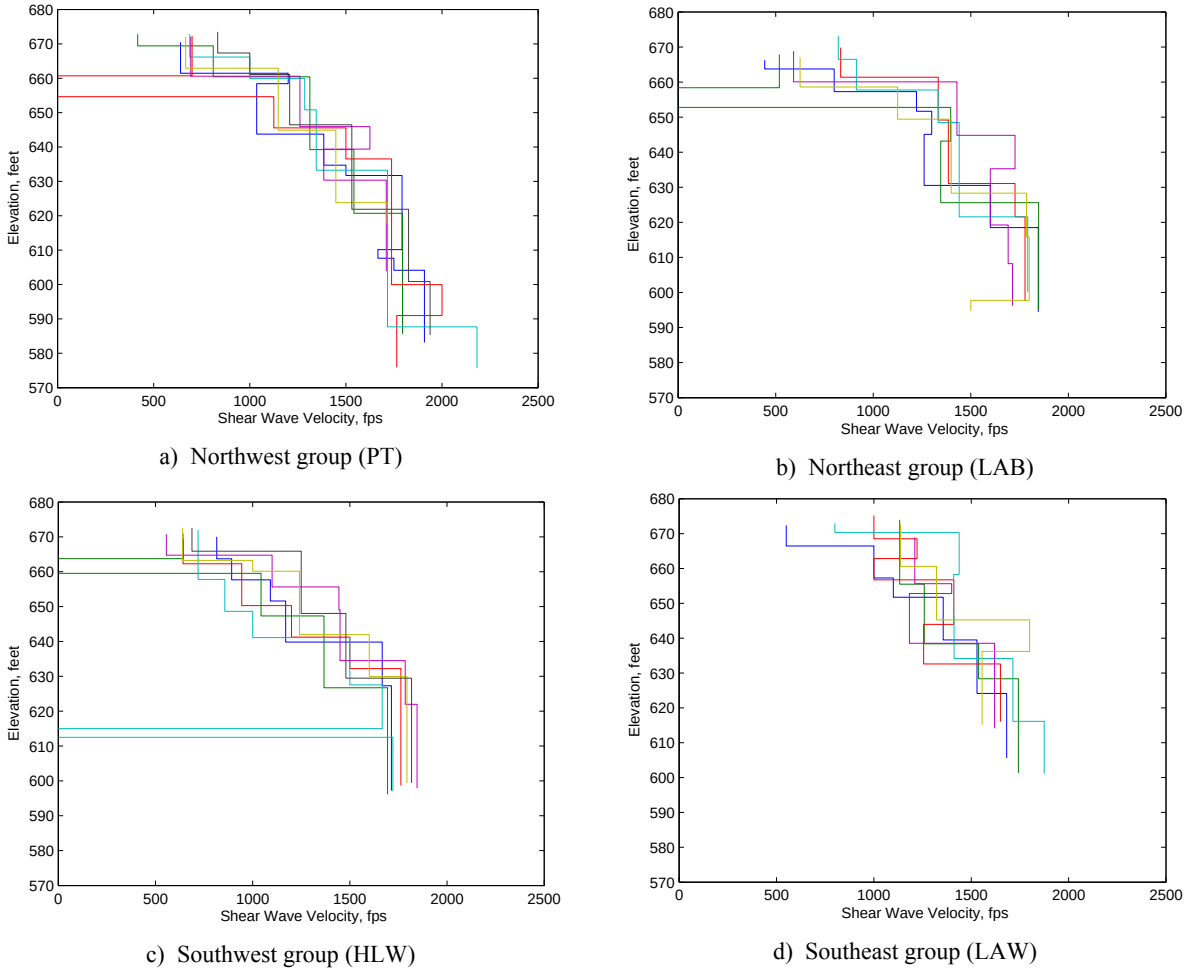

a) Northwest group (PT)

b) Northeast group (LAB)

c) Southwest group (HLW)

d) Southeast group (LAW)

Figure 6.9. Preconstruction Seismic Cone Penetrometer Testing Shear Wave Velocity Profiles

Table 6.5 shows the sediment unit thicknesses as reported by Barnett et al. (2007). In the seismic site response modeling, layer depths and/or thicknesses are randomized to include the range observed. Because of this approach, it is appropriate to ignore the implied thickness of this transition zone and use the average velocities above and below. The randomization will then have a sharp velocity contrast at a variable elevation for the modeling.

Figure 6.10 also shows the averaging of the downhole data with the SCPT data. There are 14 SCPT profiles and 7 downhole profiles. At shallow depth, the data from the new boreholes have been censored because of the backfill issues described previously, so the shallow portion of the profile is dominated by the SCPT data, taken directly beneath the PT and HLW buildings, as desired.

6.3.4 Velocity Data and Model from 2005 WTP Site Response Modeling

Figure 6.16 shows the sediment Vs data used in Rohay and Reidel (2005), and the average profile and associated standard error bounds are shown in Figure 6.17. The data used in 2005 included all of the SCPT data that were found at that time, downhole Vs data taken in boreholes surrounding the WTP site, and SASW measurements. When averaged, the 2005 data reflect slightly lower Vs than the average model developed in Section 6.3.3. The most significant difference is the very high velocity found for the

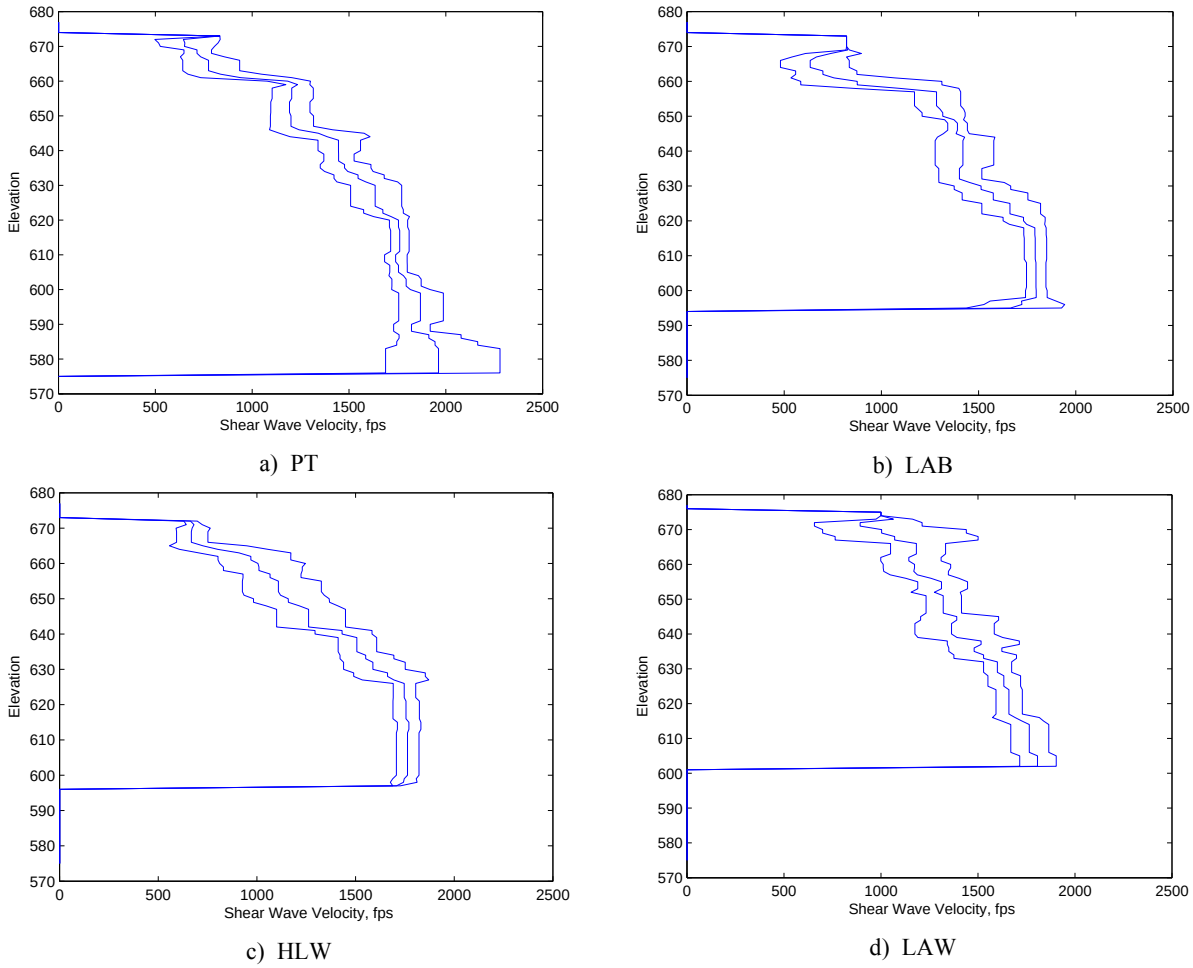

Figure 6.10. Geometric Average (median) Shear Wave Velocity Profiles for the Four Groups of Seismic Cone Penetrometer Test Measurements Showing 16th and 84th Percentiles

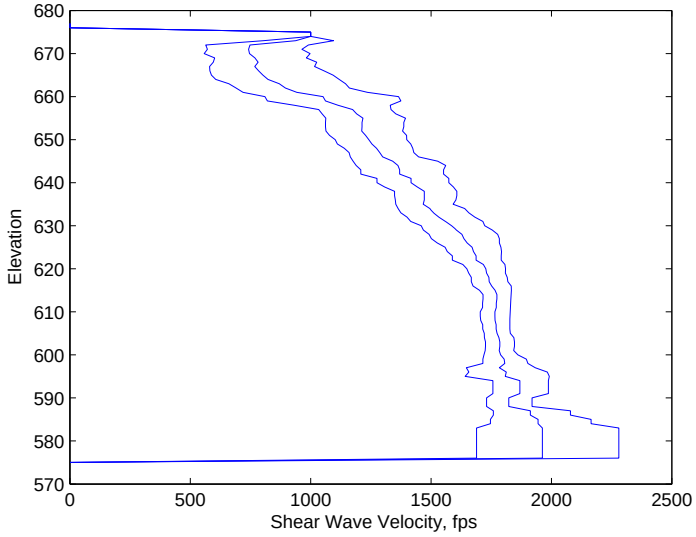

Figure 6.11. Average Shear Wave Velocity Profile for All Seismic Cone Penetrometer Test Data Showing 16th and 84th Percentiles

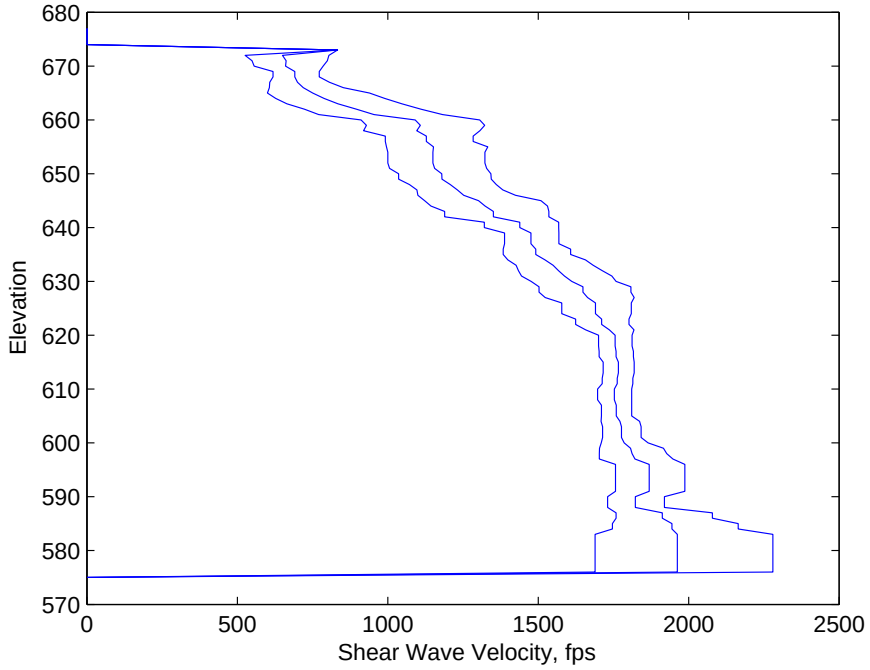

Figure 6.12. Average Shear Wave Velocity Profiles for the Seismic Cone Penetrometer Test Beneath the High-Level Waste and Pretreatment Buildings Showing 16th and 84th Percentiles

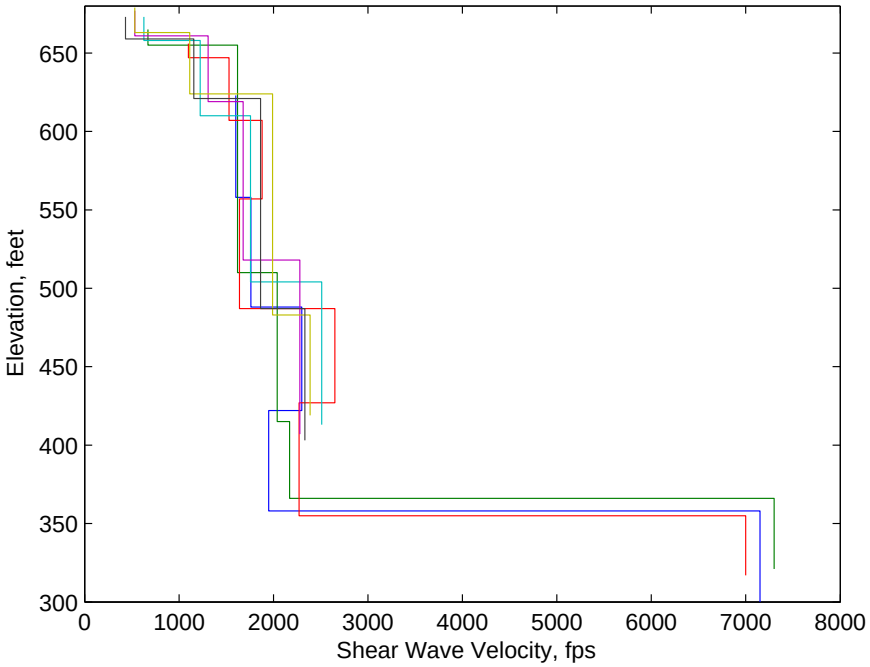

Figure 6.13. Comparison of Redpath and Shannon & Wilson Downhole Data. The Redpath and Shannon & Wilson data are identified in Figures 6.6 and 6.8, respectively.

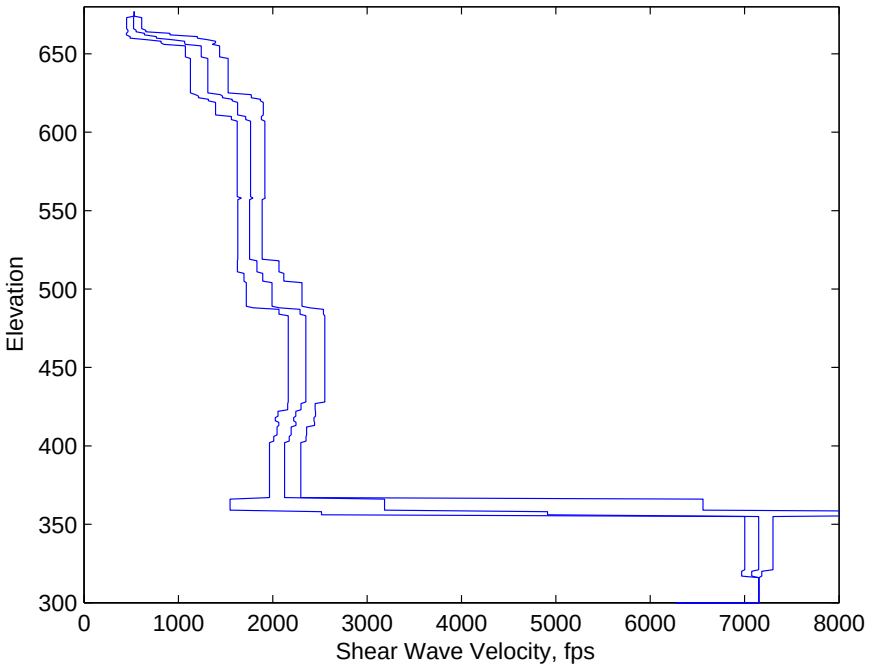

Figure 6.14. Comparison of the Average of Redpath and Shannon & Wilson Downhole Data. The 16th and 84th percentiles are also shown.

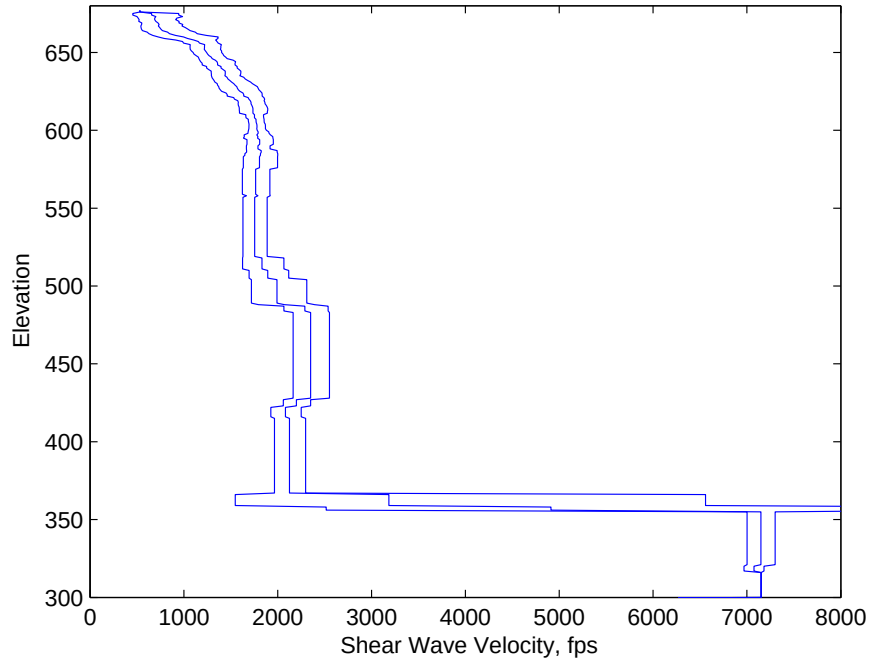

Figure 6.15. Average of All Downhole Data and Seismic Cone Penetrometer Test Data for the High-Level Waste and Pretreatment Buildings. The 16th and 84th percentiles are also shown. The Shannon & Wilson data have been truncated to sharpen the H3-CCU contact near the 425-ft elevation.

Table 6.5. Thickness Variation in Sedimentary Layers

Sediment Unit Thicknesses in Feet				
	C4993	C4996	C4997	C4998
Hanford formation H2 unit	185	173	166	160
Hanford formation H3 unit	70	89	90	90
Cold Creek unit	54	49	63	72
Ringold Unit A	68	45	64	60

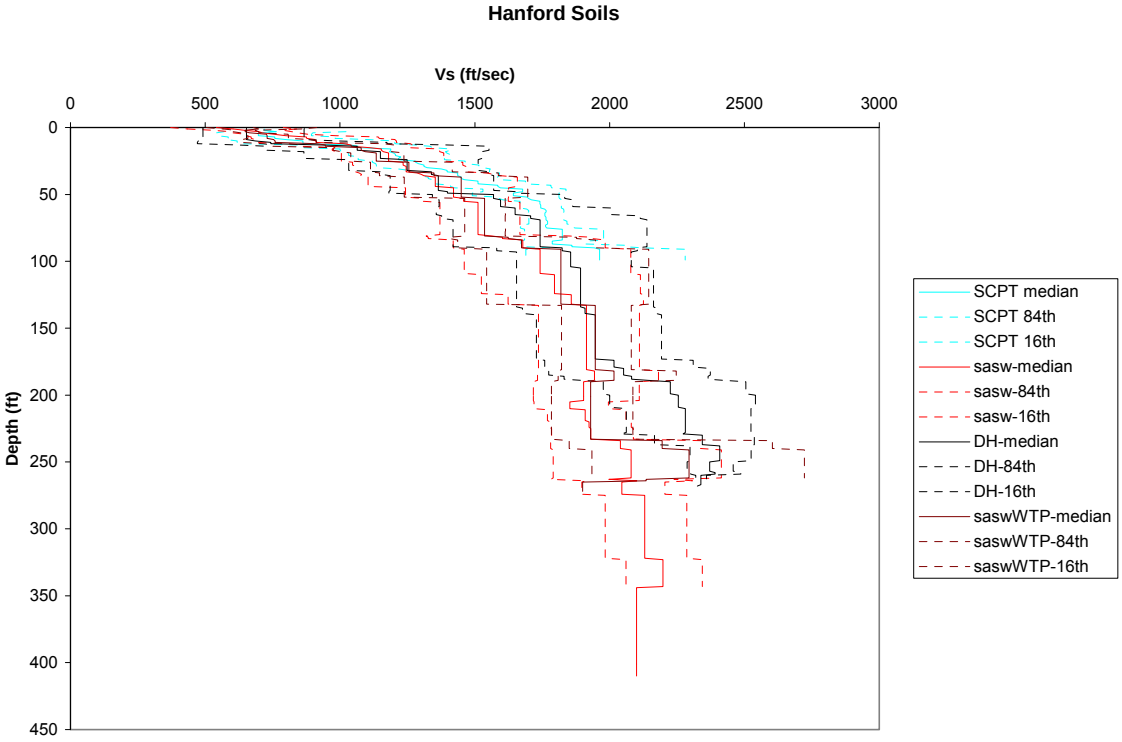

Figure 6.16. Comparison of 2005 Velocity Profiles Including Spectral Analysis of Shear Wave, Seismic Cone Penetrometer Test, and Downhole

Ringold Unit A that lies directly on the topmost basalt, which was not detected in the previous site investigations due to the limited borehole velocity depth range and the indirect nature of the SASW measurements. In addition, the standard errors for the 2005 data, approximately 500 fps, are significantly larger than the result from Section 6.3.3, where they are near 200–250 fps.

6.4 Density Models for Basalts, Interbeds, and Sediments

Densities measured with the borehole gravity meter for each of the stratigraphic units in all three boreholes were averaged to determine mean unit densities. The stratigraphic units included the four suprabasalt sedimentary units (Hanford sand [H2], Hanford gravel [H3], Cold Creek unit gravel [CCU], and Ringold Formation A), in addition to the six basalt members and flows and four sedimentary interbeds shown in Figure 6.4. A fifth sedimentary interbed approximately 5 ft thick (Byron interbed) was encountered in borehole C4996 but not in C4993 or C4997. The Byron interbed is not an important

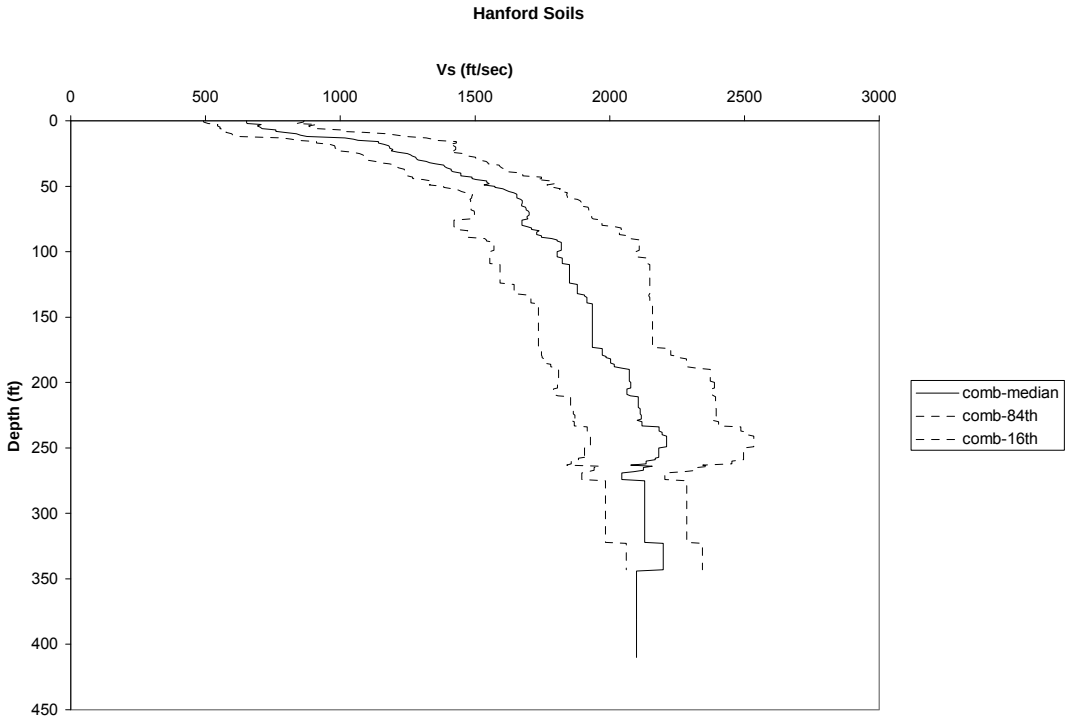

Figure 6.17. Average Velocity Profile Averaging All Spectral Analysis of Shear Wave, Seismic Cone Penetrometer Test, and Downhole Data from 2005

consideration in seismic analysis because of the small thickness of this interbed and its discontinuity across the WTP site. The interbed thickness was also less than the BHGM measurement interval; therefore, no meaningful density values are reported.

6.4.1 Transitions Zones Between Interbeds and Basalt Units

As described in Barnett et al (2007), the Columbia River Basalt Group lava flows consist of a flow top, a dense flow interior, and a flow bottom of variable thicknesses. The flow top is represented by vesicular to rubbly and/or brecciated basalt and may have features and physical properties distinctly different from those of the flow interior. Based on review of the geologists' logs of the corehole C4998 (Barnett and Garcia 2006) and each of the three deep boreholes (Adams et al. 2007; Difebbo 2007; Rust et al. 2007), the geophysical logs (Gardner and Price 2007), and the density logs (Figure 5.3), the flow tops of the basalt units tend to include significant breccia (e.g., Pomona Member), vesicular basalt (Priest Rapids member), or a mix of sedimentary clay and basalt breccia (e.g., Esquatzel, Umatilla, Priest Rapids members)In addition, these flow top transition zones between each of the sedimentary layers and the basalt flow interiors are significantly thicker for the basalt flow tops than for the basalt flow bottoms. Therefore, it is important to distinguish the flow top characteristics, such as density and shear wave velocity, from those of the basalt flow interior and sedimentary interbeds. The approach taken to calculate mean densities for each of the stratigraphic units was to 1) parse the BHGM density data by clearly demarcating each stratigraphic unit using the depths of upper contact from Barnett et al. (2007); 2) identify the flow top transition zones using depth of upper contact and measured density values as an indicator; and 3) calculate the mean unit densities for each stratigraphic unit, excluding any measurements from the flow top transition zones.

As seen in Figure 6.18, densities increase from approximately 2.0 g/cm^3 within the sedimentary interbeds to approximately 2.8 g/cm^3 within the basalt flow interiors of most units. The transition zone was defined as the region from the upper contact of a basalt flow to the depth at which the measured density reaches 2.75 g/cm^3. This value was selected as a reasonable approximation of the upper boundary of the basalt flow top, based on review of the data in Figure 5.3. The Umatilla Member has a lower mean density than the other basalt units and also comprises two separate flows—the upper Sillusi flow and the lower Umatilla flow. Therefore, an upper boundary density value of 2.60 g/cm^3 was used for the Umatilla Member instead of 2.75 g/cm^3. In addition, a flow top feature exists on both flows. The lower Umatilla flow top is evident from the zone of lower density at approximately 320 ft below mean sea level (MSL), as seen on Figure 6.18.

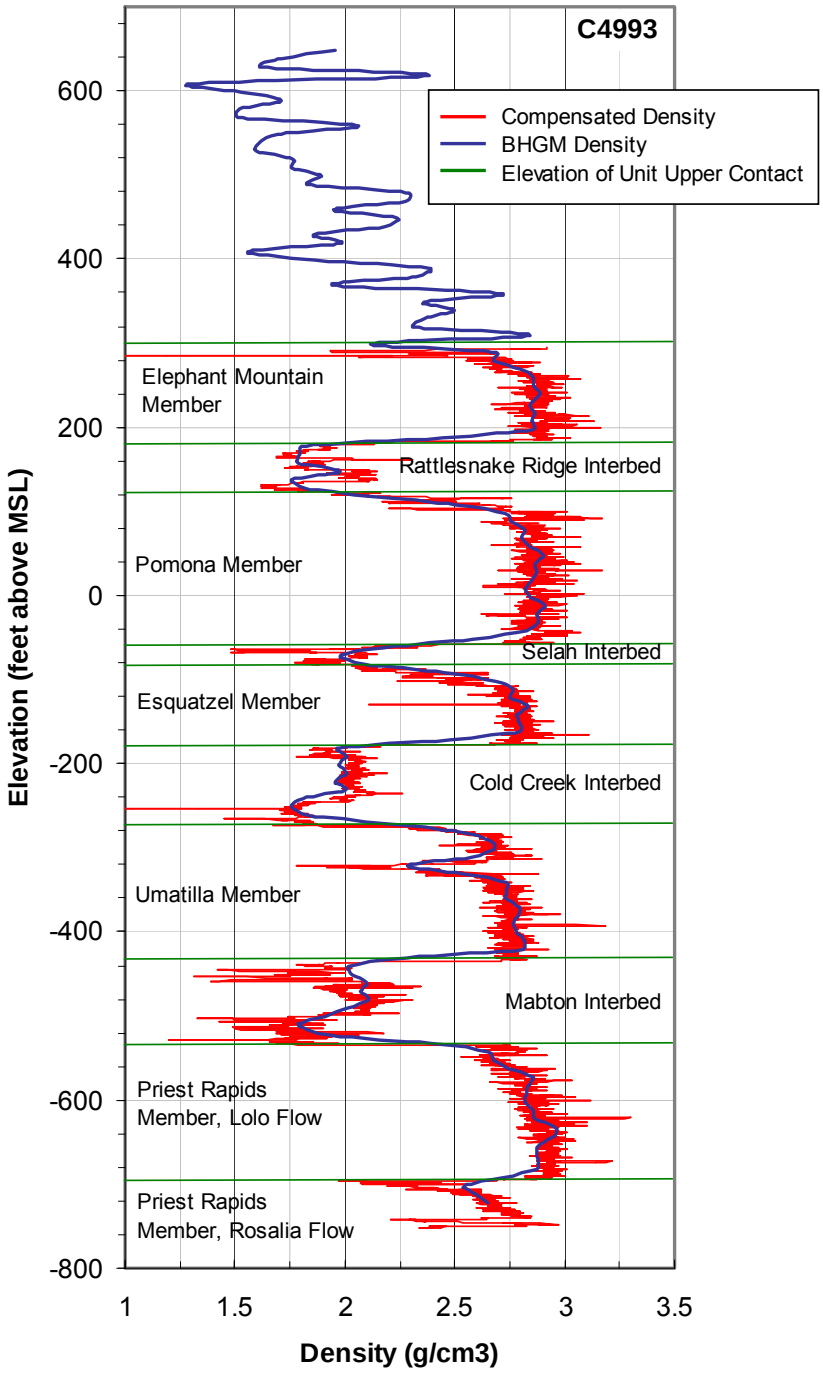

Figure 6.18. Borehole Gravity Meter and Compensated Density Logs of Borehole C4993

Density measurements from both BHGM and compensated density logs were used to assess the flow top transition zone thicknesses. Although there are some suspect data with the compensated density logs, likely due to washout zones, the 0.1-ft measurement interval of these logs provided higher resolution for assessing the thicknesses of the transition zones and identifying measurements to be excluded from the mean unit density calculation. The estimated flow top transition zone thicknesses for each basalt member/flow are shown in Table 6.6. Estimates of flow bottom thicknesses also were made using the same approach as described above but using the depth of

Table 6.6. Estimated Basalt Flow Top Thicknesses

Basalt Unit, Flow	Flow Top Mean Thickness (ft)	Std. Dev. (ft)
Elephant Mountain Member	20.0	10.8
Pomona Member	30.6	6.3
Esquatzel Member	26.3	16.2
Umatilla Member, Sillusi flow	9.3	2.1
Umatilla Member, Umatilla flow	24.5	12.4
Priest Rapids Member, Lolo flow	12.3	11.8
Priest Rapids Member, Rosalia flow[(a)]	22.8	13.0
(a) Based on limited data. The Rosalia flow interior was not fully penetrated in the three deep boreholes.		

upper contact of the underlying sedimentary interbed rather than basalt member. The mean thickness of the flow bottoms ranged from 1.5 to 4.4 ft, much less than the BHGM measurement interval of 10 ft. Therefore, assessment of flow bottom transition zones was deemed unnecessary and impractical.

6.4.2 Mean Unit Densities

The BHGM density data for each borehole and depth interval were tabulated and organized by common stratigraphic unit using the depths of upper contact from Barnett et al. (2007). Density data for depth intervals corresponding to the flow top transition zones described above were identified in the tabulated data. Arithmetic mean unit densities for each stratigraphic unit across all three boreholes were calculated along with standard deviations. The density data from the flow top transition zones were excluded from the estimate of unit mean densities. The results of the mean density calculations for each stratigraphic unit are shown in Table 6.7.

6.5 Shape-Factor Refinements to Velocity and Density Models

Basalt flow top transition zones are represented by significant changes in both density and velocity as described in Section 6.4. The density flow top characteristics were distinguished from those of the basalt flow interior and sedimentary interbeds when the mean unit densities in Section 6.4.2 were calculated. In addition, velocity refinements are necessary to the velocity model presented in Section 6.2, to specifically address the transition zones. This section describes how the density and velocity profiles within the transition zones are represented in the overall velocity and density model for the WTP site.

6.5.1 Transition Zone Density Shapes

The density of the flow top transitions zones, as described in Section 6.4.1, increases from approximately 2.0 g/cm^3 within the sedimentary interbeds to approximately 2.8 g/cm^3 within the basalt flow interiors of most units.[(a)] A density shape function for each basalt flow top was developed to

(a) Except for the Umatilla Member, where the flow interior mean unit density is 2.656 g/cm^3, and an interior flow top is present between the Sillusi and Umatilla flows.

Table 6.7. Mean Stratigraphic Unit Densities

Stratigraphic Unit, Flow	Arithmetic Mean Unit Density (g/cm^3)	Std. Dev. (g/cm^3)	84th Percentile (g/cm^3)	16th Percentile (g/cm^3)
Backfill	1.934	0.240	2.173	1.694
Hanford formation H2 unit (sand)	1.703	0.198	1.901	1.505
Hanford formation H3 unit (gravel)	2.037	0.158	2.196	1.879
Cold Creek unit (gravel)	2.168	0.246	2.414	1.922
Ringold Formation A	2.493	0.134	2.627	2.360
Elephant Mountain Member	2.806	0.197	3.003	2.609
Rattlesnake Ridge Interbed	1.891	0.091	1.982	1.801
Pomona Member	2.812	0.096	2.908	2.716
Selah Interbed	2.129	0.101	2.229	2.028
Esquatzel Member	2.735	0.119	2.854	2.616
Cold Creek Interbed	1.947	0.115	2.061	1.832
Umatilla Member	2.656	0.132	2.788	2.524
Mabton Interbed	2.035	0.112	2.148	1.923
Priest Rapids Member, Lolo flow	2.826	0.104	2.930	2.722
Priest Rapids Member, Rosalia flow	2.688	0.090	2.777	2.598

represent the density transition. A three-step function as depicted in Figure 6.19 was chosen as the means of aggregating and averaging data from the three deep boreholes to generate an approximate transition shape. The flow top transition zone described in Section 6.4.1 was divided into three steps or segments of density change identified as Flow top1, Flow top2, and Flow top3, corresponding to densities of 2.25, 2.5, and 2.75[(a)] g/cm^3, respectively. The Flow top1 step represents the thickness of the flow top from the top of contact of the flow to the depth at which the density reaches 2.25 g/cm^3. Flow top2 represents the difference between the depth at 2.25 g/cm^3 and that at which the density reaches 2.5 g/cm^3. Likewise, Flow top3 represents the depth difference between measured densities of 2.5 and 2.75 g/cm^3. The mean thickness and range of thickness for these three steps for each flow top and borehole were assessed from BHGM and compensated density logs as described earlier for the overall transition zone thickness. The densities at each of the three steps were then reflected as a percentage less than or greater than each flow interior mean unit density. The calculated density shape functions are shown in Table 6.8.

6.5.2 Transition Zone Velocity Shapes

Similar to density, the shear wave velocity within the flow top transition zones increases from lower velocities at the base of the sedimentary interbeds to higher velocities within the basalt flow interior. This transition is not readily observed from the results of downhole seismic logging, due to the typical measurement intervals of 10 ft (3 m) or more. However, the change in velocity can be observed from the

(a) An upper boundary density value of 2.60 g/cm^3 was used for the Umatilla Member instead of 2.75 g/cm^3 because of the lower flow interior mean unit density.

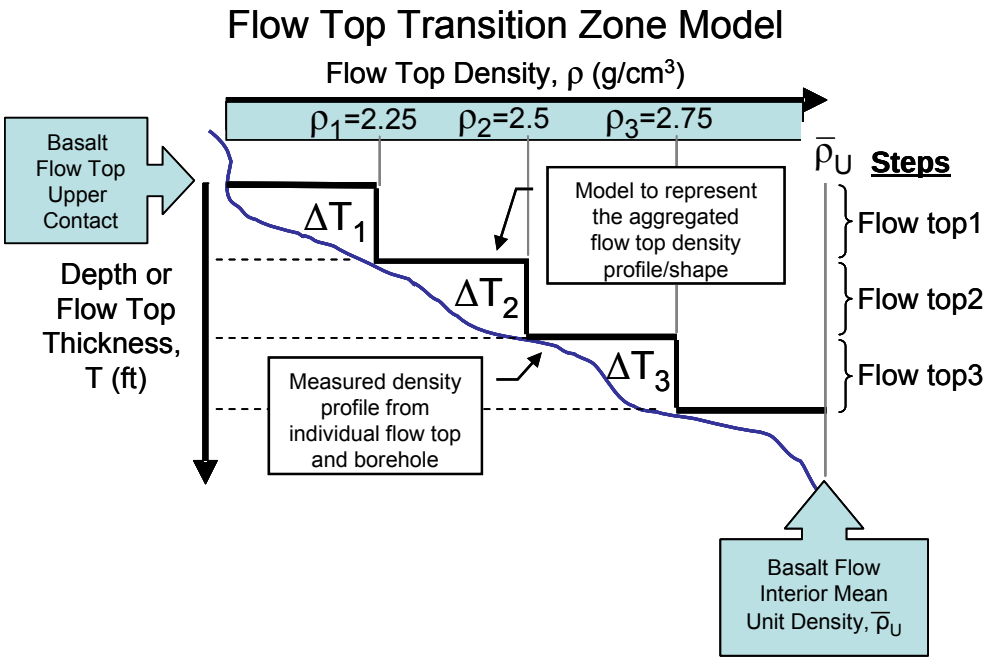

Figure 6.19. General Model for Depicting Flow Top Density Profile

0.5- and 1.0-m interval suspension logging data, as seen in Figure 6.20. In this 0.5-m interval log from borehole C4996, shear wave velocity increases from approximately 5,000 ft/sec at the Esquatzel Member top of contact at 718 ft bgs, to approximately 10,000 ft/sec in the flow interior at greater than 750 ft bgs. To account for transition zones where velocities do not increase as a single step function from the interbeds to the basalt flow interior, a velocity shape function for each basalt flow top was developed to represent the velocity transition.

Unlike densities, the shear wave velocities from suspension logging show greater scatter, as can be seen between 720 and 730 ft bgs in Figure 6.20. The velocity increases rapidly to 9,000 ft/sec and then drops back to less than 6,000 ft/sec before climbing again. Although the general trend of the velocity increase within the flow top transition zone can be observed, the variability of the suspension logging data made it difficult to apply the same transition zone steps approach used with the density data. Transition zone thicknesses estimated using velocity changes were consistently lower than thicknesses estimated using densities and other physical observations (Barnett et al. 2007). Therefore, a combined approach using density and velocity data was chosen to develop velocity shape functions for each basalt flow top.

The same flow top steps and corresponding thicknesses defined for the density shape functions (Figure 6.19 and Table 6.7) were used for the velocity shape functions. To calculate the percentage less than or greater than the mean unit Vs, average Vs values corresponding to the three density step values of 2.25, 2.5, and 2.75 g/cm^3 were estimated. All suspension logging Vs measurements from within the flow top transition zones were correlated with the BHGM density measurements from those same zones. Because of the difference in measurement intervals between density (3 m) and Vs (1 m), the harmonic mean of the three Vs measurements corresponding to the same density depth interval was calculated. A total of 42 discrete density and velocity data pairs were tabulated and a linear regression applied to produce a numerical relationship representing average Vs as a function of density.

Table 6.8. Density Shape Functions for Basalt Flow Tops

Stratigraphic Unit, Flow	Step/Feature	Arithmetic Mean Step/ Feature Thickness (ft)	Minimum Step/Feature Thickness (ft)	Maximum Step/Feature Thickness (ft)	Percentage Less Than (−) or Greater Than (+) the Flow Interior Mean Unit Density[(a)]
Elephant Mountain Member	Flow top1	2.0	2.0	2.0	-19.81%
	Flow top2	6.0	1.0	10.0	-10.91%
	Flow top3	13.3	10.0	20.0	-2.00%
Pomona Member	Flow top1	12.8	3.2	26.1	-19.99%
	Flow top2	10.2	1.3	21.0	-11.10%
	Flow top3	7.6	0.8	13.5	-2.20%
Esquatzel Member	Flow top1	4.0	0.6	8.6	-17.73%
	Flow top2	2.2	0.9	4.5	-8.59%
	Flow top3	20.2	0.5	33.3	0.55%
Umatilla Member, Sillusi flow[(b)]	Flow top1	4.1	0.5	8.1	-15.29%
	Flow top2	3.5	1.8	5.5	-5.87%
	Flow top3	1.7	1.0	2.4	-2.11%
	Flow interior				-0.98%
Umatilla Member, Umatilla flow[(b)]	Flow top1	18.4	4.6	32.9	-15.29%
	Flow top2	4.6	0.9	8.4	-5.87%
	Flow top3	1.5	0.5	3.2	-2.11%
	Flow interior				0.68%
Priest Rapids Member, Lolo flow	Flow top1	0.4	0.3	0.7	-20.38%
	Flow top2	2.0	0.2	5.4	-11.54%
	Flow top3	9.8	0.4	25.0	-2.69%
Priest Rapids Member, Rosalia flow	Flow top1	3.7	0.0	6.1	-16.29%
	Flow top2	3.3	1.2	6.9	-6.99%
	Flow top3	NM	NM	NM	NM

(a) Flow interior mean unit densities from Table 6.7. Percentage (%) $\rho_U = (\rho_U - \rho_i)/\rho_U \times 100$, where ρ_U is mean flow interior unit density for unit U, ρ_i is ρ_1, ρ_2, or ρ_3 for each step i (see Figure 6.19).

(b) Sillusi and Umatilla flow density shapes are a percentage of the single Umatilla Member mean flow interior unit density from Table 6.7. The mean flow interior densities of each flow are slightly lower and higher, respectively, than the overall mean density of the Umatilla Member.

NM – Not measured. The flow interior of the Rosalia flow was not penetrated in all three boreholes.

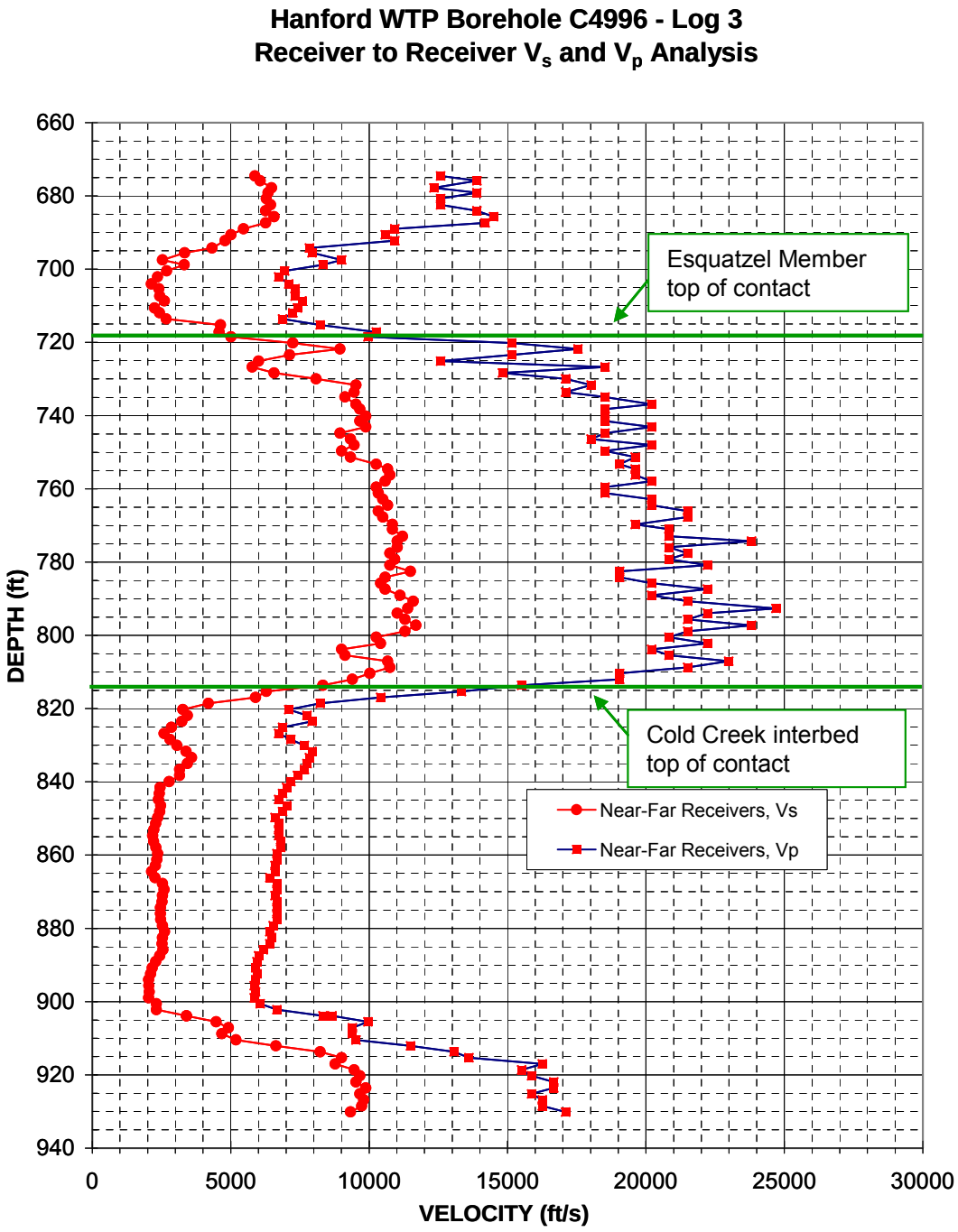

Figure 6.20. Suspension Logging P- and S-Wave Velocities for Borehole C4996, Log 3, 0.5-m Intervals (adapted from Diehl and Steller 2007a)

The linear regression resulted in average Vs values of 5,821, 6,911, and 8,000 ft/sec corresponding to the three density step values of 2.25, 2.5, and 2.75 g/cm^3, respectively. These average Vs step values developed from suspension logging data do not correlate directly to velocities measured using downhole logging methods. However, by presenting the velocity shapes for each flow top step as a percentage of flow interior mean unit velocity, the results can be used directly with the mean unit velocity model from Section 6.2 that was developed from downhole logging data.

Mean unit velocities from suspension logging data for the flow interior of each basalt unit were developed using the same methodology used to produce mean unit densities (see Section 6.4.2). The 1-m suspension logging Vs data (Diehl and Steller 2007b) for each borehole and depth interval were tabulated and organized by common stratigraphic unit using the depths of upper contact from Barnett et al. (2007). Velocity data for depth intervals corresponding to the flow top transition zones described above were identified in the tabulated data. Geometric mean unit velocities for each stratigraphic unit across all three boreholes were calculated along with geometric standard deviations. The velocity data from the flow top transition zones were excluded from the estimate of mean unit velocities. The results of the mean velocity calculations for each stratigraphic unit are shown in Table 6.9.

Using the mean unit velocities in Table 6.9, the velocities at each of the three steps were then reflected as a percentage less than or greater than each flow interior mean unit velocity. The calculated velocity shape functions are shown in Table 6.10.

Table 6.9. Basalt Flow Interior and Interbed Mean Unit Velocities from 1-m Interval Suspension Logging Data

Stratigraphic Unit, Flow	Geometric Mean Unit Velocity (Vs) (ft/sec)	Std. Dev. (lnV)	84th Percentile (ft/sec)	16th Percentile (ft/sec)
Elephant Mountain Member	9,547	0.0955	10,504	8,678
Rattlesnake Ridge Interbed	2,729	0.1342	3,121	2,386
Pomona Member	10,233	0.1027	11,340	9,235
Selah Interbed	3,190	0.3487	4,521	2,251
Esquatzel Member	9,687	0.1367	11,106	8,449
Cold Creek Interbed	2,492	0.1436	2,876	2,158
Umatilla Member	9,417	0.1276	10,698	8,289
Mabton Interbed	2,566	0.1559	2,998	2,195
Priest Rapids Member, Lolo flow	9,884	0.1111	11,045	8,845
Priest Rapids member, Rosalia flow	8,843	0.1550	10,326	7,574

6.6 Final Shear Wave Velocity and Density Profiles for Use in Seismic Response Modeling

A set of final site-specific velocity and density profiles or models of the WTP site were generated based on the analyses presented in Sections 6.1 through 6.5. The final set of profiles integrates data from the new boreholes and past studies, and provides a set of updated input parameters for subsequent use in evaluating the seismic site response of the WTP site.

The final velocity and density profiles are represented by a set of input parameters required for seismic site response analyses that include densities of all stratigraphic units, stratigraphic unit thicknesses, basalt flow top thicknesses, Vs of all stratigraphic units, and basalt flow top velocity gradients. The recommended density profile is represented by the mean density for each stratigraphic unit

Table 6.10. Velocity Shape Functions for Basalt Flow Tops

Stratigraphic Unit, Flow	Step/Feature	Arithmetic Mean Step/Feature Thickness (ft)	Minimum Step/Feature Thickness (ft)	Maximum Step/Feature Thickness (ft)	Percentage Less Than (−) or Greater Than (+) the Flow Interior Mean Unit Vs[(a)]
Elephant Mountain Member	Flow top1	2.0	2.0	2.0	-39.03%
	Flow top2	6.0	1.0	10.0	-27.61%
	Flow top3	13.3	10.0	20.0	-16.20%
Pomona Member	Flow top1	12.8	3.2	26.1	-43.12%
	Flow top2	10.2	1.3	21.0	-32.46%
	Flow top3	7.6	0.8	13.5	-21.82%
Esquatzel Member	Flow top1	4.0	0.6	8.6	-39.91%
	Flow top2	2.2	0.9	4.5	-28.66%
	Flow top3	20.2	0.5	33.3	-17.42%
Umatilla Member, Sillusi flow[(b)]	Flow top1	4.1	0.5	8.1	-38.19%
	Flow top2	3.5	1.8	5.5	-26.61%
	Flow top3	1.7	1.0	2.4	-15.05%
	Flow interior				-3.08%
Umatilla Member, Umatilla flow[(b)]	Flow top1	18.4	4.6	32.9	-38.19%
	Flow top2	4.6	0.9	8.4	-26.61%
	Flow top3	1.5	0.5	3.2	-15.05%
	Flow interior				1.95%
Priest Rapids Member, Lolo flow	Flow top1	0.4	0.3	0.7	-41.11%
	Flow top2	2.0	0.2	5.4	-30.08%
	Flow top3	9.8	0.4	25.0	-19.06%
Priest Rapids Member, Rosalia flow	Flow top1	3.7	0.0	6.1	-34.17%
	Flow top2	3.3	1.2	6.9	-21.85%
	Flow top3	NM	NM	NM	NM

(a) Calculated using flow interior mean shear wave velocities (Vs) from Table 6.9. Can also be applied to shear wave mean unit velocities from downhole seismic logging (Section 6.2).
(b) Sillusi and Umatilla flow velocity shapes are a percentage of the single Umatilla Member mean flow interior unit velocity from Table 6.9. The mean flow interior velocities of each flow are slightly lower and higher, respectively, than the overall mean velocity of the Umatilla Member.
NM – Not measured. The flow interior of the Rosalia flow was not penetrated in all three boreholes.

which was provided in Table 6.7. These recommended densities are comparable to, but represent more accurate and slightly wider range of values than the densities used in the 2005 seismic site response analyses.

The thickness of the suprabasalt sediments, basalts, and sedimentary interbeds measured in each of the four new boreholes were shown in Tables 6.1 and 6.4. The range of thicknesses is summarized in Table 6.11 and is recommended for use in randomly selecting values for seismic site response modeling. The combined thickness of the Rattlesnake Ridge interbed and the underlying Pomona Member is nearly constant across the boreholes; therefore, a correlation is to be used with the randomization to keep this combined thickness constant. Thicknesses of stratigraphic layers used in the 2005 seismic site response analyses are comparable to and bounded by those recommended here. In a few cases (i.e., Elephant Mountain Member, Rattlesnake Ridge interbed, and Pomona Member) the minimum or maximum thicknesses slightly exceeded the range used in 2005 (Rohay and Reidel 2005).

Table 6.11. Range of Stratigraphic Unit Thicknesses

Stratigraphic Unit, Flow	Minimum Thickness (ft)	Maximum Thickness (ft)
Suprabasalt Sediments		
Hanford formation H2 unit	160	185
Hanford formation H3 unit	70	90
Cold Creek unit	49	72
Ringold Unit A	45	68
Basalt and Interbed Layers		
Elephant Mountain Member	104	118
Rattlesnake Ridge Interbed	34	56
Pomona Member	186	209
Selah Interbed	22	23
Esquatzel Member	94	96
Cold Creek Interbed	91	98
Umatilla Member	156	161
Mabton Interbed	94	98
Priest Rapids Member, Lolo flow	156	165

The range of basalt flow top thicknesses was represented by a total flow top mean and standard deviation in Table 6.5. The flow top thickness is most important in estimation of the velocity gradients between the interbeds and basalt flow interiors. Therefore, the range of flow top thicknesses recommended for use in randomly selecting values for seismic site response modeling are represented by the unit-specific step thickness ranges in Table 6.10. In 2005, the flow top thickness was represented by a 50-ft thick zone on each of the shallowest four basalt members only. Shear wave velocity was reduced by a maximum of 20% (of the Vs for the basalt flow interior), at the top of the basalt, and increased linearly with depth. The flow top thickness was not unit-specific or randomized in 2005.

The final Vs profiles for the suprabasalt sediments recommended for seismic site response modeling are shown in Figure 6.21 along with the profiles used in the 2005 analyses. Vs gradually increases with depth in the sand-dominated H2 unit to a depth of approximately 60 ft (see Figure 6.15), where it reaches

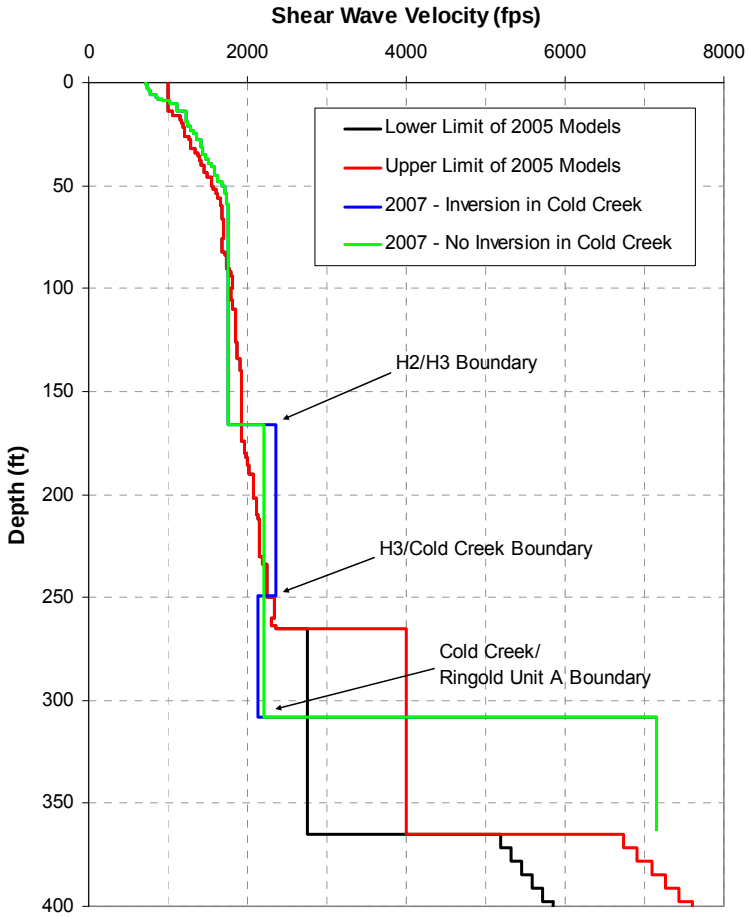

Figure 6.21. Comparison of Final Sediment Shear Wave Velocity Model to Rohay and Reidel (2005). Figure taken from Youngs (2007).

a near-constant value near 1,750 ft/sec. The velocity increases abruptly in the gravel-dominated H3 unit. Two alternatives of the deeper sediment layers are recommended for the 2007 analyses based on the data presented in Section 6.3. A uniform Vs profile (2,200 ft/sec) across the H3 unit and CCU as shown by the green line in Figure 6.21, and an inverted Vs profile represented by the blue line with a higher Vs (2,350 ft/sec) in the H3 unit and lower Vs (2,126 ft/sec) in the CCU.

A significant difference between the 2005 model and this model exists for the Ringold velocity structure shown in Figure 6.21. The upper part (the CCU or "reworked Ringold) has much lower velocity, in either of the alternatives described above, compared to the 2005 model. The lower part (Ringold Unit A) has a very high velocity (7,150 fps), nearly as high as that in the basalts.

The final recommended Vs profiles for the basalt and interbeds are shown in Figure 6.22 along with the profiles used in the 2005 analyses. The recommended basalt flow top velocity gradients identified in Table 6.10 are also shown graphically in Figure 6.22. Two alternatives are recommended for the 2007 analyses based on the data presented in Section 6.2. Individual unit (i.e., unit-specific) Vs profile for each basalt and interbed unit is shown by the blue line in Figure 6.22. A composite Vs profile representing a

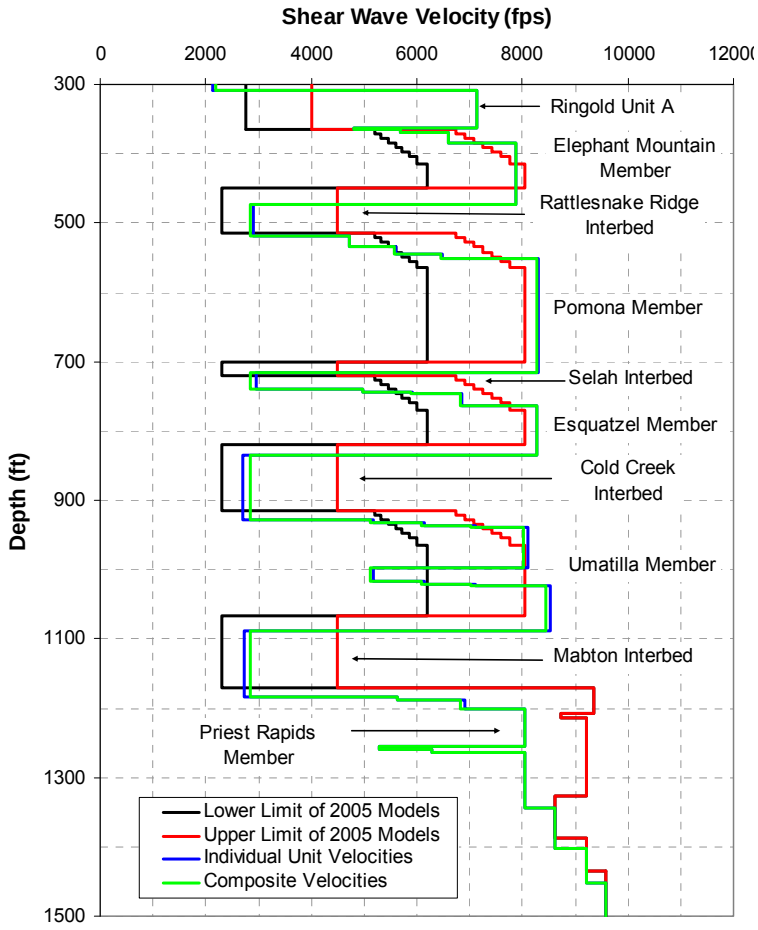

Figure 6.22. Comparison of Final Basalt and Interbed Shear Wave Velocity Model to Rohay and Reidel (2005). Figure taken from Youngs (2007).

single mean Vs for the basalt units and single mean Vs for the interbeds is shown by the green line. In comparison to 2005, the basalt Vs values are comparable to the upper limit of the 2005 analyses, and the interbed Vs values are significantly less than the upper limit of the 2005 analyses. The flow top gradients are also noticeably different based on the analyses presented in Section 6.5. The 2007 gradients are unit-specific, and gradually rise from a much lower Vs value than estimated in 2005. Finally, the 2007 profile represents the interflow features present in the Umatilla and Priest Rapids members, introducing flow top gradients between basalt flows.

7.0 References

Abramowitz M and IA Stegun. 1964. *Handbook of Mathematical Functions with Formulas, Graphs, and Mathematical Tables*. Dover, New York.

Adams SC, ST Ahlquist, JR Fetters, BJ Garcia, and CF Rust. 2007. *Borehole Summary Report for Waste Treatment Plant Seismic Borehole C4996*. WMP-32076/PNNL-16416. Prepared by Fluor Hanford, Inc., Richland, Washington, for Pacific Northwest National Laboratory, Richland, Washington.

Barnett DB and BJ Garcia. 2006. *Borehole Summary Report for Core Hole C4998 – Waste Treatment Plant Seismic Boreholes Project*. PNNL-16303, Pacific Northwest National Laboratory, Richland, Washington.

Barnett DB, BN Bjornstad, KR Fecht, DC Lanigan, SP Reidel, and CF Rust. 2007. *Geology of the Waste Treatment Plant Seismic Boreholes*. PNNL-16407 Revision 1, Pacific Northwest National Laboratory, Richland, Washington.

Beyer LA. 1983. *Borehole Gravity Surveys: Theory, Mechanics, and Nature of Measurements*. Number 83-76 in the Open-File Report Series. U.S. Geological Survey, Washington, D.C.

Carmichael RS. 1989. *CRC Practical Handbook of Physical Properties of Rocks and Minerals*. CRC Press, Inc., Boca Raton, Florida.

Crum JV and BJ Riley. 2006. *Mineral Identification of Geologic Samples from Borehole C4998*. PNNL-16297, Rev. 0, Pacific Northwest National Laboratory, Richland, Washington.

Diehl J and R Steller. 2007a. *Final Data Report: P- and S-Wave Velocity Logging Borings C4993, C4996, and C4997 Part A: Interval Logs*. 6303-01, Vol. 1, Rev. 1/PNNL-16381, Rev. 1, prepared by GEOVision Geophysical Services Corona, California, for Pacific Northwest National Laboratory, Richland, Washington.

Diehl J and R Steller. 2007b. *Final Data Report: P- and S-Wave Velocity Logging Borings C4993, C4996, and C4997 Part B: Overall Logs*. 6303-01, Vol. 2, Rev. 1/PNNL-16476, prepared by GEOVision Geophysical Services, Corona, California, for Pacific Northwest National Laboratory, Richland, Washington.

Difebbo TJ. 2007. *Borehole Summary Report for C4997 Rotary Drilling, WTP Seismic Boreholes Project, CY 2006*. WMP-31815/PNNL-16415, prepared by Environmental Quality Management, Inc. and Fluor Hanford, Inc., Richland, Washington, for Pacific Northwest National Laboratory, Richland, Washington.

Gardner MG and RK Price. 2007. *Summary Report of Geophysical Logging for the Seismic Boreholes Project at the Hanford Site Waste Treatment Plant*. DTS-RPT-090/PNNL-16395, prepared by Energy*Solutions* and Pacific Northwest Geophysics, Richland, Washington, for Pacific Northwest National Laboratory, Richland, Washington.

Gardner MG, KD Reynolds, and DE Skoglie. 2005. *Drilling Plan for the Waste Treatment Plant Seismic Test Borehole Project*. FS-RW-SWS-PN-005, Revision 0, Duratek Federal Services, Inc., Richland, Washington.

Geomatrix Consultants. 1996. *Probabilistic Seismic Hazard Analysis – DOE Hanford Site, Washington*. WHC-SD-W236A-TI-002, Rev. 1, Westinghouse Hanford Company, Richland, Washington.

Horner J. 2007. *Entry Boreholes Summary Report for the Waste Treatment Plant Seismic Boreholes Project*. WMP-32119 Revision 0 (Reissue)/PNNL-16417 Rev. 0, prepared by Gram, Inc., for Fluor Hanford, Inc., Richland, Washington.

Hutchinson MF. 1989. "A New Method for Gridding Elevation and Streamline Data with Automatic Removal of Pits." *Journal of Hydrol*ogy 106:211-232.

Hutchinson MF. 1996. "A Locally Adaptive Approach to the Interpolation of Digital Elevation Models." *Third International Conference/Workshop on Integrating GIS and Environmental Modelling*. NCGIA, University of California, Santa Barbara. Available at http://www1.gsi.go.jp/geowww/globalmap-gsi/gtopo30/papers/local.html.

MacQueen JD and EA Mann. 2007. *Borehole Gravity Meter Surveys at the Waste Treatment Plant, Hanford, Washington*. MGL-2007-001/PNNL-16490, prepared by Micro-g LaCoste, Lafayette, Colorado, for Pacific Northwest National Laboratory, Richland, Washington.

Pacific Northwest National Laboratory. 2006. *Sampling and Analysis Plan – Waste Treatment Plant Seismic Boreholes Project*. PNNL-15848 Rev. 2, Pacific Northwest National Laboratory, Richland, Washington.

Redpath B. 2007. *Downhole Measurements of Shear- and Compression-Wave Velocities in Boreholes C4993, C4996, C4997, and C4998 at the Waste Treatment Plant, DOE Hanford Site*. PNNL-16559, prepared by Redpath Geophysics, Murphys, California, for Pacific Northwest National Laboratory, Richland, Washington.

Rohay AC and SP Reidel. 2005. *Site-Specific Seismic Site Response Model for the Waste Treatment Plant, Hanford, Washington*. PNNL-15089, Pacific Northwest National Laboratory, Richland, Washington.

Rust CF, DB Barnett, NA Bowles, and JA Horner. 2007. *Borehole Summary Report for Waste Treatment Plant Seismic Borehole C4993*. PNNL-16343, Pacific Northwest National Laboratory, Richland, Washington.

Selby SM. 1972. *CRC Standard Mathematical Tables*. 20th ed. Chemical Rubber Co., Cleveland, Ohio.

Shannon & Wilson, Inc. 2000. *Final Report, Geotechnical Investigation, River Protection Project-Waste Treatment Plant*. Project No. DE-AC06-96RL-13308, Subcontract No. W375-WTSC99-1036, 200 East Area, Hanford Site, Richland, Washington, report prepared for British Nuclear Fuels, Ltd.

Stokoe KH II, S Li, B Cox and F-Y Menq. 2007. *Deep Downhole Seismic Testing at the Waste Treatment Plant Site, Hanford, WA*. Geotechnical Engineering Report GR07-10/PNNL-16678, Volumes I through VI, prepared by Geotechnical Engineering Center, University of Texas at Austin, for Pacific Northwest National Laboratory, Richland, Washington.

Youngs RR. 2007. *Updated Site Response Analyses for the Waste Treatment Plant, DOE Hanford Site, Washington*. GMX-9995.002-001/PNNL-16653, prepared by Geomatrix Consultants, Inc., Oakland, California, for Pacific Northwest National Laboratory, Richland, Washington.

Distribution

No. of Copies

OFFSITE

C. J. Costantino
4 Rockingham Road
Spring Valley, NY 10977

J. A. McCloskey
U.S. Department of Energy
Headquarters, EM-23
19901 Germantown Road
Germantown, MD 20874

B. B. Redpath
Redpath Geophysics
P.O. Box 540
Murphys, CA 95247

K. H. Stokoe II
University of Texas at Austin
Department of Civil Engineering
College of Engineering
1 University Station C1700
Austin, TX 78712

6 U.S. Army Corps of Engineers
Seattle District
P.O. Box 3755
Seattle, WA 98124-3755
ATTN: A. P. Dimbirs (4)
R. O. Garrison
R. E. Smith

E. A. Mann
Micro-g LaCoste
1401 Horizon Ave.
Lafayette, CO 80026

S. P. Reidel
7207 West Old Inland Empire Highway
Benton City, WA 99320

No. of Copies

ONSITE

7 **DOE Office of River Protection**

W. Abdul	H6-60
J. R. Eschenberg	H6-60
T. R. Hoertkorn	H6-60
L. F. Miller	H6-60
Correspondence Control (3)	H6-60

2 **Bechtel National, Inc.**

L. T. Lamm	MS4-A2
M. R. Braccia	MS 5-K

Energy*Solutions*

M. G. Gardner	G1-62

5 **Fluor Hanford, Inc.**

D. B. Barnett	E6-35
S. A. Fargo	H8-60
D. G. Horton	K6-75
S. H. Worley	E6-35
C. S. Wright	E6-35

Washington Closure Hanford, LLC

K. R. Fecht	H4-21

Washington State Department of Ecology

J. A. Caggiano	H0-57

11 **Pacific Northwest National Laboratory**

B. N. Bjornstad	K6-81
T. M. Brouns (5)	K9-69
D. C. Lanigan	K6-75
A. C. Rohay	K6-75
Information Release (3)	P8-55